Activated sludge batch settling : from experimental investigation using an ultrasonic transducer to 1D modelling, sensitivity analysis and parameter identification

Florent Locatelli

UNIVERSITÉ DE STRASBOURG

ÉCOLE DOCTORALE MSII

Laboratoire ICube

THÈSE présentée par :

Florent LOCATELLI

soutenue le : **24 septembre 2015**

pour obtenir le grade de : **Docteur de l'université de Strasbourg**

Discipline/ Spécialité : Mécanique des Fluides

Activated sludge batch settling: from experimental investigation using an ultrasonic transducer to 1D modelling, sensitivity analysis and parameter identification

THÈSE dirigée par :

M. BEKKOUR Karim	Maître de Conférences, université de Strasbourg

RAPPORTEURS :

M. NOPENS Ingmar	Professeur, université de Gand
M. POTIER Olivier	Maître de Conférences, ENSGSI – université de Lorraine

---

AUTRES MEMBRES DU JURY :

M. DAGOT Christophe	Professeur, ENSIL – université de Limoges
M. MOSE Robert	Professeur, ENGEES – université de Strasbourg
M. FRANCOIS Pierre	Maître de Conférences, université de Strasbourg
M. LAURENT Julien	Maître de Conférences, ENGEES – université de Strasbourg

Remerciements

En premier lieu, je tiens à remercier le professeur Robert Mosé, directeur du Département Mécanique du laboratoire ICube, pour m'avoir permis d'y réaliser l'intégralité de cette thèse dans les meilleures conditions.

Je remercie également mon directeur de thèse, monsieur Karim Bekkour. Son encadrement rigoureux et ses conseils m'ont été précieux et permis de donner une direction à ce travail, de prendre du recul par rapport à mes objectifs, et d'appréhender les subtilités du domaine complexe de la rhéologie.

A messieurs Ingmar Nopens et Olivier Potier, je souhaite exprimer ma profonde gratitude d'avoir accepté d'être les rapporteurs de ce travail. Je remercie vivement messieurs Christophe Dagot, Robert Mosé, Pierre François et Julien Laurent d'avoir bien voulu en être les examinateurs. Je suis également très heureux que messieurs Matthieu Dufresne et Stéphane Fischer aient pris part au jury de cette thèse en tant que membres invités. A monsieur Christophe Dagot, qui a présidé ce jury, j'adresse à nouveau mes sincères remerciements.

Je souhaite exprimer ma reconnaissance à Julien Laurent, qui a encadré cette thèse. Son dynamisme communicatif, ses nombreuses idées et son exigence, associés à un immense investissement, ont été autant d'éléments cruciaux à la bonne marche et à l'achèvement de ce travail.

Je tiens à remercier Pierre François, dont la contribution a permis de développer au-delà de toutes espérances la partie expérimentale de ce travail, et d'extraire la substantifique moelle des résultats obtenus.

Encore une fois, merci à Robert Mosé pour de multiples séances de travail, des explications claires et nombreuses, et son enthousiasme, sans lesquels le chapitre modélisation de cette thèse n'aurait été qu'un pâle reflet de ce qui est présenté ici.

Je souhaite également remercier Isabelle Charpentier pour m'avoir initié aux arcanes de la différentiation automatique et à ses formidables applications, ainsi que pour sa disponibilité, sa patience et son perfectionnisme, grâces auxquels des développements considérables ont pu être apportés à ce travail.

Je remercie à nouveau Matthieu Dufresne pour l'aide et les conseils qu'ils ma prodigués et qui, tout au long de cette thèse, m'ont permis d'aborder et de progresser énormément dans l'application de la CFD à la sédimentation des boues activées.

Je souhaite exprimer ma gratitude à José Vazquez, qui a favorisé et encouragé activement le développement de ce travail de recherche.

Je voudrais également remercier Jean-Charles Jehl, qui a soutenu ce projet dès les premiers instants et m'a procuré des données cruciales.

Bien sûr, de nombreuses personnes ont contribué à ce travail, de diffé-

rentes façons. J'ai maintenant le plaisir de leur adresser mes remerciements. Merci à Fabrice Lawniczak, Abdelkrim Azizi et Johary Rasamimanana, qui ont construit le pilote sur lequel repose l'essentiel de la partie expérimentale de cette thèse. Merci à Adrien Wanko, qui m'a grandement aidé au cours de cette thèse et beaucoup apporté durant toute ma présence au sein du laboratoire. Merci à Elena Torfs, avec qui j'ai eu le privilège et l'immense plaisir de travailler, et grâce à qui j'ai beaucoup appris. Merci à Joseph Ehrhardt, grâce à qui j'ai pu réaliser tous les prélèvements nécessaires à l'étude expérimentale à la station de traitement de Rosheim, et qui m'y a toujours accueilli avec la plus grande sympathie. Merci à Marie-Pierre Ottermatte, qui a participé à un grand nombre d'analyses expérimentales au cours de ce travail, en a, heureusement, supervisé une bonne partie, et a grandement amélioré mes compétences dans ce domaine. Merci à Marcelline Hartz pour sa formidable gentillesse et les innombrables services qu'elle m'a rendus pendant cette thèse. Merci à Thierry Schaetzle, qui est toujours parvenu à trouver les articles dont j'avais besoin, et ce avec une admirable promptitude. Merci à Simon Schatz, dont les lumières mathématiques m'ont été d'un grand secours. Merci à Olivier et Cécile Rolland, qui m'ont soutenu lors de l'ultime phase de rédaction de ce manuscrit, et pour leur aide inestimable lors de la relecture et de l'impression de celui-ci. Merci à mes collègues et amis « jeunes chercheurs », qui ont contribué à faire de cette thèse une belle expérience. Merci à ma famille, sur le soutien et les encouragements de laquelle j'ai toujours pu compter. Enfin, merci à Louise, pour tant de raisons qu'il faudrait une deuxième thèse pour les écrire.

Résumé

Introduction

Afin d'optimiser la gestion des stations de traitement des eaux usées à boues activées, il est nécessaire de disposer d'outils performants, tels que des modèles numériques. La conception et l'amélioration de ces modèles nécessite une investigation expérimentale détaillée des processus simulés. Dans le cas des décanteurs secondaires, où l'eau traitée est séparée des particules de boues (flocs), cette investigation expérimentale est délicate, et la démarche de développement des modèles est souvent en butte à un manque de données adaptées (c'est-à-dire suffisamment précises et nombreuses). Dans le cadre de cette thèse, un processus expérimental est donc élaboré afin d'obtenir des données permettant de mieux comprendre le comportement des boues activées sédimentant en système fermé et de tester et développer des modèles numériques. Un modèle de sédimentation est élaboré à partir d'une méthode validée dans la littérature et intégrant des fonctions expérimentales. Une méthodologie est ensuite proposée pour analyser la sensibilité du modèle aux paramètres des fonctions utilisées et identifier les valeurs de ces paramètres à partir des données expérimentales. En premier lieu, une revue de la bibliographie permet de faire l'état de l'art sur la modélisation et l'étude expérimentale de la sédimentation des boues activées.

1 Etat de l'art sur la modélisation et l'étude expérimentale des boues activées

1.1 Modélisation

Le choix du modèle utilisé pour simuler la décantation secondaire doit être principalement orienté par les objectifs de la modélisation (Dochain et Vanrolleghem, 2001), bien que la puissance de calcul disponible puisse être un facteur limitant. Les modèles les plus simples, à zéro dimension (0D) décrivent le fonctionnement des ouvrages par des fonctions de transfert. Les modèles les plus détaillés, 2D ou 3D, font appel à la mécanique des fluides numérique (CFD, de l'Anglais « Computational Fluid Dynamics ») et permettent de modéliser les écoulements au sein des ouvrages. Les modèles 1D fournissent un compromis entre temps de calcul et finesse des détails. Dans le cadre de la modélisation des décanteurs secondaires, dont le fonctionnement concerne principalement la dimension verticale (surverse, recirculation et sédimentation), ces modèles sont adaptés à la simulation des principaux phénomènes.

Quel que soit le nombre de dimensions du modèle, les équations employées peuvent être établies par le biais de deux approches principales. L'approche

mécaniste consiste à dériver les équations de l'application des lois fondamentales de la physique, de la chimie et de la biologie. Bien que rigoureuse, cette approche peut conduire à des équations dont certains paramètres ne sont pas accessibles à la mesure. La seconde approche, dite *phénoménologique*, consiste à déterminer les relations mathématiques les plus adaptées à la représentation des données expérimentales. L'absence de recours aux lois fondamentales réduit la fiabilité d'un modèle entièrement phénoménologique. Néanmoins, cette approche permet d'obtenir des relations substituables aux équations faisant appel à des paramètres non mesurables au sein de modèles mécanistes.

Modèles 0D Les modèles 0D permettent de calculer la concentration au fond des décanteurs en fonction des conditions de fonctionnement (Roche et al., 1995; Giokas et al., 2002). Les ouvrages sont modélisés soit par une seule fonction de transfert regroupant les différents phénomènes (clarification, sédimentation, épaississement), soit par une association de plusieurs fonctions afin de raffiner la représentation de chaque phénomène. Dans tous les cas, les fonctions utilisées sont empiriques. Une association de fonctions, bien que plus réaliste du point de vue du fonctionnement des ouvrages, s'accompagne d'une augmentation du nombre des paramètres phénoménologiques et de l'incertitude du modèle. Les modèles 0D sont donc plutôt adaptés à la construction d'outils empiriques rapides applicables à des dimensionnements et calculs de flux généraux qu'à une compréhension détaillée des phénomènes.

Modèles 1D L'approche 1D stratifiée de Takács et al. (1991) est utilisée dans de nombreux modèles. Elle consiste à discrétiser le décanteur en un nombre variable de couches (généralement 10) contenant chacune une concentration homogène. Les flux de matière entre chaque couche sont calculés à l'aide d'une fonction phénoménologique de vitesse de sédimentation à double exponentielle. Bien que le calibrage de cette fonction soit relativement aisé, la méthode numérique de Takács manque de fiabilité (Bürger et al., 2012) : le modèle ne converge pas vers une solution stable lorsque les paramètres de discrétisation tendent vers 0. Cette approche a donc des capacités prédictives limitées.

L'application d'une approche 1D mécaniste (Bürger, 2000) conduit à l'équation

$$\frac{\partial C}{\partial t} + \frac{\partial f_{\mathrm{bk}}(C)}{\partial z} = \frac{\partial}{\partial z}\left(d_{\mathrm{comp}}(C)\,\frac{\partial C}{\partial z}\right), \tag{1}$$

où t est le temps (s), z est la hauteur dans l'ouvrage (m), C est la concentration en boues ($\mathrm{kg{\cdot}m^{-3}}$), f_{bk} est la fonction de sédimentation de Kynch

($\mathrm{kg{\cdot}m^{-2}{\cdot}s^{-1}}$) et d_{comp} est la fonction de compression,

$$d_{\mathrm{comp}}(C) = \begin{cases} 0, & \text{si } 0 \leq C < C_{\mathrm{c}}, \\ \dfrac{\rho_{\mathrm{s}}}{\Delta\rho g C} f_{\mathrm{bk}}(C)\, \sigma'_{\mathrm{e}}(C), & \text{si } C \geq C_{\mathrm{c}}, \end{cases} \tag{2}$$

où ρ_{s} est la masse volumique de la boue ($\mathrm{kg{\cdot}m^{-3}}$), $\Delta\rho$ est l'écart entre les masses volumiques de la boue et de l'eau ($\mathrm{kg{\cdot}m^{-3}}$), g est l'accélération gravitationnelle ($\mathrm{m{\cdot}s^{-2}}$) et σ_{e} est la contrainte solide effective (Pa). Les expressions mécanistes de f_{bk} et σ_{e} contenant des paramètres physiques non mesurables, elles sont remplacées par des expressions phénoménologiques. On considère le plus souvent que $f_{\mathrm{bk}} = C v_{\mathrm{hs}}$, où v_{hs} est une fonction phénoménologique de vitesse de sédimentation de zone. La sédimentation de zone correspond à la phase au cours de laquelle la boue est suffisamment concentrée pour que les interactions entre flocs limitent leur vitesse de sédimentation, et suffisamment diluée pour que le contact entre particules ne soit pas permanent.

Modèles CFD Ces modèles peuvent représenter la suspension de boues activées comme le transport d'une phase secondaire particulaire, la boue, par une phase primaire, l'eau (Lakehal, 1999), ou bien comme un mélange de deux phases qui interagissent selon l'approche Euler–Euler (Brennan, 2001). Dans le premier cas, le mouvement de l'eau est calculé par les équations de Navier–Stokes, et celui de la boue par une équation d'advection–dispersion. Dans le second cas, le mouvement de chaque phase est calculé à l'aide des équations de Navier–Stokes en tenant compte d'un terme d'interaction entre les phases. Dans les deux cas, il peut être nécessaire de calculer une ou plusieurs viscosités (celle de l'eau, de la boue, ou du mélange eau + boue), la vitesse de sédimentation ou la contrainte solide effective. Des modèles rhéologiques et fonctions phénoménologiques sont alors mis en œuvre.

Fonctions phénoménologiques Outre la fonction de Takács, d'autres fonctions fréquemment utilisées calculent la vitesse de sédimentation de zone v_{hs} par le biais de fonctions simples, de type exponentielle (Vesilind, 1968) ou puissance (Cole, 1968). La fonction de Vesilind est l'une des plus fréquemment utilisées :

$$v_{\mathrm{hs}}(C) = v_0 e^{-r_{\mathrm{V}} C}, \tag{3}$$

où C est la concentration de la boue ($\mathrm{kg{\cdot}m^{-3}}$), v_0 est la vitesse de sédimentation maximale théorique ($\mathrm{m{\cdot}s^{-1}}$) et r_{V} est un paramètre ($\mathrm{kg^{-1}{\cdot}m^3}$). D'autres fonctions plus complexes ont été développées, e.g. by Kinnear (2002). Elles font intervenir un plus grand nombre de propriétés fondamentales, telles que la porosité du voile de boue, mais leur calibrage est plus complexe.

La contrainte solide effective σ_e peut être modélisée par la fonction de De Clercq et al. (2008),

$$\sigma_e = \begin{cases} 0, & \text{si } 0 \leq C < C_c, \\ \alpha \ln\left(1 + \dfrac{C - C_c}{\beta}\right), & \text{si } C \geq C_c, \end{cases} \tag{4}$$

où C_c est la concentration critique au-delà de laquelle le contact entre particules est permanent, c'est-à-dire en compression, et $(\alpha\,;\,\beta)$ est un couple de paramètres (Pa et kg·m^{-3} respectivement).

1.2 La rhéologie des boues activées

Aux concentrations de fonctionnement des ouvrages, les boues activées ont un comportement non-Newtonien (Seyssiecq et al., 2003). La plupart des auteurs relèvent l'existence d'une contrainte seuil τ_s, son absence étant fréquemment attribuée à des glissements à l'intérieur de la cellule de mesure du rhéomètre. Les boues ont généralement un comportement rhéofluidifiant jusqu'à un certain taux de cisaillement, au-delà duquel la viscosité μ devient quasi-constante, sauf en cas d'instabilités de Taylor ou de turbulence. Le foisonnement filamenteux peut produire de la thixotropie (Tixier, 2003). Le modèle de Cross (1965) associé à une contrainte seuil peut permettre de prendre en compte les différentes caractéristiques du comportement des boues saines (rhéofluidification et viscosité quasi-constante au-delà d'un certain taux de cisaillement) :

$$\mu = \frac{\mu_0 - \mu_\infty}{1 + (k\dot{\gamma})^n} + \mu_\infty, \tag{5}$$

où μ_0 (Pa·s) est la viscosité limite lorsque le taux de cisaillement $\dot{\gamma}$ (s^{-1}) tend vers 0, μ_∞ (Pa·s) est la viscosité limite lorsque le taux de cisaillement $\dot{\gamma}$ tend vers $+\infty$, k est la consistance (s) et n est l'indice d'écoulement.

1.3 Méthodes expérimentales

1.3.1 Rhéologie

Les rhéomètres rotationnels cylindriques sont fréquemment employés. Toutefois, en cas d'entrefer trop large, la boue risque de sédimenter au cours de la mesure et, en cas d'entrefer trop étroit, les particules de taille importante peuvent être à l'origine de frottements solides (Seyssiecq et al., 2003). Des géométries de mesure de type cône-plan sont souvent utilisées. Le risque de sédimentation est ainsi écarté, mais l'étroitesse de l'entrefer à l'apex de la géométrie de mesure augmente le risque de frottements solides. Une géométrie de mesure de type plan-plan permet d'éviter la sédimentation et réduire

le risque de frottements, mais nécessite de corriger les données obtenues. C'est ce type de géométrie qui est mis en œuvre dans cette étude, et une méthode d'ajustement des résultats est proposée.

1.3.2 Sédimentation

Une étude précise du comportement interne des boues activées au cours de leur sédimentation requiert une méthode de mesure non-invasive de façon à limiter la perturbation du processus. L'application de méthodes optiques est délicate du fait des propriétés des liqueurs mixtes (Vanrolleghem et Lee, 2003; De Clercq, 2003). De Clercq et al. (2005) ont mesuré avec une grande précision des profils de concentration complets au cours de tests de sédimentation ex situ à l'aide d'un traceur radioactif. Néanmoins, l'application de cette technique à des ouvrages réels est difficile du fait de la complexité du matériel nécessaire. Dans le cadre de la présente étude, la méthode de mesure de profil vélocimétrique par effet Doppler (UVP, de l'Anglais « Ultrasonic Velocity Profile »), présentée par Takeda (1995), a donc été appliquée. Cette méthode permet en effet de mesurer des profils de vitesse complets au sein d'ouvrages et au cours d'expériences ex situ (De Clercq, 2003).

2 Etude expérimentale des boues activées

Une procédure d'étude expérimentale de la rhéologie et de la sédimentation libre des boues activées a été développée afin d'apporter des interprétations et des relations applicables au développement de la modélisation de la décantation secondaire. Les échantillons de boues utilisés ont été prélevés à la station de traitement des eaux usées du syndicat du Rosenmeer (Rosheim, Bas-Rhin). Différentes concentrations ont pu être obtenues en prélevant soit dans le réacteur biologique, soit dans le canal de recirculation, en concentrant la boue en laboratoire, ou en la diluant par ajout d'eau de sortie de la station.

2.1 Rhéologie

Un rhéomètre équipée d'une géométrie de mesure de type plan-plan a été utilisé. La procédure de mesure rhéologique mise en œuvre a permis de mesurer la contrainte seuil τ_s pour des boues activées de différentes concentrations. Les paramètres du modèle de Cross (μ_0 ; μ_∞ ; k ; n) ont également été déterminés. Les valeurs des paramètres μ_0 et μ_∞ ont pu être mesurées à partir des viscosités aux faibles et forts taux de cisaillement respectivement. La détermination des paramètres k et n nécessite de corriger les données (car le logiciel de pilotage du rhéomètre calcule la contrainte de cisaillement subie par le fluide, nécessaire pour calculer la viscosité, selon l'hypothèse que le

fluide cisaillé est Newtonien) et de mettre en place une procédure d'identification de paramètres. Pour ce faire, une méthode d'identification classique utilisant l'algorithme BFGS (Byrd et al., 1995) a ensuite été appliqué afin de déterminer le couple de paramètres k et n optimal minimisant une fonction objectif quadratique. Dans ce cadre, le logiciel de différentiation automatique Tapenade (Hascoët et Pascual, 2004) a été utilisé afin de déterminer le modèle linéaire tangent et l'état adjoint utilisé pour le calcul du gradient de la fonction objectif. Des relations ont pu être établies afin de lier les différents paramètres à la concentration de la boue :

$$\tau_{\mathrm{s}} = 4{,}20 \cdot 10^{-3} e^{0{,}324C}, \tag{6}$$

$$\mu_0\left(C\right) = 8{,}40 \cdot 10^{-4}\left(e^{0{,}386C} - 1\right) + \mu_{\mathrm{e}}, \tag{7}$$

$$\mu_\infty\left(C\right) = 5{,}0 \cdot 10^{-4} C + \mu_{\mathrm{e}}, \tag{8}$$

$$k = 6{,}61 \cdot 10^{-4} e^{0{,}546C}, \tag{9}$$

$$n = 6{,}80 C^{-0{,}868}, \tag{10}$$

où μ_{e} est la viscosité de l'eau (Pa·s).

Les relations obtenues permettent de modéliser le comportement rhéologique des boues activées sur des plages de concentrations et taux de cisaillement correspondant au fonctionnement des décanteurs secondaires.

2.2 Sédimentation en système fermé

Un pilote expérimental a été conçu afin d'étudier le processus de sédimentation et de compression des boues activées. Ce pilote se compose principalement d'une colonne de sédimentation équipée d'un transducteur ultrasonore. Ce capteur permet de détecter l'interface entre le voile de boues et le surnageant. Il est ainsi possible de tracer des courbes de sédimentation. En outre, par application de la méthode UVP, le profil de vitesse de sédimentation de la suspension peut être mesuré.

2.2.1 Effet de la concentration

Selon la théorie de Kynch (1952), la vitesse de sédimentation dépend principalement de la concentration de la suspension, une augmentation de la concentration s'accompagnant généralement d'une diminution de la vitesse. L'effet de la concentration a pu être étudié à l'aide des courbes de sédimentation. Celles-ci montrent clairement l'existence d'une concentration critique au-delà de laquelle la période de sédimentation de zone disparaît car les flocs sont en contact permanent dès le début de la sédimentation. Les profils de vitesse mettent également en évidence différents comportements bien distincts. La figure 1 montre des profils de vitesse de sédimentation obtenus

avec différentes boues après 10 min de décantation. Ces résultats permettent de distinguer la région de sédimentation de zone (fluctuations dans la partie supérieure des profils) et la région de compression (partie inférieure stable des profils). Les fluctuations de la sédimentation de zone n'ont pas un caractère aléatoire et peuvent être associées à des migrations de groupes de flocs de propriétés différentes, en particulier en termes de granulométrie (Torfs et al., 2015).

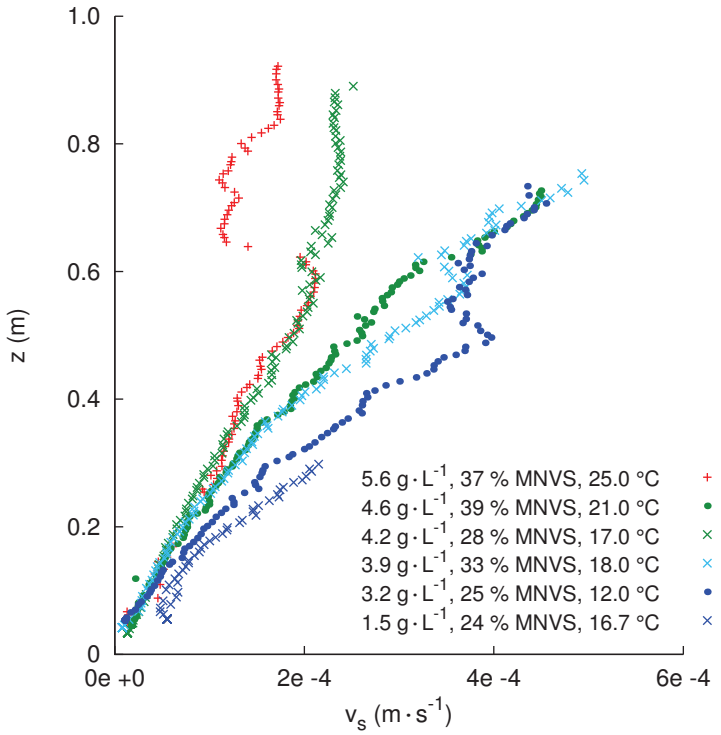

FIGURE 1 – Profils de vitesse de sédimentation obtenus après 10 min de sédimentation avec différentes boues.

Les résultats obtenus indiquent que la concentration n'est pas le seul paramètre influençant la vitesse de sédimentation. La figure 1 montre que la teneur en Matières Non-Volatiles en Suspension (MNVS) des boues est variable. Ceci peut se traduire par des différences de densité et avoir un impact sur la vitesse de sédimentation. La température est également un paramètre extrêmement fluctuant au sein d'ouvrages réels et a un impact sur la viscosité des suspensions. L'influence de ces deux paramètres a donc été investiguée plus en détail.

2.2.2 Effet de la teneur en MNVS

La proportion en MNVS des échantillons de boues a été artificiellement modifiée par ajout de lœss. Il apparaît que, bien que l'ajout de loess entraîne une augmentation de la concentration de la boue, il s'accompagne d'une augmentation de la vitesse de sédimentation et d'une diminution de la hauteur du voile de boue à un instant donné par rapport à une boue brute. La diminution de la hauteur du voile de boue indique que l'augmentation de la fraction en MNVS par ajout de lœss accroît la compressibilité de la boue. Les résultats montrent que la modification de la fraction en MNVS a un impact important sur la vitesse de sédimentation pendant la sédimentation de zone. La vitesse de sédimentation au cours de la compression est, en revanche, peu modifiée. Une relation linéaire a pu être établie entre le pourcentage d'augmentation de la vitesse de sédimentation de zone $\Delta v_{\mathrm{hs}}^{\%}$ et le pourcentage de lœss ajouté à la concentration initiale de la boue brute $\Delta C_{\mathrm{l}}^{\%}$:

$$\Delta v_{\mathrm{hs}}^{\%} = 0{,}8101 \Delta C_{\mathrm{l}}^{\%}. \tag{11}$$

Des mesures pycnométriques ont été effectuées, permettant d'établir une relation affine entre la densité d_{b} d'une boue de densité initiale $d_{\mathrm{b},0} = 1,01$ et le pourcentage de lœss ajouté à la concentration initiale de la boue brute $\Delta C_{\mathrm{l}}^{\%}$:

$$d_{\mathrm{b}} = 7{,}84 \cdot 10^{-4} \Delta C_{\mathrm{l}}^{\%} + d_{\mathrm{b},0}. \tag{12}$$

Ces deux relations montrent que l'augmentation de la densité de la boue par ajout de lœss est faible par rapport à celle de la vitesse de sédimentation.

2.2.3 Effet de la température

Une petite colonne de sédimentation équipée d'un manchon thermique a été mise en œuvre de façon à contrôler plus facilement la température de la suspension. Des tests de sédimentation ont été effectués avec différentes boues. La courbe de sédimentation de chaque échantillon a été réalisée à différentes températures. Les résultats obtenus montrent que l'augmentation de la température entraîne une diminution de la hauteur du voile de boue. Ceci peut s'expliquer par le fait que la diminution de viscosité de l'eau associée à l'accroîssement de température permet aux flocs de mieux sédimenter. En compression, l'eau peut également mieux circuler à l'intérieur du lit de boues. D'autre part, comme les flocs contiennent une importante proportion d'eau, ils sont mieux à même de se déformer au cours de la compression lorsque la température augmente et que la viscosité de l'eau diminue.

2.2.4 Comportement à long terme

L'étude des contours de vitesse de sédimentation au cours des premières heures d'expérience fait apparaître un comportement linéaire des lignes isovitesses. La figure 2 montre les contours de vitesse de sédimentation obtenus

durant 2 heures de sédimentation avec une boue de concentration initiale 3,9 g·L^{-1}. La quasi-linéarité des lignes isovitesses (limites entre les niveaux de la carte colorimétrique) y apparaît clairement. Ceci a permis d'établir une relation entre la vitesse de sédimentation v_s (m·s^{-1}), la hauteur z (m) et le temps de sédimentation t (s) :

$$v_s = \frac{z}{\lambda t}, \tag{13}$$

où λ est un paramètre. Celui-ci a été évalué pour plusieurs boues différentes. Il s'est avéré que λ varie peu en fonction de la concentration initiale de la boue et du temps. La valeur de λ obtenue est 3,40 $\pm$ 0,49. Les résultats expérimentaux ont montré que la relation (13) est applicable au cours de la compression jusqu'à 2 ou 3 heures de sédimentation. Cette relation montre qu'à un instant t donné, la vitesse de sédimentation est une fonction linéaire de la hauteur et ne dépend pas de la concentration initiale de la boue. En revanche, l'ajout de lœss tend à augmenter la valeur de λ.

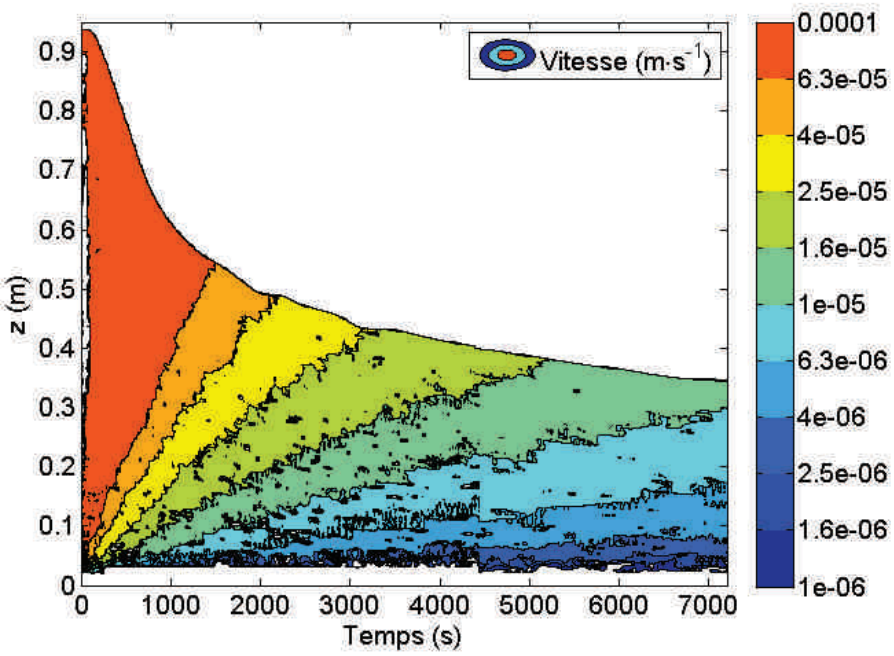

FIGURE 2 – Contours de vitesse de sédimentation obtenus durant 2 heures de sédimentation avec une boue de concentration initiale 3,9 g·L^{-1}.

Au-delà de 2 à 3 heures de sédimentation, les résultats expérimentaux montrent que le gradient de vitesse de sédimentation tend à disparaître dans la partie supérieure du voile, sur une hauteur de quelques centimètres. Dans cette région du voile de boue, la contrainte subie par les flocs est inférieure à la contrainte solide effective σ_e (cf. section 1.1).

Les données de vitesse de sédimentation ont permis d'obtenir les valeurs de concentration par discrétisation de l'équation de conservation de la concentration. La figure 3 montre les contours de concentration obtenus durant 22 h de sédimentation avec une boue de concentration initiale 3.9 g·L^{-1}. Les résultats obtenus montrent que la concentration demeure relativement

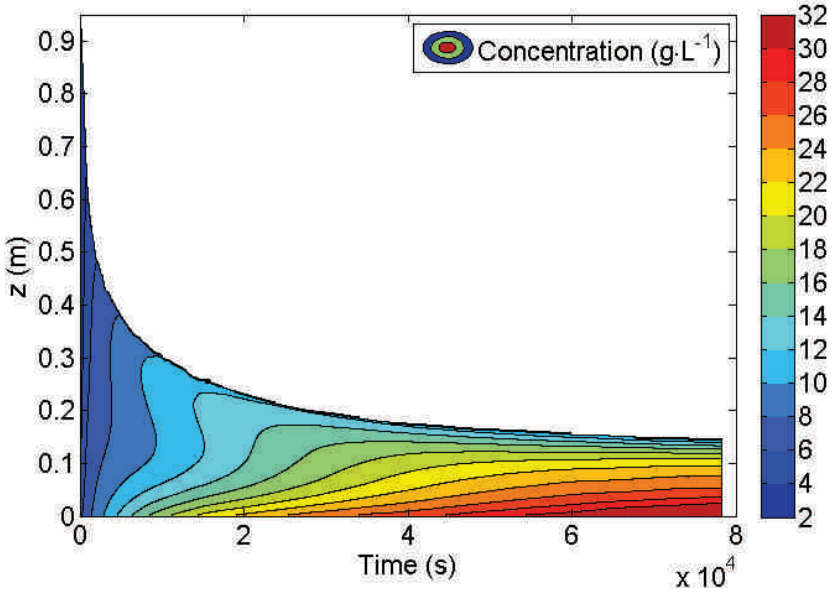

FIGURE 3 – Contours de concentration obtenus durant 22 h de sédimentation avec une boue de concentration initiale 3.9 g·L^{-1}.

homogène à l'intérieur du voile de boue durant 1 à 2 heures de sédimentation. De plus, suivant l'hypothèse de De Clercq et al. (2008) selon laquelle la concentration critique C_c est celle mesurable juste sous l'interface du voile de boue, les profils de concentration obtenus ont permis de montrer que la variation temporelle de C_c peut être exprimée par la relation

$$\frac{dC_c}{dt} = b\left(\frac{1}{C_c^2} - \frac{1}{C_m^2}\right), \tag{14}$$

où b est un paramètre et C_m est la concentration critique maximale. En effet, il est apparu que la concentration critique tend vers une valeur maximale proche de 12 g·L^{-1} pour la plupart des boues brutes testées. La valeur de C_m augmente lorsque la boue est additionnée de lœss. La relation (14) est facilement paramétrable sur la base de résultats expérimentaux (C_c est déterminable asymptotiquement, de sorte que b possède une unique valeur optimale) et fournit une fonction utilisable au sein de modèles de sédimentation.

En partant de l'hypothèse que la concentration demeure homogène à

l'intérieur du voile de boue durant les première heures de sédimentation (hypothèse fondée sur les résultats expérimentaux), l'équation de conservation de la concentration et la relation (13) permettent d'obtenir une relation décrivant l'évolution de la hauteur du voile de boue au cours du temps,

$$h(t) = h_0 \left(\frac{t}{t_0} \right)^{-\frac{1}{\lambda}}, \tag{15}$$

où h_0 est la hauteur du voile de boue à l'instant t_0. Cette relation a pu être vérifiée à l'aide des courbes de sédimentation expérimentales, en prenant pour valeur de t_0 celle du temps auquel la phase de sédimentation de zone prend fin. La relation (15) montre que la hauteur de l'interface entre le voile de boue et le surnageant suit une loi simple de type puissance. Elle permet de prédire la position de cet interface durant 2 à 3 heures de sédimentation. Pour des temps de sédimentation plus longs, la relation (15) tend à surestimer la hauteur de l'interface. Ceci peut être expliqué par l'expulsion de l'eau contenue par les flocs lorsque la contrainte qu'ils subissent dépasse la contrainte solide effective σ_e, ce dépassement se produisant dans une portion de plus en plus importante du voile de boue au fur et à mesure de la compression.

2.3 Conclusion de l'étude expérimentale

La procédure expérimentale développée a permis d'obtenir des résultats de grande précision et mettre en évidence les différents comportements de la boue activée au cours de sa sédimentation, et ce au cours de temps très longs. Plusieurs relations ont été proposées pour décrire l'évolution temporelle de certains paramètres, en particulier la concentration critique C_c. Ces relations et la précision des résultats sont adaptées à l'identification de paramètres et au développement de modèles de sédimentation. Une méthodologie est proposée à cet effet dans le chapitre 3 de la thèse.

3 Modélisation de la sédimentation des boues activées

Un modèle mécaniste 1D de sédimentation a été élaboré sur la base du modèle de Bürger–Diehl (Bürger et al., 2013), utilisant la fonction (3) de vitesse de sédimentation de Vesilind et la fonction (4) de compression de De Clercq et al. (2008). La fonction expérimentale (14) décrivant l'évolution temporelle de la concentration critique y a été incorporée.

Le chapitre 3 se compose de deux articles. Le premier, correspondant à la section 3.1 de ce résumé, traite de la méthode mise en œuvre pour analyser la sensibilité du modèle aux paramètres des fonctions phénoménologiques

employées. Le second article, correspondant à la section 3.2, présente le processus d'identification des paramètres à partir des données expérimentales et les résultats de simulations y afférents.

3.1 Analyse de sensibilité du modèle de sédimentation

L'analyse de sensibilité des modèles est un outil crucial pour comprendre les relations entre les données et les résultats des simulations. L'analyse de sensibilité du modèle considéré est réalisée par application du logiciel de différentiation automatique Tapenade (Hascoët et Pascual, 2004)

3.1.1 Méthode numérique

L'équation principale du modèle est l'équation (1) (cf. section 1.1). Cette équation peut être considérée comme une équation mixte hyperbolique-parabolique. La stratégie de séparation des opérateurs est donc adoptée afin de décomposer cette équation en un problème de convection (hyperbolique) et un problème de diffusion (parabolique) dont les solutions peuvent être déterminées indépendamment par application de schémas de discrétisation à haute efficacité (Karlsen et Risebro, 1997).

Le problème hyperbolique est résolu par application de la méthode des volumes finis sous la forme proposée par Godunov (1959). Le problème parabolique est résolu par application du schéma aux différences finies classique présenté par Bürger et al. (2000).

3.1.2 Sensibilité du modèle de sédimentation

L'analyse de sensibilité vise à mesurer la réponse d'un modèle $\mathcal{M}$ à un changement de ses paramètres P. Des informations qualitatives et quantitatives peuvent être obtenues à cet effet par le calcul des dérivées du modèle par rapport aux paramètres d'intérêt. Pour ce faire, la différentiation automatique (DA) constitue la méthode la plus générale, précise et commode. Le modèle de sédimentation est différentié en mode linéaire tangent, consistant à considérer les calculs exécutés par le programme comme une succession d'opérations mathématiques élémentaires (additions, multiplications) et à les différentier par application de règles de dérivation classiques. Le code linéaire tangent ainsi obtenu permet de propager une direction de perturbation afin de calculer la sensibilité des variables dépendantes du modèle à cette perturbation.

Le modèle est différentié par rapport aux paramètres v_0 et r_V de la fonction de Vesilind (3) et aux paramètres α et β de la fonction de compression (4) de De Clercq et al. (2008). La fiabilité du code différentié est évaluée par tests de Taylor, c'est-à-dire par comparaison du résultat du code linéaire tangent à celui d'un calcul approché par différence finie de la perturbation

de la solution obtenus avec des valeurs décroissantes de perturbation des paramètres δP.

3.1.3 Analyse de sensibilité

Le modèle de sédimentation permet d'obtenir des profils de concentration. Le code linéaire tangent calcule les valeurs des perturbations de la solution pour des perturbations données des paramètres. La figure 4 montre un profil de concentration calculé par le modèle à 0.25 h de sédimentation avec une boue de concentration initiale 3.9 g·L^{-1} et les profils de sensiblité (perturbations) correspondant à une perturbation de + 10 % des paramètres du modèle. La sensibilité du modèle a été analysée à différents temps de sédimentation et avec deux jeux de paramètres différents. D'une façon générale, augmenter le

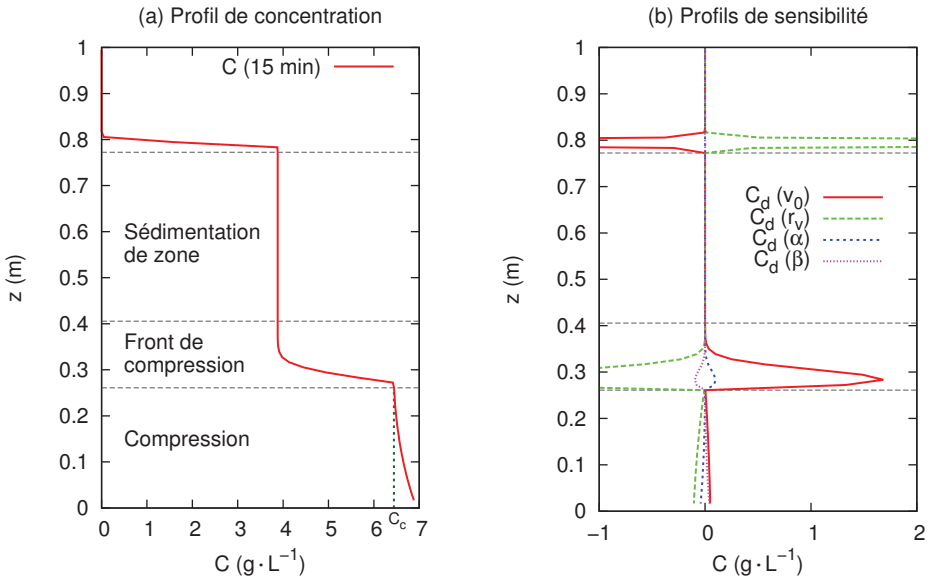

FIGURE 4 – Profil de concentration calculé par le modèle à 0.25 h de sédimentation avec une boue de concentration initiale 3.9 g·L^{-1} (a) et profils de sensiblité C_d correspondant à une perturbation de + 10 % des paramètres du modèle (b).

paramètre v_0 tend à diminuer la hauteur du voile de boue, et augmenter le paramètre r_V tend à l'accroître. D'autre part, augmenter le paramètre α tend à élever la hauteur de la région de compression, et augmenter le paramètre β tend à la réduire. Ceci est cohérent avec les rôles respectifs de ces paramètres au sein des fonctions de vitesse de sédimentation (3) et de compression (4). Comme l'indique la figure 4, les paramètres testés n'ont pas d'influence sur le profil de concentration à l'intérieur de la région de sédimentation de zone. En revanche, les paramètres de la loi de Vesilind ont une importante influence

sur le profil de concentration dans la région de compression. Ceci indique qu'une meilleure séparation des fonctions de vitesse de sédimentation et de compression est nécessaire à l'optimisation des modèles de sédimentation (Torfs et al., 2015).

Les profils de sensibilité des paramètres de la fonction de Vesilind v_0 et r_V sont généralement concaves, et ceux des paramètres de compression α et β sont généralement convexes. Cet aspect des profils peut toutefois évoluer avec le temps : avec le premier jeu de paramètres testé, le profil de sensibilité associé à r_V tend à devenir convexe. D'autre part, l'influence du paramètre v_0 tend à s'amenuiser avec le temps.

3.1.4 Conclusion

L'application de la différentiation automatique à l'analyse de sensibilité du modèle de sédimentation permet de décrire précisément et comprendre l'influence des différents paramètres phénoménologiques sur la solution. La méthodologie employée, utilisant la DA, facilite et accélère le processus d'analyse de sensibilité, tout en supprimant le risque d'erreur lors du calcul des dérivées du modèle par rapport aux paramètres considérés. Les résultats obtenus mettent en évidence des pistes pour l'optimisation des modèles. Par ailleurs, la différentiation du modèle peut être mise en œuvre dans un processus d'identification de paramètres, qui fait l'objet de la section suivante.

3.2 Identification des paramètres

Le jeu de paramètres optimal est celui permettant de modéliser au mieux les données expérimentales. Afin de déterminer ces paramètres, il est nécessaire d'appliquer des algorithmes efficaces pour minimiser l'écart entre les résultats du modèle et les données de référence.

3.2.1 Assimilation de données et différentiation

L'application de la technique d'assimilation variationnelle de données (Le Dimet et Talagrand, 1986) permet de résoudre le problème de minimisation grâce à une méthode de descente de gradient. Les données expérimentales sont injectées dans le processus de modélisation en composant le modèle $\mathcal{M}$ par une fonction objectif $\mathcal{J}$, à savoir une fonction calculant l'écart quadratique entre les résultats du modèle et les données. Les valeurs des paramètres à identifier (v_0 ; r_V ; α ; β) sont regroupées dans un vecteur, noté p. Le jeu optimal de paramètres p_m est celui pour lequel la composée de la fonction objectif et du modèle $\mathcal{J} \circ \mathcal{M}$ est minimale :

$$\min_{p \in \mathbf{P}} \left(\mathcal{J} \circ \mathcal{M}(p) \right) = \mathcal{J} \circ \mathcal{M}(p_\mathrm{m}), \tag{16}$$

où $\mathbf{P}$ est l'ensemble des vecteurs de paramètres admissibles. La solution p_{m} de ce problème peut être calculée en résolvant

$$\nabla(\mathcal{J} \circ \mathcal{M})(p) = 0. \tag{17}$$

La détermination de p_{m} fait donc appel au calcul du gradient de $\mathcal{J} \circ \mathcal{M}$. Pour ce faire, le code initial est tout d'abord différentié en mode linéaire tangent à l'aide du logiciel de différentiation automatique Tapenade. Le code linéaire tangent permet de calculer $\mathcal{J} \circ \mathcal{M}(p)$ ainsi qu'une dérivée directionnelle $\delta j = \nabla(\mathcal{J} \circ \mathcal{M})(p).\delta p$, où δp est une direction de perturbation du vecteur de paramètre p. Ces fonctions peuvent ensuite être utilisées par Tapenade pour différentier le code en mode adjoint. Le code adjoint donne accès au gradient de $\mathcal{J} \circ \mathcal{M}$. La fiabilité des codes différentiés est vérifiée à l'aide de tests de Taylor (cf. section 3.1.2). Afin de déterminer le vecteur p_{m} des paramètres optimaux, le gradient est minimisé à l'aide d'un algorithme de descente de type BFGS.

3.2.2 Résultats d'identification

Deux catégories de valeurs (expérimentales et numériques) ont été utilisées pour identifier les paramètres : les valeurs de hauteur de voile de boue et les profils de concentration. Les données expérimentales à 0.25 h et 0.5 h de sédimentation ont été retenues comme données de référence. En combinant ces données de différentes manières, huit expériences numériques ont pu être réalisées. La figure 5 montre des courbes de sédimentation expérimentale et modélisées correspondant à différentes expériences numériques. Les noms d'expériences indiquent quelles valeurs sont utilisées comme références : la lettre I indique que la hauteur de l'interface entre le voile de boues et le surnageant est utilisée, la lettre P indique que le profil de concentration est utilisé, les chiffres 1 et 2 indiquent respectivement que les données à 0.25 h et 0.5 h sont utilisées.

L'expérience I1P2 (utilisant la position de l'interface à 0.25 h et le profil de concentration à 0.5 h) est celle permettant de reproduire au mieux les données. Le jeu de paramètres optimaux correspondant est $v_0 = 12.0$ m·h^{-1}, $r_{\mathrm{V}} = 0.60$ kg^{-1}·m^3, $\alpha = 4.64$ Pa et $\beta = 3.39$ kg·m^{-3}. Au-delà de 3 h de sédimentation, le modèle tend toutefois à surestimer la hauteur du voile de boues et ne suit pas le comportement de type loi de puissance relevé en section 2.2.4.

3.2.3 Conclusion

La méthode d'identification mise en œuvre permet de calculer le jeu de paramètres optimal pour les fonctions utilisées dans le modèle. Les résultats obtenus montrent que le modèle est à même de bien reproduire les données expérimentales jusqu'à 3 h de sédimentation. La divergence entre le modèle

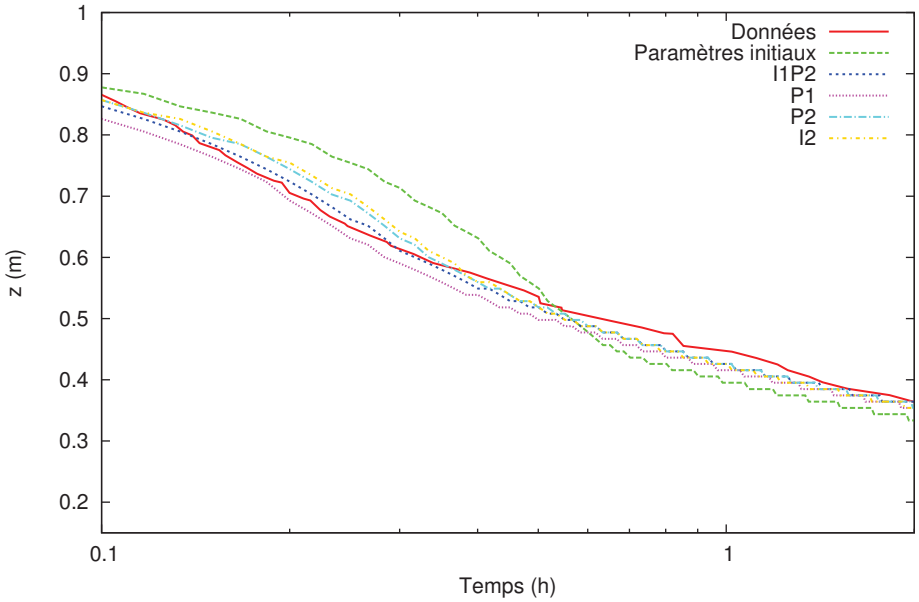

FIGURE 5 – Courbes de sédimentation expérimentale et modélisées correspondant à différentes expériences numériques (temps en échelle logarithmique).

et les données peut être due au fait que les paramètres varient potentiellement en fonction du temps, comme c'est le cas pour la concentration critique C_c, ou bien au fait que la fonction exponentielle de vitesse de sédimentation de Vesilind modélise partiellement le phénomène de compression et altère les résultats de la fonction de contrainte solide effective σ_e de De Clercq et al. (2008) (Torfs et al., 2015).

4 Conclusions et perspectives

L'étude expérimentale réalisée au cours de cette thèse a aboutit à la conception d'un dispositif performant et permis d'obtenir des données précises, adaptées au développement de modèles numériques. Des relations ont pu être proposées pour décrire certains comportements de la boue activée en fonction du temps et d'autres paramètres tels que la fraction en matières non-volatiles en suspension. Un modèle numérique de sédimentation a été réalisé sur la base de la méthode proposée par Bürger et al. (2013) et intégrant une fonction expérimentale pour la concentration critique. L'analyse de sensibilité de ce modèle a été réalisée à l'aide d'une méthode efficace mettant en œuvre la différentiation automatique. Les influences précises de chaque paramètre phénoménologique ont ainsi pu être décrites et comprises. Les paramètres ont ensuite été identifiés à partir des données expérimentales par le

biais d'une méthode numérique utilisant également la DA et un algorithme de descente de gradient. Ceci a permis de déterminer un jeu de paramètre optimal et suggérer des pistes d'optimisation du modèle.

Un processus d'optimisation peut ainsi être élaboré, en appliquant la méthode d'analyse de sensibilité et d'identification développée au cours de cette étude à d'autres fonctions. D'avantage d'expériences peuvent être réalisées à l'aide du pilote conçu afin de préciser l'influence d'autres paramètres de fonctionnement, telles que la température. L'application de la méthode expérimentale à des boues provenant d'autres stations permettrait de préciser l'influence du processus de traitement sur la sédimentation. Les nouveaux éléments ainsi apportés permettrait de développer une approche de modélisation CFD de la colonne de sédimentation expérimentale. Le modèle CFD pourrait intégrer des fonctions phénoménologique testées au sein du modèle 1D, et ainsi permettre de mieux comprendre l'influence de l'hydrodynamique du système sur ces fonctions. A terme, cette approche CFD serait applicable à des ouvrages réels afin d'en optimiser le fonctionnement.

Références

Brennan, D. The numerical simulation of two-phase flows in settling tanks. Thèse de doctorat, université de Londres, Londres, RU.

Bürger, R., 2000. Phenomenological foundation and mathematical theory of sedimentation-consolidation processes. Chem. Eng. J. 80, 177-188.

Bürger, R., Evje, S., Karlsen, K. H., Lie, K. A., 2000. Numerical methods for the simulation of the settling of flocculated suspensions. Chem. Eng. J. 80 (1–3), 91–104.

Bürger, R., Diehl, S., Farås, S., Nopens, I., 2012. On reliable and unreliable numerical methods for the simulation of the secondary settling tanks in wastewater treatment. Comput. Chem. Eng. 41, 93–105.

Bürger, R., Diehl, S., Farås, S., Nopens, I., Torfs, E., 2013. A consistent modelling methodology for secondary settling tanks : A reliable numerical method. Water Sci. Technol. 68 (1), 192–208.

Byrd, R. H., Lu, P., Nocedal, J. et Zhu, C., 1995. A limited memory algorithm for bound constrained optimization. SIAM J. Sci. Comput. 16, 1190–1208.

Cole, R. F., 1968. Experimental evaluation of the Kynch theory. Thèse de doctorat, université de Caroline du Nord, Chapel Hill, États-Unis d'Amérique.

Cross, M. M., 1965. Rheology of non-Newtonian fluids : a new flow equation for pseudoplastic systems. J. Coll. Sci. Imp. U. Tok. 20 (5), 417–437.

De Clercq, B., 2003. Computational fluid dynamics of settling tanks : development of experiments and rheological, settling, and scraper submodels. Thèse de doctorat, université de Gand, Gand, Belgique.

De Clercq, J., Jacobs, F., Kinnear, D. J., Nopens, I., Dierckx, R. A., Defrancq, J., Vanrolleghem, P. A., 2005. Detailed spatio-temporal solids concentration profiling during batch settling of activated sludge using a radiotracer. Water Res. 39, 2125–2135.

De Clercq, J., Nopens, I., Defrancq, J.,Vanrolleghem, P.A., 2008. Extending and calibrating a mechanistic hindered and compression settling model for activated sludge using in-depth batch experiments. Water Res. 42 (3), 781–791.

Dochain, D., Vanrolleghem, P. A., 2001. Dynamical modelling and estimation in wastewater treatment processes. IWA Publishing, Alliance House, 12 Caxton Street, Londres, RU.

Giokas, D. L., Kim, Y., Paraskevas, P.A., Paleologos, E.K., Lekkas, T.D., 2002. A simple empirical model for activated sludge thickening in secondary clarifiers. Water Res. 36 (13), 3245–3252.

Godunov, S. K., 1959. A difference method for numerical calculation of discontinuous solutions of the equations of hydrodynamics. Mat. Sb. 89 (3), 271–306.

Hascoët, L., Pascual, V., 2004. Tapenade 2.1 user's guide.

Karlsen, K. H., Risebro, N. H., 1997. An operator splitting method for nonlinear convection-diffusion equations. Numer. Math. 77 (3), 365–382.

Kinnear, D. J., 2002. Biological solids sedimentation : a model incorporating fundamental settling parameters. Thèse de doctorat, université de l'Utah, Salt Lake City, États-Unis d'Amérique.

Kynch, G. J., 1952. A theory of sedimentation. T. Faraday Soc. 48, 166–176.

Lakehal, D., Krebs, P., Krijgsman, J., Rodi, W., 1999. Computing shear flow and sludge blanket in secondary clarifiers. J. Hydraul. Eng.–ASCE 125 (3), 253–262.

Le Dimet, F.-X., Talagrand, O., 1986. Variational algorithms for analysis and assimilation of meteorological observations : theoretical aspects. Tellus A 38 (2), 97–110.

Roche, N., Vaxelaire, J., Prost, C., 1995. A simple empirical model for hindered settling in activated sludge clarifier. Water Environ. Res. 67(5), 775–780.

Seyssiecq, I., Ferrasse, J. H., Roche, N., 2003. State-of-the-art : rheological characterisation of wastewater treatment sludge. Biochem. Eng. J. 16 (1), 41–56.

Takács, I., Patry, G. G., Nolasco, D., 1991. A dynamic model of the clarification-thickening process. Water Res. 25 (10), 1263–1271.

Takeda, Y., 1995. Velocity profile measurement by ultrasonic Doppler method. Exp. Therm. Fluid Sci. 10, 444–453.

Tixier, N., 2003. Approche des propriétés rhéologiques de suspensions biologiques floculées. Thèse de doctorat, université de Limoges, Limoges, France.

Torfs, E., Locatelli, F., Balemans, S., Diehl, S., Bürger, R., François, P., Laurent, J.and Nopens, I., 2015. Impact of the flocculation state on hindered and compression settling : experimental evidence and overview of available modelling frameworks. Actes de la conférence « 9th IWA symposium on systems analysis and integrated assessment » (Watermatex 2015), Gold Coast, Australie, 14–17 Juin 2015.

Torfs, E., Balemans, S., Locatelli, F., Bürger, R., Laurent, J., François, P., Diehl, S., Nopens, I., 2015. Critical analysis of constitutive functions for hindered settling velocity in 1–D settler models. Actes de la conférence « 9th IWA symposium on systems analysis and integrated assessment » (Watermatex 2015), Gold Coast, Australie, 14–17 Juin 2015.

Vanrolleghem, P. A., Lee, D. S., 2003. On-line monitoring equipment for wastewater treatment processes : state of the art. Water Sci. Technol. 47 (2), 1–34.

Vesilind, P. A. 1968. Discussion of "Evaluation of activated sludge thickening theories" by Dick R. I. and Ewing B. B.. J. San. Eng. Div. ASCE 94 (SA1).

Summary

In order to optimise the design and operation of activated sludge wastewater treatment plants, powerful tools, such as numerical models, are required. A thorough experimental investigation of the simulated phenomena is key to the development and improvement of these models. It is however delicate in the case of secondary clarifiers, where treated water and sludge particles are separated, and the process of model development is thus often impaired by a lack of precise enough data. During this Ph.D., an experimental setup combining a settling column and an ultrasonic transducer was designed. It was used to measure detailed settling velocity and concentration profiles, which allowed understanding the mechanisms of sedimentation and compression of activated sludge better. These results have been applied to the development of a numerical approach. A settling model using a well-known approach and completed with experimental functions was built. A methodology based on the automatic differentiation of the model was developed. It was used, on the one hand, to analyse the sensitivity of the results to the model parameters and, on the other hand, to identify the parameter values on the basis of experimental data. The combination of the proposed experimental and numerical methods yields an efficient process for the development of sedimentation models.

Publications internationales

Locatelli, F., François, P., Laurent, J., Lawniczak, F., Dufresne, M., Vazquez, J., Bekkour, K. (2015). Detailed velocity and concentration profiles measurement during activated sludge batch settling using an ultrasonic transducer. Separation Science and Technology, 50(7), 1059-1065.

François, P., Locatelli, F., Laurent, J., Bekkour, K. Experimental study of activated sludge batch settling velocity profile. Flow Measurement and Instrumentation, Submitted.

Locatelli, F., Laurent, J., François, P., Dufresne, M., Vazquez, J., Bekkour, K. (2013). Impact de la loi de comportement rhéologique sur la sédimentation en batch de boues activées: approche expérimentale et numérique. La Houille Blanche, 4, 31-36.

Actes de conférences

François, P., Locatelli, F., Laurent, J., Bekkour, K. (2014). Experimental study of activated sludge batch settling velocity profile. 9th International Symposium on Ultrasonic Doppler Methods for Fluid Mechanics and Fluid Engineering.

Locatelli, F.,Laurent, J.,François, P., Lawniczak, F., Bekkour, K. (2013). In situ monitoring of activated sludge batch settling using an ultrasonic device. 11th IWA Conference on Instrumentation Control and Automation.

Locatelli, F., François, P., Laurent, J., Lawniczak, F., Bekkour, K. (2013). Etude expérimentale de la sédimentation des boues activées par mesures acoustiques ultrasonores. Récents Progrès en Génie des Procédés – XIVe Congrès de la Société Française de Génie des Procédés.

It is the malpractice of the courts to confine evidence and discussion to the bounds of apparent relevancy. Yet experience has shown, and a true philosophy will always show, that a vast, perhaps the larger, portion of truth arises from the seemingly irrelevant. It is through the spirit of this principle, if not precisely through its letter, that modern science has resolved to *calculate upon the unforeseen.*

—Edgar Allan Poe, *The Mystery of Marie Roget*

Contents

Nomenclature

Abbreviations

0D, 1D, 2D, 3D	Zero-, One-, Two-, Three-Dimensional
AD	Automatic Differentiation
CFD	Computational Fluid Dynamics
CSTR	Completely Stirred Tank Reactor
NVSS	Non-Volatile Suspended Solids [M L^{-3}]
SS	Suspended Solids [M L^{-3}]
TSS	Total Suspended Solids [M L^{-3}]
VSS	Volatile Suspended Solids [M L^{-3}]
WWTP	Wastewater Treatment Plant

Symbols

C	Concentration [M L^{-3}]
C_c	Critical concentration [M L^{-3}]
f_{bk}	Kynch batch flux density function [M L^{-2} T^{-1}]
g	Gravitational acceleration [L T^{-2}]
t	Time [T]
v_{hs}	Hindered settling velocity [L T^{-1}]
v_s	Settling velocity [L T^{-1}]
z	Height [L]

Greek letters

$\dot{\gamma}$	Shear rate [T^{-1}]
μ	Dynamic viscosity [M L^{-1} T^{-1}]
ρ	Density [M L^{-3}]
σ_e	Effective solids stress [M L^{-1} T^{-2}]
τ	Shear stress [M L^{-1} T^{-2}]

Introduction

The field of wastewater treatment processes is in constant need for optimisation. The requirements defined by the European Water Framework Directive in response to environmental issues as well as the increasing pressure of population growth on water resources (Willuweit and O'Sullivan, 2013) call for ever more accurate prediction tools, such as modelling software. Activated sludge process is a widespread method for the treatment of urban wastewater. The diagram of figure 1 shows the general principle of an activated sludge wastewater treatment plant (WWTP) and the connexions between the different steps of the process. The well-balanced development of a diversified bacterial biomass in the biological reactor allows an efficient treatment of pollution. The bacteria consume and degrade the pollution, which results in the formation of particulate aggregates called flocs. After the biological treatment step, the water must be rid of the resulting suspended matter before it can be returned safely to the environment: this is one of the functions of the secondary settling tank. The latter also plays the role of thickener, most of the settled sludge being recycled to the biological reactor in order to maintain a sufficient biomass in the whole system. As a result, the behaviour of the biological reactor and that of the clarifier are strongly connected. Figure 2 shows a schematics of a circular settling tank. Upon entering the structure, activated sludge coming from the biological reactor is deviated downward by the inlet baffle, thus directing the suspended matter toward the bottom of the tank. The supernatant overflows through a weir into a culvert circling the tank. It is then returned to the environment or, if necessary, undergoes tertiary treatment steps. The efficiency of the treatment depends on a precise control of this process.

Engineers have long relied on rules of thumb in order to design secondary clarifiers. These methods, often based on the maximum value of the vertical velocity of water, provide dimensions adapted to most situations. However, in order to enhance WWTP control and design, dynamic tools are necessary. The conditions inside of the settling tank can be influenced by such variables as precipitations, temperature, volatile suspended solids (VSS) to total suspended solids (TSS) ratio, filamentous bulking, etc. As a consequence, changes in the thickening process, effluent concentration or sludge blanket

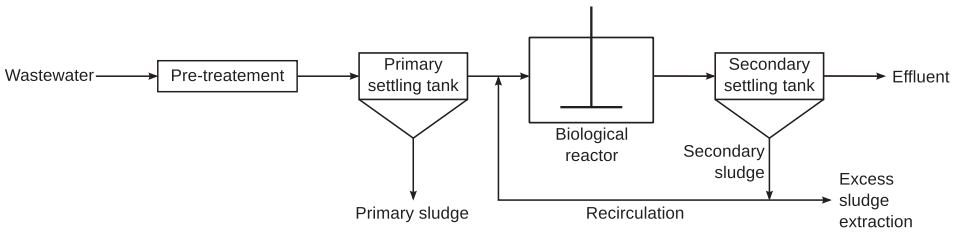

Figure 1 – Schematics of the principle of an activated sludge wastewater treatment plant

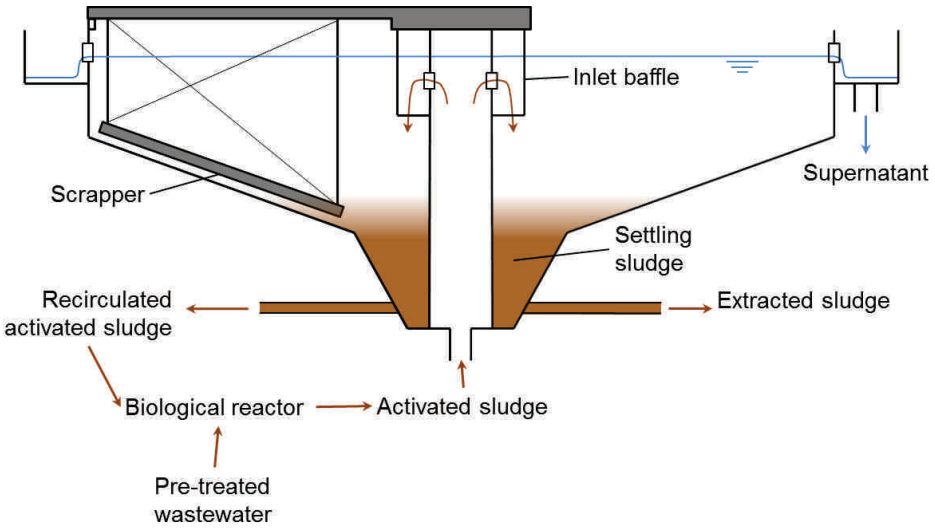

Figure 2 – Schematics of a circular clarifier

height can occur. Models can help understand how the secondary settling process reacts to changes of the operating conditions, as well as provide information to foresee the possible scenarios and develop appropriate response strategies. However, there is a lack data extensive and precise enough to test and develop models that can satisfyingly simulate all the aspects of activated sludge sedimentation. Furthermore, building and enhancing settling models requires implementing quantitative, fast and reproducible analysis processes. The key points on which the present study focuses in order to tackle these issues are:

- the development of an experimental procedure designed to provide data adapted to the enhancement of models,
- the elaboration of a method to study the sensitivity of the model solutions to the parameters of the functions simulated and calibrate these parameters using the experimental data.

In order to orientate the field of investigation, the state of the art is reviewed in chapter 1. The different modelling approaches are considered so as to identify the one best suited to the aims of the present study. Various experimental methods applicable to the study of activated sludge are then examined in order to select an appropriate procedure. In chapter 2, the developed experimental process is presented. The obtained results are then detailed and interpreted. They bring new insight into the internal behaviour of activated sludge suspension during the batch settling process. Additionally, relations linking the settling and rheological properties of the sludge to its characteristics are proposed. Building on these results, chapter 3 presents the model designed to simulate the experiments performed and the sensitivity analysis method applied to this model. This analysis allows describing the specific influences of each parameter. Subsequently, an identification method is applied to the model using the experimental data. The optimal set of parameters can thus be designated. The model thus parametrised can be compared to the data and potential improvements can be suggested.

The following chapter begins by reviewing the different approaches that may be applied to the modelling of activated sludge settling.

CHAPTER 1

Literature review: modelling and experimental study of activated sludge settling and rheology

1.1 Modelling secondary clarifiers

Over the last two decades, a consensus on the study and modelling of the biological treatment process has been well established, leading to the development of the Activated Sludge Models (Henze et al., 2000). The models used to describe the behaviour of the sludge suspensions in the clarifier, however, have not been the subject of such a wide and coordinated effort as yet. The numerical tools used in the field of wastewater treatment have seen the development of integrated plant models, allowing the simulation of entire WWTPs as well as their interactions with their environment (i.e. the sewer system and receiving waters). The different models describing each process taking place in a WWTP are linked together, and thus have to be relatively simple in order to prevent excessive calculation times. Secondary settler models are therefore usually one-dimensional (1D). Many models use phenomenological functions to calculate the fluxes between the layers of the discretised settler, but apply numerical methods which are not derived from the underlying physical equations and associated stability conditions. Hence, though they provide fast tools for the simulation of secondary clarification, they often lack reliability (Bürger et al., 2012). As a result, they do not allow accurately predicting the behaviour of a settler and reduce the efficiency of integrated models. The improvement of clarifier models requires better experimental characterisation coupled with thorough numerical methodologies (Dochain and Vanrolleghem, 2001).

In the field of wastewater treatment, most models rely on Completely Stirred Tank Reactors (CSTRs) or Tank-In-Series approaches to describe the hydrodynamics of the systems. Nevertheless, these simplified approaches

cannot reproduce the complex flow patterns and concentration gradients which exist within biological reactors and alter the biokinetic and physico-chemical parameters calibration process (Le Moullec et al., 2010; Laurent et al., 2014). This is particularly true for secondary settling, which generates strong spatial heterogeneity in terms of suspended solids (SS) concentration. Whereas the spatial dimensions do not appear in the mathematical relations describing systems modelled as completely stirred tanks, they have to be considered in order to account for this heterogeneity in secondary settler models, which increases their complexity. The functions involved are dependent on time as well as space, the influence of which requires the definition of boundary conditions (Dochain and Vanrolleghem, 2001).

Models can be described according to the approach used for their development (Dochain and Vanrolleghem, 2001). Models stemming from the application of physical, chemical or biological principles to the problem at hand are called *mechanistic*. The equations obtained are derived from the fundamental laws governing the phenomena that have been identified in the process to be simulated. One of the main obstacles on the path of mechanistic model building is the use of fundamental parameters that cannot always be measured. Many models are therefore built the other way around, i.e. their developers started by considering the data available or attainable given the experimental methods at hand, then endeavoured to identify the mathematical functions most adapted to fit the data. Such models are called *phenomenological*. They usually involve few parameters and are therefore faster to develop and calibrate than fully mechanistic models. However, their structure does not necessarily match that of the actual behaviour of the modelled system. Their outputs can therefore be questionable when the input values are outside the range with which they were developed and tested. Thus, the numerical method has to be carefully designed and implemented, lest the final model be unreliable (Bürger et al., 2012).

There are different levels of settling tank model complexity. The degree of complexity will of course be partly oriented by the computational power available, but should be mainly dependent on the user's objectives. Model complexity is often associated with the number of space dimensions taken into account. As mentioned in the previous section, modelling the behaviour of an activated sludge suspension inside a settler requires taking the influence of the space variables into account. However, end-users of models such as WWTP managers are often interested principally in the underflow and effluent concentrations. Therefore, simplified models have been developed in order to evaluate specific parameters. The simplest models do not consider any space dependency, thus the variables are functions of time only. Such models are called *lumped parameter models*.

1.1.1 Lumped parameter models

As Dick and Ewing (1967b) point out, settling tanks are usually called either "clarifier" or "thickener" depending on the main objective of the structure. The settling process always leads to a thickening phenomenon. Therefore, a 0D model systematically represents an approximation of an actual clarifier, for at least two distinct regions, one for clarification and one for thickening, have to be considered (which is still a simplification of the actual process, since there is no clear discontinuity between them). One of the main motivations for the development of 0D models is the desire to propose fast, easy to use models. Very often, end-users of clarifier models are indeed primarily interested in obtaining a value of the underflow concentration under different operating conditions for design or control purposes. Several approaches can be used in such models, but the main difficulty associated with their development lies in the model abstraction: The model has to capture enough details to provide realistic results without requiring excessive computational efforts. The final model is generally of convenient use, but requires parameters that have to be either measured or calculated.

Roche et al. (1995) proposed a simple model to calculate the concentration of the recycled sludge. They based their work on the results of twenty-three experiments conducted with different sludge samples. They measured the concentration of an activated sludge suspension at the bottom of a batch settling column at different instant and deduced a relation for the evolution of that concentration with time. They obtained the following relation:

$$C_{\mathrm{r}}(t) = a\,(t + \Delta t)^b\,, \tag{1.1}$$

with

$$\Delta t = 0.086 C_0^{2.234}, \tag{1.2}$$

$$a = 2.065 C_0^{0.382}, \tag{1.3}$$

$$b = 0.545 SVI^{-0.152}, \tag{1.4}$$

where

- C_{r} is the concentration of the recycled sludge ($\mathrm{g{\cdot}L^{-1}}$),
- t is the time (s),
- C_0 is the initial sludge concentration ($\mathrm{g{\cdot}L^{-1}}$),
- SVI is the sludge volume index ($\mathrm{m^3{\cdot}g^{-1}}$).

This empirical model provides an evaluation of the concentration of the sludge at the bottom of a settling tank and takes into account the thickening of the sludge.

Using the work of Roche et al. (1995), Giokas et al. (2002) endeavoured to propose a more detailed model. They considered three regions in the settling tank where the average concentration of the sludge was to be evaluated: 1) the diluted sludge, between the inlet and the sludge blanket; 2) the sludge blanket itself; 3) the bottom of the settler.

This model was calibrated and verified on the basis of field measurements. If this model represents a good compromise in terms of simplicity and precision, it indirectly highlights the necessity of considering different strata in settling tank models in order to increase their precision. In addition, the drawback of such a model as compared to simpler ones (e.g. the model of Roche et al. (1995)) is the increased number of equations and parameters, which increase the difficulty of parameter estimation. This kind of models materialises the limit of precision achievable using lumped models. In this work, efforts will be devoted to the study and description (experimental as well as numerical) of activated sludge compression and rheology. As a consequence, the models involved will have to be at least 1D to be able to provide the required level of detail.

1.1.2 One dimensional models

Since 1D models are able to simulate vertical gradients, they represent a reasonably realistic approach to settling. They have the advantage of running comparatively fast on most computers, and can therefore be associated with models of other processes of the wastewater treatment cycle (Benedetti et al., 2013). In a 1D approach, the settling tank is discretised using a vertical mesh, each cell of which represents a settling tank layer of homogeneous concentration.

The Takács model

In the classical Takács approach (Takács et al., 1991), the fluxes between each layer of the tank model are calculated. Figure 1.3 presents the principle of this approach. Calulating the fluxes requires a value of settling velocity v_s. Different phenomenological functions have been proposed to calculate v_s and will be presented and discussed in section 1.1.4.

Though straightforward, this model has been proven *unreliable*, in the sense that its solution is not stable when the discretisation parameters are refined (Bürger et al., 2012).

The mechanistic approach

The premise of the mechanistic approach to settling is the application of the fundamental equations, i.e. mass conservation (or continuity equation) and momentum conservation. The equations were described in detail by Karl and Wells (1999) and Bürger et al. (2000c), and a summary of the reasoning was

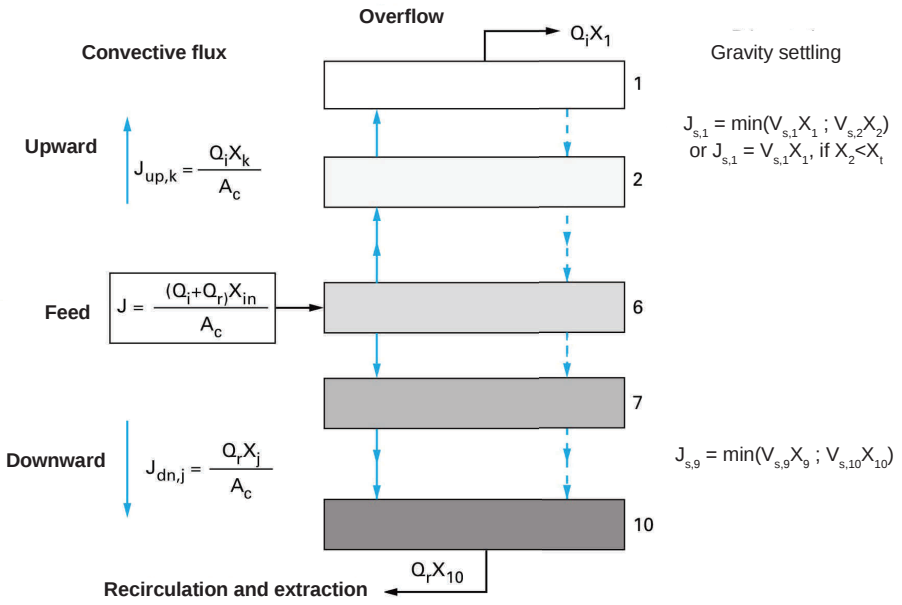

Figure 1.3 – Diagram of the principle of the 1D layered approach (Spérandio et al., 2007).

given by Bürger (2000). The establishment of the equation for the volume fraction of the sludge blanket in compression will now be detailed. Table 1.1 presents the nomenclature of the parameters and variables used in equations (1.5) to (1.23).

The continuity equation for the solids is

$$\frac{\partial \phi}{\partial t} + \frac{\partial \phi v_{\mathrm{s}}}{\partial z} = 0, \tag{1.5}$$

and the continuity equation for water is

$$\frac{\partial \left(1-\phi\right)}{\partial t} + \frac{\partial \left(1-\phi\right) v_{\mathrm{w}}}{\partial z} = 0. \tag{1.6}$$

The momentum conservation equation for solids is

$$\rho_{\mathrm{s}}\phi\left(\frac{\partial v_{\mathrm{s}}}{\partial t} + v_{\mathrm{s}}\frac{\partial v_{\mathrm{s}}}{\partial z}\right) = -\frac{\partial \phi \tilde{p}}{\partial z} - \frac{\partial \sigma_{\mathrm{e}}}{\partial z} + \left(\nabla \cdot \overline{\overline{T_{\mathrm{s}}^{\mathrm{E}}}}\right) \cdot \vec{k} + \rho_{\mathrm{s}}\phi g + \vec{m} \cdot \vec{k}. \tag{1.7}$$

In this equation, the effective solid stress σ_{e} appears. It models the solid-like properties developed by concentrated activated sludge in compression. The momentum conservation equation for water is

$$\rho_{\mathrm{w}}\left(1-\phi\right)\left(\frac{\partial v_{\mathrm{w}}}{\partial t} + v_{\mathrm{w}}\frac{\partial v_{\mathrm{w}}}{\partial z}\right) = -\frac{\partial \left(1-\phi\right)\tilde{p}}{\partial z} + \left(\nabla \cdot \overline{\overline{T_{\mathrm{w}}^{\mathrm{E}}}}\right) \cdot \vec{k} + \rho_{\mathrm{w}}\left(1-\phi\right) g - \vec{m} \cdot \vec{k}. \tag{1.8}$$

Table 1.1 – Nomenclature

C	Solids concentration ($\mathrm{kg{\cdot}m^{-3}}$)
C_c	Critical solids concentration ($\mathrm{kg{\cdot}m^{-3}}$)
f_bk	Kynch batch flux density function ($\mathrm{kg{\cdot}m^{-2}{\cdot}s^{-1}}$)
g	Gravitational acceleration ($\mathrm{m{\cdot}s^{-2}}$)
$\overrightarrow{k}$	Downward-pointing vertical unit vector
$\overrightarrow{m}$	Solid-fluid interaction force per unit volume ($\mathrm{N{\cdot}m^{-3}}$)
$\tilde{p}$	Pore pressure (Pa)
r	Resistance coefficient ($\mathrm{kg{\cdot}m^{-3}{\cdot}s^{-1}}$)
t	Time (s)
$\overline{\overline{T_\mathrm{s}^\mathrm{E}}}$	Solids component viscous stress tensor (Pa)
$\overline{\overline{T_\mathrm{w}^\mathrm{E}}}$	Water component viscous stress tensor (Pa)
v_d	Drift velocity ($\mathrm{m{\cdot}s^{-1}}$)
v_hs	hindered settling velocity function ($\mathrm{m{\cdot}s^{-1}}$)
v_s	Settling velocity ($\mathrm{m{\cdot}s^{-1}}$)
v_w	Water velocity ($\mathrm{m{\cdot}s^{-1}}$)
z	Coordinate along the upward-pointing vertical axis (m)
	Greek letters
γ	Virtual mass ($\mathrm{kg{\cdot}m^{-3}}$)
ϕ	Solids volume fraction (–)
ρ_s	Solids density ($\mathrm{kg{\cdot}m^{-3}}$)
ρ_w	Water density ($\mathrm{kg{\cdot}m^{-3}}$)
σ_e	Effective solids stress (Pa)

In the two previous equations, the vector $\overrightarrow{m}$ describes the interaction force per unit volume existing between the flocs and the water. According to Newton's third law of movement, this vector has the same norm in both equations, but opposite directions. It is expressed as follows:

$$\overrightarrow{m} = \tilde{p}\nabla\phi - r\left(\phi\right)\overrightarrow{v_\mathrm{d}} + \gamma\left(\phi\right)\left(\frac{\partial\overrightarrow{v_\mathrm{d}}}{\partial t} + \left(\overrightarrow{v_\mathrm{d}}\cdot\nabla\right)\overrightarrow{v_\mathrm{d}}\right). \tag{1.9}$$

The local difference between the velocity of water and the velocity of flocs is called the drift velocity:

$$v_\mathrm{d} = v_\mathrm{s} - v_\mathrm{w}. \tag{1.10}$$

Combining equation (1.7) and equation (1.9) leads to

$$\begin{aligned}\frac{\partial\sigma_\mathrm{e}}{\partial z} = &-\phi\frac{\partial\tilde{p}}{\partial z} - r\left(\phi\right)v_\mathrm{d} + \phi\rho_\mathrm{s}g + \left(\nabla\cdot\overline{\overline{T_\mathrm{s}^\mathrm{E}}}\right)\cdot\overrightarrow{k} - \phi\rho_\mathrm{s}\left(\frac{\partial v_\mathrm{s}}{\partial t} + v_\mathrm{s}\frac{\partial v_\mathrm{s}}{\partial z}\right)\\ &+\gamma\left(\phi\right)\left(\frac{\partial v_\mathrm{d}}{\partial t} + v_\mathrm{d}\frac{\partial v_\mathrm{d}}{\partial z}\right),\end{aligned} \tag{1.11}$$

and combining equation (1.8) and equation (1.9) leads to:

$$\frac{\partial \tilde{p}}{\partial z} = \rho_{\mathrm{w}} g - \rho_{\mathrm{w}} \left(\frac{\partial v_{\mathrm{w}}}{\partial t} + v_{\mathrm{w}} \frac{\partial v_{\mathrm{w}}}{\partial z} \right) + \frac{1}{1-\phi} \Bigg[\left(\nabla \cdot \overline{\overline{T_{\mathrm{w}}^{\mathrm{E}}}} \right) \cdot \vec{k} - \gamma(\phi) \left(\frac{\partial v_{\mathrm{d}}}{\partial t} + v_{\mathrm{d}} \frac{\partial v_{\mathrm{d}}}{\partial z} \right) + r(\phi) v_{\mathrm{d}} \Bigg]. \tag{1.12}$$

This gives an expression for the space derivative of the pore pressure, which can be injected in equation (1.11), yielding:

$$\begin{aligned} \frac{\partial \sigma_{\mathrm{e}}}{\partial z} = {} & \frac{-r(\phi)}{1-\phi} v_{\mathrm{d}} + \phi \Delta \rho g + \left[\left(\nabla \cdot \overline{\overline{T_{\mathrm{s}}^{\mathrm{E}}}} \right) - \frac{\phi}{1-\phi} \left(\nabla \cdot \overline{\overline{T_{\mathrm{w}}^{\mathrm{E}}}} \right) \right] \cdot \vec{k} \\ & + \phi \left[\rho_{\mathrm{w}} \left(\frac{\partial v_{\mathrm{w}}}{\partial t} + v_{\mathrm{w}} \frac{\partial v_{\mathrm{w}}}{\partial z} \right) - \rho_{\mathrm{s}} \left(\frac{\partial v_{\mathrm{s}}}{\partial t} + v_{\mathrm{s}} \frac{\partial v_{\mathrm{s}}}{\partial z} \right) \right] \\ & + \frac{\gamma}{1-\phi}(\phi) \left(\frac{\partial v_{\mathrm{d}}}{\partial t} + v_{\mathrm{d}} \frac{\partial v_{\mathrm{d}}}{\partial z} \right), \end{aligned} \tag{1.13}$$

hence the drift velocity:

$$\begin{aligned} v_{\mathrm{d}} = {} & -\frac{1-\phi}{r(\phi)} \Bigg[\frac{\partial \sigma_{\mathrm{e}}}{\partial z} - \phi \Delta \rho g - \left(\left(\nabla \cdot \overline{\overline{T_{\mathrm{s}}^{\mathrm{E}}}} \right) - \frac{\phi}{1-\phi} \left(\nabla \cdot \overline{\overline{T_{\mathrm{w}}^{\mathrm{E}}}} \right) \right) \cdot \vec{k} \\ & - \phi \left(\rho_{\mathrm{w}} \left(\frac{\partial v_{\mathrm{w}}}{\partial t} + v_{\mathrm{w}} \frac{\partial v_{\mathrm{w}}}{\partial z} \right) - \rho_{\mathrm{s}} \left(\frac{\partial v_{\mathrm{s}}}{\partial t} + v_{\mathrm{s}} \frac{\partial v_{\mathrm{s}}}{\partial z} \right) \right) \\ & + \frac{\gamma(\phi)}{1-\phi} \left(\frac{\partial v_{\mathrm{d}}}{\partial t} + v_{\mathrm{d}} \frac{\partial v_{\mathrm{d}}}{\partial z} \right) \Bigg]. \end{aligned} \tag{1.14}$$

A dimensional analysis leads to the following simplification of the previous formula:

$$v_{\mathrm{d}} = -\frac{1-\phi}{r(\phi)} \left(\frac{\partial \sigma_{\mathrm{e}}}{\partial z} - \Delta \rho g \phi \right). \tag{1.15}$$

The volume average velocity of the mixture can be expressed as

$$q = \phi v_{\mathrm{s}} + (1-\phi) v_{\mathrm{w}}. \tag{1.16}$$

Combining equation (1.10) and equation (1.16) leads to

$$v_{\mathrm{s}} = (1-\phi) v_{\mathrm{d}} + q. \tag{1.17}$$

In the case of batch settling with no discharge, $q = 0\ \mathrm{m}^3.\mathrm{s}^{-1}$. The continuity equation for the solids (1.5) leads to

$$\frac{\partial \phi}{\partial t} - \frac{\partial}{\partial z} \left[\frac{\phi (1-\phi)^2}{r(\phi)} \left(\frac{\partial \sigma_{\mathrm{e}}}{\partial z} - \Delta \rho g \phi \right) \right] = 0, \tag{1.18}$$

or

$$\frac{\partial \phi}{\partial t} + \frac{\partial f_{\mathrm{bk}}(\phi)}{\partial z} = \frac{\partial}{\partial z} \left(\frac{f_{\mathrm{bk}}(\phi)}{\Delta \rho g \phi} \frac{d\sigma_{\mathrm{e}}(\phi)}{d\phi} \frac{\partial \phi}{\partial z} \right), \tag{1.19}$$

with

$$f_{\mathrm{bk}}(\phi) = \frac{\Delta\rho g\phi^2 (1-\phi)^2}{r(\phi)}. \tag{1.20}$$

Equations (1.19) and (1.20) can be rewritten in terms of solids concentration:

$$\frac{\partial C}{\partial t} + \frac{\partial f_{\mathrm{bk}}(C)}{\partial z} = \frac{\partial}{\partial z}\left(\frac{\rho_{\mathrm{s}}}{C\Delta\rho g} f_{\mathrm{bk}}(C) \frac{d\sigma_{\mathrm{e}}(C)}{dC} \frac{\partial C}{\partial z}\right), \tag{1.21}$$

$$f_{\mathrm{bk}}(C) = -\frac{\Delta\rho g C^2 \left(\rho_{\mathrm{s}}^2 - C^2\right)}{\rho_{\mathrm{s}}^2 r(\phi)}. \tag{1.22}$$

The function f_{bk} is the Kynch Batch flux density function accounting for hindered settling. Since the Kynch function as expressed above is difficult to calculate, it is generally evaluated using a phenomenological settling velocity function v_{hs}:

$$f_{\mathrm{bk}}(C) = C v_{\mathrm{hs}}(C). \tag{1.23}$$

Similarly, the effective solids stress σ_{e} has to be calculated. The functions used for v_{s} and σ_{e} will be presented in section 1.1.4.

1.1.3 Multidimensional models: Computational Fluid Dynamics (CFD)

The different settling regimes and properties of activated sludge, as well as the effluent and underflow concentration, can be simulated using 1D models. However, in order to precisely simulate actual structures and take the hydrodynamic currents and rheological properties of activated sludge suspensions into account, CFD models are required (De Clercq, 2003; Locatelli et al., 2013). Several studies involving multidimensional models have been conducted (Lakehal et al., 1999; Brennan, 2001; De Clercq, 2003; Griborio, 2004; Hosseini et al., 2010; Xanthos et al., 2011; Pollert et al., 2012). They have been useful to propose modifications in settler systems and improve their efficiency.

When modelling secondary settling tanks with a CFD model, the choice of a multiphase approach is fundamental. Some of the main approaches available are presented hereafter.

- The Lagrangian approach: this approach is relevant when dealing with grit and/or diffuse secondary species/phases that do not have a significant influence on the bulk flow. It is therefore not suitable as there is a strong coupling between the primary and secondary phases in activated sludge suspensions.

- The Eulerian approach with a transport model: in this case, the continuity and momentum equations are solved for the primary phase

(usually water) only. A concentration scalar is used to describe the secondary phase (suspended solids), the motion of which is simulated using a convection–diffusion equation.

- The Euler–Euler approach: by solving the continuity and momentum equations for each phase, this approach simulates the modelled case as a system of interacting fluids. The Euler–Euler approach allows taking the specific properties of each phase into account and precisely modelling their interactions. However, it is computationally very demanding.

Some of these approaches will be detailed in the following subsections.

The Eulerian approach with a transport model

A three-dimensional time-dependent incompressible monophasic fluid flow is governed by the Navier–Stokes equation, i.e. the continuity equation (1.24) and the momentum conservation equation (1.25) (Versteeg and Malalasekera, 1995; Lakehal et al., 1999; Brennan, 2001; De Clercq, 2003; Griborio, 2004; Xanthos et al., 2011; ANSYS®, 2012):

$$\frac{\partial \rho}{\partial t} + \nabla \cdot (\rho \vec{u}) = 0, \tag{1.24}$$

$$\frac{\partial \rho \vec{u}}{\partial t} + \nabla \cdot (\rho \vec{u}\,\vec{u}) = -\nabla p + \nabla \cdot \left[\mu \left(\nabla \vec{u} + \nabla \vec{u}^{T}\right)\right] + C\frac{\rho_\mathrm{p} - \rho_\mathrm{w}}{\rho_\mathrm{p}}\vec{g} \tag{1.25}$$

where

- ρ is the local fluid-solid mixture density ($\mathrm{kg{\cdot}m^{-3}}$),
- $\vec{u}$ is the velocity vector ($\mathrm{m{\cdot}s^{-1}}$),
- p is the static pressure (Pa),
- μ is the dynamic viscosity (Pa·s),
- g is the gravitational acceleration ($\mathrm{m{\cdot}s^{-2}}$),
- C is the suspended solids concentration ($\mathrm{kg{\cdot}m^{-3}}$),
- ρ_p is the density of the flocs ($\mathrm{kg{\cdot}m^{-3}}$) and
- ρ_w is the density of clear water ($\mathrm{kg{\cdot}m^{-3}}$).

The term $C\frac{\rho_\mathrm{p} - \rho_\mathrm{w}}{\rho_\mathrm{p}}g$, sometimes called reduced gravitational force, accounts for buoyancy effects (Baines and Chu, 1996; Lakehal et al., 1999). In the case of this approach, a transport equation must be defined to account

for the movement of particles in the clarifier. This is usually achieved using a convection–diffusion equation,

$$\frac{\partial C}{\partial t} + \nabla \cdot \left[(\vec{u} + \vec{v_{\mathrm{s}}})\, C \right] = \nabla \cdot (D \nabla C)\,, \tag{1.26}$$

where

- v_{s} is the particle settling velocity ($\mathrm{m \cdot s^{-1}}$) and
- D is the diffusion coefficient ($\mathrm{m^2 \cdot s^{-1}}$).

If the flow is turbulent, perturbations appear in the variables of the previous equations. According to the Reynolds decomposition, these perturbations can be modelled by considering each variable as the sum of an average component and a fluctuating component, the average of which is zero. For a stationary turbulence, the average component can be calculated by time-averaging over a time interval Δt, which has to be larger than the time scale of the slowest fluctuations. In the case of a time-dependent flow, the average of a variable at a given time t is calculated over a large series of identical experiments, which is called "ensemble averaging" (Versteeg and Malalasekera, 1995; Brennan, 2001). Brennan (2001) recommends the use of ensemble averaging, explaining that it does not impose any restrictions on the time and space discretisations, and is mathematically rigorous

The instantaneous variables of equations (1.24) and (1.25) can be rewritten according to the Reynolds decomposition (for the sake of clarity, equations (1.27) to (1.31) are written using the convention of Einstein summation, where i and j are direction indices),

$$u_{\mathrm{i}} = U_{\mathrm{i}} + u'_{\mathrm{i}}, \tag{1.27}$$

where u_{i} is the instantaneous velocity value, U_{i} is the average velocity component and u'_{i} is the fluctuating velocity component. Likewise, the pressure becomes

$$p = P + p'. \tag{1.28}$$

This averaging method allows rewriting the Navier–Stokes equations, yielding the Reynolds–Averaged Navier–Stokes (RANS) equations. The continuity equation (1.24) becomes

$$\frac{\partial \rho}{\partial t} + \frac{\partial \rho U_{\mathrm{i}}}{\partial x_{\mathrm{i}}} = 0, \tag{1.29}$$

and the momentum conservation equation (1.25) becomes

$$\begin{aligned} \frac{\partial \rho U_{\mathrm{i}}}{\partial t} + \frac{\partial \rho U_{\mathrm{i}} U_{\mathrm{j}}}{\partial x_{\mathrm{j}}} = &- \frac{\partial P}{\partial x_{\mathrm{i}}} + \frac{\partial}{\partial x_{\mathrm{j}}} \left[\mu \left(\frac{\partial U_{\mathrm{i}}}{\partial x_{\mathrm{j}}} + \frac{\partial U_{\mathrm{j}}}{\partial x_{\mathrm{i}}} \right) \right] + C \frac{\rho_{\mathrm{p}} - \rho_{\mathrm{w}}}{\rho_{\mathrm{p}}} g_{\mathrm{i}} + \\ &+ \frac{\partial}{\partial x_{\mathrm{j}}} \left(-\rho \overline{u'_{\mathrm{i}} u'_{\mathrm{j}}} \right), \end{aligned} \tag{1.30}$$

where the term $-\rho\overline{u_\mathrm{i}' u_\mathrm{j}'}$ represents additional stress components, the turbulent stresses (or Reynolds stresses), and has to be modelled. Some of the modelling approaches used to account for the effects of turbulence will be discussed in section 1.1.4.

The convection–diffusion equation (1.26) is also modified to take the turbulence into account (Versteeg and Malalasekera, 1995; Lakehal et al., 1999; De Clercq, 2003; Griborio, 2004):

$$\frac{\partial C}{\partial t} + \frac{\partial \left(U_\mathrm{i} + v_{\mathrm{s,i}}\right) C}{\partial x_\mathrm{i}} = \frac{\partial}{\partial x_\mathrm{i}} \left(\frac{\nu_\mathrm{t}}{\sigma_\mathrm{t}} \frac{\partial C}{\partial x_\mathrm{i}} \right), \tag{1.31}$$

where

- ν_t is the eddy viscosity ($\mathrm{m^2 \cdot s^{-1}}$), which will be discussed in section 1.1.4, and
- σ_t is the turbulent Schmidt number (–), which is defined as the ratio between the turbulent diffusivities of momentum and mass (Rodi, 1993).

This approach requires relations for the viscosity μ (equations (1.25) and (1.30)), the settling velocity v_s (equations (1.26) and (1.31)) and the turbulent stresses (equation (1.30)). Some of these relations will be discussed in section 1.1.4.

Secondary clarification can lead to the formation of dense sludge beds, in which case the sludge becomes the primary phase in the thickened parts of the suspension. Therefore, simulating the sludge motion in these places can be better achieved by resorting to the Navier-Stokes equations instead of a transport equation. This can be done using the Euler-Euler approach, discussed hereafter.

The Euler-Euler approach

As previously mentionned, the sedimentation of activated sludge in quiescent conditions favours the formation of a floc matrix with specific rheological properties. It is therefore possible to model the particles as a second continuous phase using the Euler–Euler approach. The continuity equation (1.32) and momentum equation (1.33) are then defined for each phase (Elghobashi, 1994; Brennan, 2001):

$$\frac{\partial \alpha_\mathrm{n} \rho_\mathrm{n}}{\partial t} + \nabla \cdot \left(\alpha_\mathrm{n} \rho_\mathrm{n} \overrightarrow{u_\mathrm{n}}\right) = 0, \tag{1.32}$$

$$\begin{aligned} &\frac{\partial \alpha_\mathrm{n} \rho_\mathrm{n} \overrightarrow{u_\mathrm{n}}}{\partial t} + \nabla \cdot \left(\alpha_\mathrm{n} \rho_\mathrm{n} \overrightarrow{u_\mathrm{n}} \overrightarrow{u_\mathrm{n}}\right) = \\ &\quad = -\alpha_\mathrm{n} \nabla p + \nabla \cdot \left[\alpha_\mathrm{n} \mu_\mathrm{n} \left(\nabla \overrightarrow{u_\mathrm{n}} + \nabla \overrightarrow{u_\mathrm{n}}^T\right)\right] + \alpha_\mathrm{n} \rho_\mathrm{n} \overrightarrow{g} + \sum_{k=1}^{N} \overrightarrow{F_{\mathrm{kn}}}, \end{aligned} \tag{1.33}$$

where

- n is the phase index,
- α_n is the volume fraction of phase n (–),
- ρ_n is the density of phase n ($kg \cdot m^{-3}$),
- $\overrightarrow{u_n}$ is the velocity vector of phase n ($m \cdot s^{-1}$),
- p is the static pressure (Pa),
- μ_n is the viscosity of phase n (Pa·s), and
- $\overrightarrow{F_{kn}}$ is the interaction force between phases k and n (N).

In the case of turbulent flow, the previous equations can be modified as explained earlier in order to take the effects of tubulence on the motion of the phases into account. Different models exist to define the interaction force $\overrightarrow{F_{kn}}$. However, these models require the input of a characteristic particle or droplet size for the phase coupling calculation, which may be an issue as a wide range of particle diameters are present and changing with time (Wicklein and Samstag, 2009).

Another method, the drift flux approach, aims at simplifying the modelling of multiphase systems by solving a single set of partial differential equations for the continuity and momentum conservation of the mixture (Brennan, 2001; ANSYS®, 2012). The motion of each phase is tracked relatively to the center of the mixture mass (concept of drift velocity). This approach is less computationally expensive than the full Euler–Euler approach, since only one set of equations has to be solved. However, as with the interaction force pertaining to the Euler–Euler approach, the drift–flux method also requires the definition of a characteristic particle (or droplet) size for the calculation of the drift velocity. In the framework of secondary settling tank modelling, the choice of an adapted model for either the interaction force or the drift velocity necessitates extensive tests and calibration.

A diphasic approach can be particularly useful for the simulation of the behaviour of cohesive suspensions such as activated sludge. It is seldom used due to a lack of computational power or insight in the required physical properties, e.g. granulometry or rheology (Brennan, 2001). However, an experimental investigation can help overcome this issue.

1.1.4 Functions applied to the different mechanisms

As mentioned in the previous sections, most of the models used to simulate secondary settling tanks require additional phenomenological functions in order to account for several mechanisms. The following sections will present the functions used to describe hindered and compression settling, turbulence, as well as the rheological behaviour of activated sludge.

Settling velocity functions

A settling velocity function is required for 1D models, using either the Takács et al. (1991) or mechanistic approaches, as well as for CFD models using a Eulerian approach with a transport equation.

The function of Vesilind (1968) Before the development of non-optical measurement techniques (tracers, ultrasonic sensors, etc.) allowing the study of the internal behaviour of dense sludge suspensions, researchers had to rely on visual methods to describe the settling of mixed liquor (Dick and Vesilind, 1969). Settling curves combined with concentration and sludge volume index (SVI) measurements were the main tools for activated sludge settling experimental characterisation. The early phenomenological settling velocity functions, such as the function of Vesilind, were based on datasets obtained using such methods. The Vesilind formula describes the hindered settling velocity as a function of the local concentration of the suspension:

$$v_{\mathrm{s}}(C) = v_0 e^{-r_{\mathrm{V}} C}, \tag{1.34}$$

where

- v_{s} is the local settling velocity ($\mathrm{m{\cdot}s^{-1}}$),
- v_0 is the maximum settling velocity of flocs (i.e. that of isolated flocs) ($\mathrm{m{\cdot}s^{-1}}$),
- r_{V} is a calibrated parameter ($\mathrm{g^{-1}{\cdot}L}$).

This function is frequently used, often in combination with other models (Bye and Dold, 1998; Giokas et al., 2002; De Clercq et al., 2008; Bürger et al., 2011), for it cannot be applied to the full simulation of compression settling and thickening. Other attempts have been made to propose more comprehensive models.

The function of Takács et al. (1991) The settling velocity function proposed by Takács et al. (1991) is one of the most frequently used in simulation software. Although it is largely empirical, its parameters all have an interpretation with respect to the settling behaviour of activated sludge. The Takács et al. (1991) function evaluates the settling velocity via the following expression:

$$v_{\mathrm{s}} = \max\left\{0,\ \min\left\{\tilde{v_0},\ v_0\left(e^{-r_{\mathrm{h}}(C-C_{\min})} - e^{-r_{\mathrm{p}}(C-C_{\min})}\right)\right\}\right\}, \tag{1.35}$$

where

- C is the suspended solids concentration ($\mathrm{g{\cdot}m^{-3}}$),

- $\tilde{v_0}$ is the maximum settling velocity ($\mathrm{m{\cdot}d^{-1}}$),
- v_0 is the theoretical maximum settling velocity, i.e. the settling velocity of an isolated activated sludge particle ($\mathrm{m{\cdot}d^{-1}}$),
- r_h is a settling parameter characteristic of the hindered settling zone ($\mathrm{m^3{\cdot}g^{-1}}$),
- r_p is a settling parameter characteristic of low solids concentration ($\mathrm{m^3{\cdot}g^{-1}}$),
- C_min is the minimum attainable suspended solids concentration, below which no settling occurs ($\mathrm{g{\cdot}m^{-3}}$).

Several sedimentation regimes can be distinguished in a settling tank. The Takács et al. (1991) approach distinguishes four sedimentation regimes based on the suspended solids concentration (figure 1.4):

- I : below the minimum concentration C_min, the suspension is composed of the non-settling fraction of the particles and $v_\mathrm{s} = 0$.
- II : between C_min and C_l, the model accounts for the small, slowly settling particles.
- III : between C_l and C_u, a maximum $\tilde{v_0}$ is defined to simulate the fact that the settling velocity tends to become independent of the concentration when the floc particles reach their maximum size.
- IV : above C_u, the hindered settling regime is established, so that the model can be assimilated to the Vesilind function. This domain of the Takács et al. (1991) function also accounts for the compression regime.

The function of Kinnear (2002) In order to account for other influences, Kinnear (2002) attempted to include more fundamental parameters, such as dry solids density, floc density, permeability and compressive resistance, in a model of settling velocity (De Clercq, 2006):

$$v_\mathrm{s}(\epsilon) = \begin{cases} \dfrac{(\rho_\mathrm{f} - \rho_\mathrm{l}) g \epsilon^3}{5 S_0^2 (1-\epsilon) \mu}, & \text{if } C < C_\mathrm{c}, \\ \dfrac{(\rho_\mathrm{f} - \rho_\mathrm{l}) g (1-\epsilon) + P_0 \left(\dfrac{1-\epsilon}{1-\epsilon_c} \right)^m \dfrac{\partial \epsilon}{\partial z}}{5 S_0^2 (1-\epsilon)^2 \mu} \epsilon^3, & \text{if } C \geq C_\mathrm{c}, \end{cases} \tag{1.36}$$

with

$$\epsilon(C) = 1 - \left(1 + \frac{\rho_\mathrm{s} - \rho_\mathrm{f}}{\rho_\mathrm{f} - \rho_\mathrm{l}} \right) \frac{C}{\rho_\mathrm{s}}, \tag{1.37}$$

where

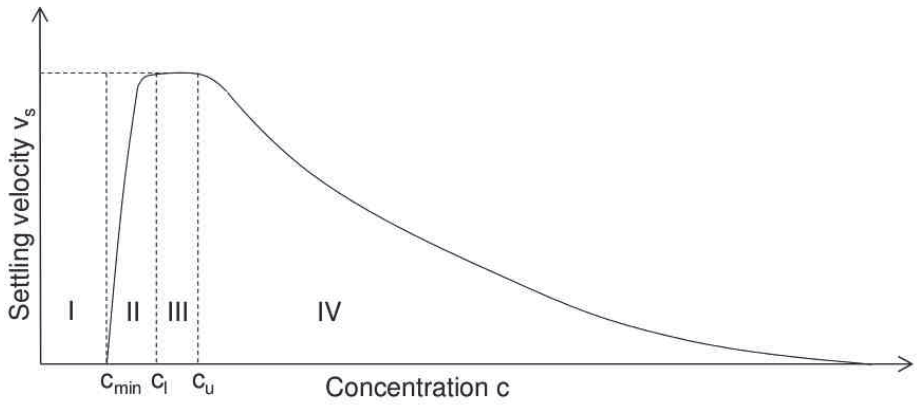

Figure 1.4 – Curve of the Takács settling velocity function with respect to the suspended solids concentration

- C_c is the critical concentration above which interparticle compressive contact exists ($g \cdot L^{-1}$),
- v_s is the settling velocity ($m \cdot s^{-1}$),
- ρ_f is the density of the floc ($kg \cdot m^{-3}$),
- ρ_l is the density of the liquid phase ($kg \cdot m^{-3}$),
- ρ_s is the density of the solids ($kg \cdot m^{-3}$),
- g is the gravitational acceleration ($m \cdot s^{-2}$),
- ϵ is the porosity (–),
- μ is the dynamic viscosity of the liquid (Pa·s),
- c is the solids concentration ($kg \cdot m^{-3}$),
- z is the vertical coordinate (m),
- S_0 is the specific area of the primary particle ($m^2 \cdot kg^{-1}$) and
- P_0 and m are empirical coefficients (–).

This model requires some calibration regarding dry solids, floc density, effective solids stress parameters and S_0 using observed initial settling velocities. Is is then able to reliably reproduce the initial phase of the hindered settling of activated sludge during batch sedimentation experiments. However, it tends to differ from reality after a while. Though a promising attempt at including a wider set of parameters in a sedimentation model, Kinnear's function remains unable to simulate complete batch settling curves.

Effective solids stress modelling

An effective solids stress function is useful for 1D models using a mechanistic approach. They also have implications for the improvement of CFD models using either full Euler–Euler or mixture approaches, by providing a method for the description of activated sludge thickening.

The function of De Clercq et al. (2008) Using detailed concentration data obtained during batch settling experiments, De Clercq et al. (2008) were able to calculate values of effective solids stress σ_e and model them using a logarithmic function,

$$\sigma_e = \begin{cases} 0, & \text{if } 0 \leq C < C_c, \\ \alpha \ln\left(1 + \dfrac{C - C_c}{\beta}\right), & \text{if } C \geq C_c, \end{cases} \tag{1.38}$$

where

- C is the sludge concentration ($g{\cdot}L^{-1}$),
- C_c is the critical concentration ($g{\cdot}L^{-1}$) above which permanent particle contact and compressive stresses exist, and
- α (Pa) and β ($g{\cdot}L^{-1}$) are calibrated parameters.

This effective solids stress function allows modelling the compression of the sludge and completes phenomenological settling velocity functions which are, as explained earlier, not able to reproduce the entire batch settling process. However, exponential settling velocity functions, such as the functions of Vesilind (1968) and Takács et al. (1991), have been shown to model also part of the compression process (Torfs et al., 2015), overlapping the effects of the effective solids stress function. It is thus necessary to devise more targeted settling velocity functions in order to develop more realistic activated sludge settling models.

Turbulence modelling

In a working settler system, turbulent motions, which are by nature three-dimensional, are generated in key places such as the inlet baffles and scraping gear (De Clercq, 2003; Griborio, 2004). A comprehensive numerical model of the hydrodynamics of a secondary settling tank therefore needs to be three-dimensional.

The k–ϵ model Most authors use the k–ϵ model, or modified versions of it, to simulate the turbulent behaviour of the flow field in settlers (Lakehal et al., 1999; Stamou et al., 2000; Armbuster et al., 2001; Brennan, 2001;

De Clercq, 2003; Xanthos et al., 2011; Pollert et al., 2012). This model uses the concept of eddy viscosity ν_t developed by Boussinesq: the turbulent stresses are assumed to be proportional to the mean-velocity gradients, with ν_t as the proportionality constant. As opposed to the molecular viscosity ν, ν_t is not a fluid property but is dependent on the state of turbulence (Rodi, 1993; Griborio, 2004). The k–ϵ model calculates the eddy viscosity using the turbulent kinetic energy k and its dissipation rate ϵ,

$$\nu_t = C_\mu \frac{k^2}{\epsilon}. \tag{1.39}$$

The transport equations for these quantities are derived in exact form from the Navier-Stokes equations. The k–ϵ approach assumes an isotropic eddy-viscosity. The transport equations for k and ϵ involve empirical constants that have been deduced from thorough experimental studies of free turbulent flow (Rodi, 1993). However, as Lesieur and Métais (1996) and Rodi (1993) pointed out, these constants occasionally need to be modified so as to fit the behaviour of the modelled system more accurately. Lakehal et al. (1999), for instance, pointed out the influence of the value of the constant associated with the buoyancy source term in the ϵ equation on the horizontal velocity profiles. Therefore, care has to be taken when calibrating the k–ϵ model.

The mixing-length model Another model using the eddy viscosity concept is the mixing-length model. In this approach, ν_t is calculated as the product of a characteristic size of the turbulence, the mixing-length, and a characteristic velocity of the turbulent fluctuations (Rodi, 1993; Lesieur and Métais, 1996). Both the k–ϵ model and the mixing-length model involve empirical constants and have been found to produce comparable results when applied to similar, simple configurations. The mixing-length model presents the advantage of being less computationally demanding than the k–ϵ model (Griborio, 2004). However, the superior complexity of the k–ϵ model makes it more adaptable to specific situations. Therefore, it should be prefered to the mixing-length model when the computational resources at hand allow it.

Though it benefits from more experience and validation than other turbulence models, it has a number of shortcomings. For instance, it has the tendency to underestimate the length of recirculation zones (Brennan, 2001).

The LES approach Another approach for the modelling of turbulence is large eddy simulation (LES). This concept is based on the observation that, though direct numerical simulation (DNS) of turbulent flows remains too computationally demanding in most cases, it is possible to solve the Navier-Stokes equations for transient motions at scales larger than the grid mesh (Lesieur and Métais, 1996; De Clercq, 2003). A low-pass filter is applied to the velocity field components in order to remove the fluctuations occurring

on a scale smaller than the chosen grid characteristic dimension. Then, the continuity and Navier-Stokes equations are applied for the filtered field and a model, often based on the eddy viscosity assumption, is employed in order to account for the subgrid phenomena. The main difficulty in this approach lies in the fact that inaccuracies in the results provided for the subgrid motions will eventually affect the larger scales (Lesieur and Métais, 1996). It is therefore important to choose a reliable model for the small scale turbulence. In this regard, the approach proposed by the meteorologist Joseph Smagorinsky (1963) is still widely and successfully used. It was initially aimed at providing a numerical solution to the equations describing the behaviour of the atmosphere on a large scale (Lesieur, 1994). Smagorinsky's model applies well to the simulation of free-shear flows.

Though more computationally demanding than the k–ϵ model, LES provides a more reliable insight on the large scale motions of the flow, since it uses less empirical parameters. Furthermore, it is well adapted to the simulation of transient flows undergoing a transition from an overall turbulent state to a laminar behaviour (Hoarau, personal communication).

Non-Newtonian effects

As presented earlier, CFD modelling approaches require viscosity values: either the viscosity of the suspension, in the cases of the Eulerian approach with a transport equation and the mixture approach, or the viscosity of each phase in the case of a Euler–Euler approach. In any case, activated sludge suspensions are known to develop non-Newtonian properties. The latter have to be accounted for using functions which can be introduced in the momentum equations (1.25), (1.30) and (1.33). The rheological properties of activated sludge and the functions used to describe them will be discussed in the following section.

1.2 The rheology of activated sudge

1.2.1 The rheological behaviour of fluids

There is a wide variety of non-Newtonian fluids, but categories of characteristic behaviours can be identified. They are commonly distinguished by comparing the aspects of their respective rheograms (Ferguson and Kemblowski, 1991; Couarraze and Grossiord, 1991). A rheogram is the curve describing the evolution of the shear stress exerted on a volume of fluid with respect to the shear rate. Figure 1.5 illustrates the notions of shear rate and shear stress: it shows the schematics of a Couette flow, i.e. that of a viscous fluid between two parallel planes, only one of which is moving at constant velocity.

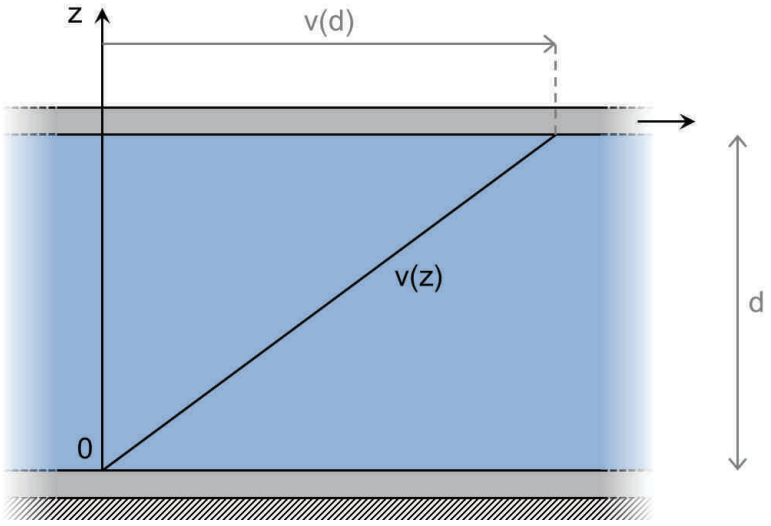

Figure 1.5 – Couette flow of a Newtonian fluid. $v(z)$ is the velocity of the fluid at distance z from the stationary plane

In this configuration, the slope of the $v(z)$ line is the shear rate $\dot{\gamma}$:

$$\dot{\gamma}(v) = \frac{\partial v}{\partial z} = \frac{v(d)}{d}, \tag{1.40}$$

where $v(d)$ is the velocity of the moving plane.

At a given velocity, thus at a given shear rate, the moving plane exerts a tangential force F on the fluid. If we denote S the surface of the plane in contact with the fluid, the shear stress τ can be expressed as:

$$\tau(\dot{\gamma}) = \frac{F(\dot{\gamma})}{S}. \tag{1.41}$$

The value of the shear stress is linked to that of the shear rate by the apparent dynamic viscosity μ (hereafter referred to as "apparent viscosity"):

$$\tau(\dot{\gamma}) = \mu\dot{\gamma}. \tag{1.42}$$

In the case of a Newtonian fluid, the apparent viscosity is a constant. In the case of non-Newtonian fluids, however, it can vary with the shear rate. Several broad categories of non-Newtonian fluids can thus be distinguished. Figure 1.6 presents the different aspects of the rheograms corresponding to those categories (Ferguson and Kemblowski, 1991; Ratkovich et al., 2013).

Newtonian fluids: curve 1 Curve 1 represents the rheogram of a Newtonian fluid: since μ is a constant, the shear stress is a linear function of the shear rate.

Shear-thinning (or pseudoplastic) fluids: curve 2 Shear-thinning can be observed when the deformation of the fluid weakens or breaks internal structures (i.e. interparticle forces in the case of suspensions). This causes the viscosity to decrease with increasing shear-rate.

Shear-thickening (or dilatant) fluids: curve 3 The viscosity can increase with the shear rate if, for example, shearing the fluids favours particle interactions that result in increased viscosity. A common example of such fluids is cornstarch mixtures.

Plastic fluids: curves 4–6 Due to the existence of internal structures, some fluids can behave as plastic solids below a certain value of shear stress, and flow only if this so-called *yield stress* is exceeded. Above this limit, they can display the same flow behaviour as fluids devoid of yield stress, only shifted by the value of the latter.

The viscosity of a fluid may vary with time. A fluid whose viscosity decreases with time is called "thixotropic", and a fluid whose viscosity increases with time is called "rheopectic". If the viscosity of a fluid changes with time, its rheogram will display hysteresis.

Several equations have been proposed to describe the behaviours of non-Newtonian fluids. Table 1.2 presents some of these equations and indicates the schematic rheogram they may correspond to.

Table 1.2 – Equations modelling the behaviour of non-Newtonian fluids. For the different equations, k is the consistency index (s or s^n), n is the flow behaviour index (–), μ_0 is the viscosity with no shear rate (Pa·s), μ_∞ is the viscosity of the Newtonian plateau at high shear rates (Pa·s) and τ_y is the yield stress (Pa)

Model name	Equation	Rheogram type (figure 1.6)
Ostwald–de Waele	$\tau = k\dot{\gamma}^n$	1–3
Sisko	$\tau = \mu_\infty\dot{\gamma} + k\dot{\gamma}^n$	2
Bingham	$\tau = \tau_y + \mu\dot{\gamma}$	4
Herschel–Bulkley	$\tau = \tau_y + k\dot{\gamma}^n$	4–6
Casson	$\sqrt{\tau} = \sqrt{\tau_y} + \sqrt{\mu\dot{\gamma}}$	5
Cross	$\mu = \dfrac{\mu_0 - \mu_\infty}{1 + (k\dot{\gamma})^n} + \mu_\infty$	1–3
Carreau	$\mu = (\mu_0 - \mu_\infty)(1 + (k\dot{\gamma})^2)^{\frac{n-1}{2}} + \mu_\infty$	1–3

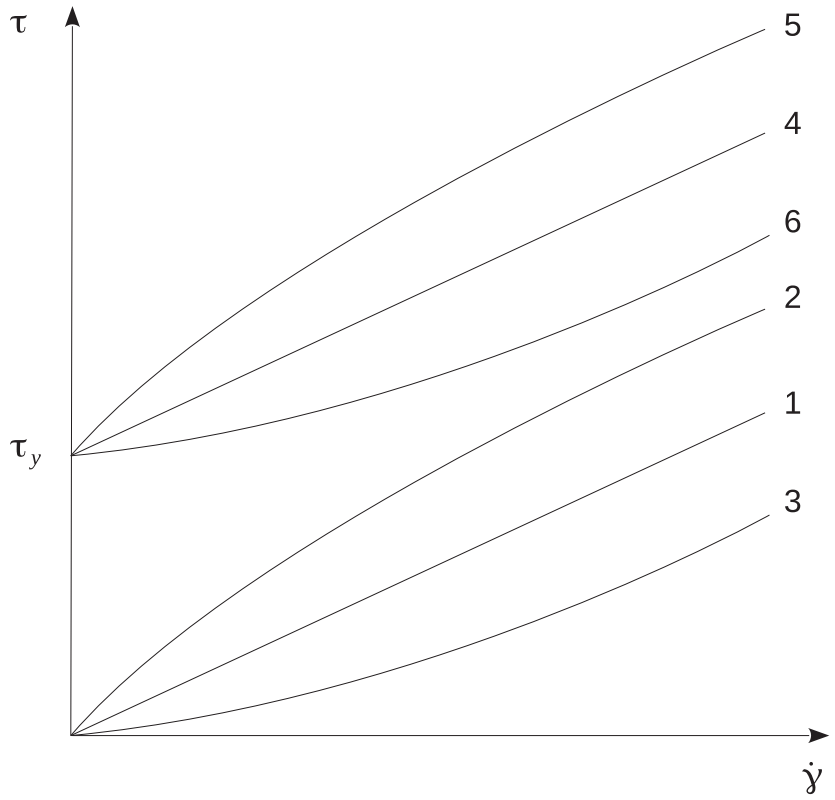

Figure 1.6 – Schematic rheograms of the main rheological behaviours

1.2.2 The rheological behaviour of activated sludge

Rheological models applied to activated sludge

Due to the complex makeup of activated sludge, its rheological behaviour is highly variable, but consistently non-Newtonian (Seyssiecq et al., 2003). Activated sludge has been identified as a plastic fluid by Dick and Ewing (1967a). The Bingham plastic model has been widely applied to activated sludge (Lotito et al., 1997; Sozanski et al., 1997; Guibaud et al., 2004; Laera et al., 2007; Yang et al., 2009; Xia et al., 2009; Garakani et al., 2011). However, the existence of a yield stress is not systematically noted (Sanin, 2002; Wang et al., 2003a). In the absence of yield stress, the Ostwald–de Waele equation is usually used (Sanin, 2002; Wang et al., 2003a). This equation, in the form of a power-law, allows modelling pure shear-thinning behaviour. However, concerning the absence of yield stress in the rheological measurements, Dick and Ewing (1967a) and Lotito et al. (1997) remark that slippage is possible inside of the rheometer due to the smooth surface of commercially available measuring geometries. This can impair the detection of a

yield stress. The authors thus suggest modifying the rheometric device by roughening the surface of the measuring geometry so as to prevent this phenomenon. Studies generally show that, though the Ostwald–de Waele is a simple model and can be applied to activated sludge with a measure of success, it often fits the experimental data less satisfactorily than models with a yield stress σ_y (Laera et al., 2007; Xia et al., 2009; Garakani et al., 2011).

The equation of Herschel-Bulkley if often applied with good results (Slatter, 1997; Mori et al., 2008, 2006; Yang et al., 2009; Xia et al., 2009; Hammadi et al., 2011). This equation allows modelling shear-thinning using, as the Ostwald–de Waele equation, a power law, and takes a yield stress into account. The equation of Casson also accounts for shear thinning and the yield stress. Yang et al. (2009) applied this equation to membrane bioreactor sludges of different concentrations and found it to provide slightly better results than the equation of Herschel–Bulkley over the range of concentrations tested.

Xia et al. (2009) compared several rheological models to data obtained at different sludge concentrations. They found that, at high shear rate, the equations of Sisko and Bingham fit the data better than Herschel–Bulkley's. Sisko's equation models an infinite-rate viscosity, i.e. an asymptotic value μ_∞ toward which the calculated viscosity tends when the shear rate increases. Similarly, the Bingham equation models a constant viscosity value. This indicates that, when the sludge is sheared fast enough, the flocs are torn apart and its viscosity becomes constant with respect to the shear rate (Guibaud et al., 2004). Indeed, at high shear rates, the flocs are reduced to their basic, indivisible elements, and the viscosity of the suspension becomes constant (Einstein, 1906, 1911).

The equations of Carreau and Cross also take shear thinning and an infinite rate viscosity μ_∞ into account, with the addition of a zero-rate viscosity μ_0, which is the limit value of the calculated viscosity when the shear rate tends toward zero. These models were compared by Garakani et al. (2011) using sludges of different concentrations. Their findings indicate that both model fit the data well, with a slight advantage for the Carreau model.

These observations suggest that a comprehensive activated sludge rheological model should take a yield stress, shear-thinning and an infinite-rate viscosity into account. The equations of Carreau and Cross both model the last two behaviours and can be combined with an experimental yield stress value. Additionally, the zero-rate viscosity μ_0 can allow calculating the viscosity of the sludge when it flows at low shear rates. Though the Carreau equation seems to give slightly better results than the Cross equation (Garakani et al., 2011), the latter was designed as a general model for a variety of shear-thinning solutions and suspensions, while the Carreau equation is oriented toward polymer solutions and melts. Therefore, the Cross model seems well-suited to the development of an activated sludge rheological model.

Influence of the sludge characteristics

Several relations have been proposed to take the impact of changes of the sludge characteristics on the rheological parameters into account. In order to integrate the influence of the sludge concentration in the Herschel–Bulkley model, Slatter (1997), using the work of Dabak and Yucel (1987), proposed the following relationship:

$$\begin{cases} \tau_{\mathrm{y}} = a\dfrac{C^3}{C_{\max} - C}\,, \\ \mu = \mu_{\mathrm{w}}\left(1 - \dfrac{C}{C_{\max}}\right)^{-m}\,, \end{cases} \tag{1.43}$$

where τ_{y} is the yield stress (Pa), μ is the sludge apparent viscosity (Pa·s), C is the sludge concentration (g·L^{-1}) and $C_{\max}$ is the maximum sludge concentration (g·L^{-1}).

Guibaud et al. (2004) found that the yield stress and viscosity of the Bingham model increase exponentially with the sludge concentration. Lotito et al. (1997) suggested two different equation forms, second degree polynomial and power, to calculate the evolution of the Bingham parameters as a function of the sludge concentration:

$$\begin{cases} \tau_{\mathrm{y}} = a_1C^2 + b_1C + d_1, \\ \mu = a_2C^2 + b_2C + d_2, \end{cases} \tag{1.44}$$

and

$$\begin{cases} \tau_{\mathrm{y}} = a_1C^{b_1}, \\ \mu = a_2C^{b_2}, \end{cases} \tag{1.45}$$

where τ_{y} is the yield stress (Pa), μ is the sludge apparent viscosity (Pa·s), C is the sludge concentration (g·L^{-1}) and $(a_1; b_1; d_1; a_2; b_2; d_2)$ are linear regression parameters.

Yang et al. (2009) proposed the following equation to calculate the value of the apparent viscosity as a function of the temperature and sludge concentration at a shear rate of 100 s^{-1}:

$$\mu = 1.0024 \times 10^{-3}C^{1.644}T^{-0.206}\ \text{(Pa·s)}, \tag{1.46}$$

where μ is the apparent viscosity (Pa), C is the sludge concentration g·L^{-1}, and T is the temperature (°C). Additionally, they proposed the following relationship to calculate the value of the apparent viscosity as a function of the shear rate and sludge concentration at a temperature of 20 °C:

$$\mu = 32.36 \times 10^{-3}C^{1.359}\dot{\gamma}^{-0.807}, \tag{1.47}$$

where μ is the apparent viscosity (Pa), C is the sludge concentration g·L^{-1}, and $\dot{\gamma}$ is the shear rate (s^{-1}).

Sanin (2002) showed that an increase of the conductivity of the suspension tends to decrease the apparent viscosity of the sludge. He explained this phenomenon by the reduction of the thickness of the electrical double layer at the interfaces between the flocs and changes in the conformation of the polymers attached to the surface of the latter. The same author showed that an increase of the pH of the suspension tends to increase the viscosity of the sludge. He explained this behaviour by an increase of the amount of negative charges carried by the surfaces of the flocs, inducing higher repulsion between them. Mori et al. (2008) observed that a decrease of the extracellular polymeric substances (EPS) concentration, achieved by starving a sludge sample, leads to a decrease of the sludge viscosity. They explained this behaviour by the modification of the flocs structure entailed by the lower EPS concentrations.

The structure of the bacteria can also have an impact on the rheological properties of activated sludge. Tixier (2003) showed that a significant thixotropic behaviour can be associated to the presence of filamentous bacteria. He suggested using the hysteresis of the sludge rheogram as a criterion to determine the filamentous nature of a sludge.

The parameters of the rheological models are thus strongly influenced by the sludge characteristics, particularly its concentration, but also the temperature of the suspension as well as other variables, such as the aeration intensity in the case of membrane bioreactors (Yang et al., 2009). The development of an activated sludge rheological model therefore requires taking steps to quantify the effects of such influences on the model parameters. Thus, an experimental process has to be devised. The following section will detail and discuss some of the experimental methods available for the investigation of rheology as well as the batch settling process.

1.3 Experimental methods for the study of activated sludge

The previous section highlighted the need for rheological and phenomenological functions in activated sludge settling models. The parameters of these functions have to be evaluated using detailed experimental data. Additionally, the development of experimental techniques can bring new insight into the batch settling process. This section thus presents and discusses experimental methods adapted to the study of the rheology and the sedimentation of activated sludge.

1.3.1 Rheological methods

The viscosity of a fluid can be measured by the mean of a rheometer. Due to the large variety of fluids encountered in industrial processes (particularly in

food processing), several kinds of rheometers have been developed. Different categories of rheometers have thus been applied to the study of activated sludge rheology.

The different categories of rheometric devices

Rotational rheometers

There are several models of rotational rheometers. A frequently encountered category of instrument is the coaxial cylinder rotational rheometer (figure 1.8, A). It is one of the oldest types of rheometers, inherited from the works of French physicist Maurice Couette (in White, 1990). The measuring geometry is composed of a cylinder rotating inside of a cylindrical cavity into which the fluid sample is poured. The torque exerted on the axle shaft of the rotating cylinder can then be measured and allows calculating the shear stress, which is linked to the angular velocity (known) by the viscosity. This type of device is frequently used to study activated sludge. However, it has some disadvantages. One of the main issues with this type of rheometer is the possibility of settling occurring during the measurement process, particularly if the gap is to large and the shear rate to low to maintain the particles in suspension. Another difficulty associated with this category of rheometers is the formation of Taylor vortices above a certain angular velocity (Taylor, 1923). This phenomenon entails a modification of the torque, thus of the apparent viscosity (Donnelly, 1958; Eagles, 1974; Di Prima and Swinney, 1985).

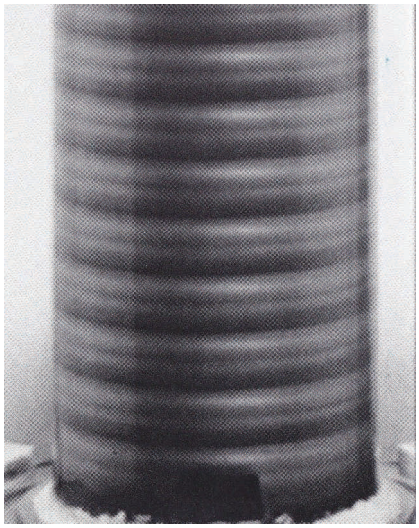

Figure 1.7 – Photograph of laminar Taylor vortices in a rotational coaxial cylinder system (Van Dyke, 1982); fluid: machine oil containing aluminium powder.

A double gap rotating cylinder geometry has also been developed. By increasing the contact surface between the fluid and the measuring geometry, this kind of rheometer is more precise than a single gap cylindrical rheometer and allows measuring smaller viscosity values. It is also possible to use this device with smaller gap values than a single gap one which, in the case of particle suspensions, tends to limit sedimentation during the measurements (Seyssiecq et al., 2003; Tixier et al., 2003a,b; Tixier, 2003; Mori et al., 2006). However, the size of the gap is a matter of concern when performing rheological measurement on fluids containing particles. Indeed, the gap has to be larger than the largest particle size class in the suspension, in order to avoid undesired deformations of the particles as well as solids friction between the particles and cylinders, which would result in abnormal viscosity measurements (Lotito et al., 1997). A frequently used rule of thumb recommends a gap ten times wider than the largest particles contained in the suspension (Van Wazer et al., 1963; Tropea et al., 2007), which is not always possible. In order to perform rheological measurements of activated sludge suspension, the size of the gap has to be weighted against the risk of settling occurring at low shear rates (Mori et al., 2006). This raises the issue of the definition of the size of activated sludge particles.

Settling issues can be avoided using rheometers equipped with horizontal measuring geometries. There are two main types of horizontal measuring designs: cone-and-plate (figure 1.8, C), and parallel-plate (figure 1.8, D) geometries. Such rheometers generally require smaller sample volumes than the other categories of devices, which makes sample conditioning, particularly temperature control, more convenient. In the case of the cone-and-plate geometry, the cone is actually truncated in order to avoid direct contact with the plate. During the measurements, the distance between the geometry and the plate is adjusted so that the tip of the cone would rest on the plate. The cone-and-plate rheometer has been developed in order to obtain a constant shear rate across the radius of the geometry (Tropea et al., 2007). This has the advantage of cancelling the need for correction of the results. However, since the angle θ of the cone is small (less than 5°), the gap between the apex of the geometry and the plate is extremely narrow (generally less than 100 μm). Thus, if the particles contained in the fluid are too large, they can cause friction and deteriorate the measurements.

It is possible to avoid the issue of particle trapping by using a parallel-plate rheometer. This type of device has the advantage of allowing a variable adjustment of the gap. The distance between the geometry and the plate can thus be modified according to the nature and size of the particles contained in the fluid. Furthermore, this type of geometry can easily be modified in order to increase its roughness and reduce slippage (Dick and Ewing (1967a) used a coaxial cylinder rheometer and increased the roughness of the cylinders in order to avoid such an issue). The sample volume remains small. However, since the shear rate is not constant across the radius of the geom-

etry, mathematical corrections have to be applied to the measured value in order to obtain the actual viscosity.

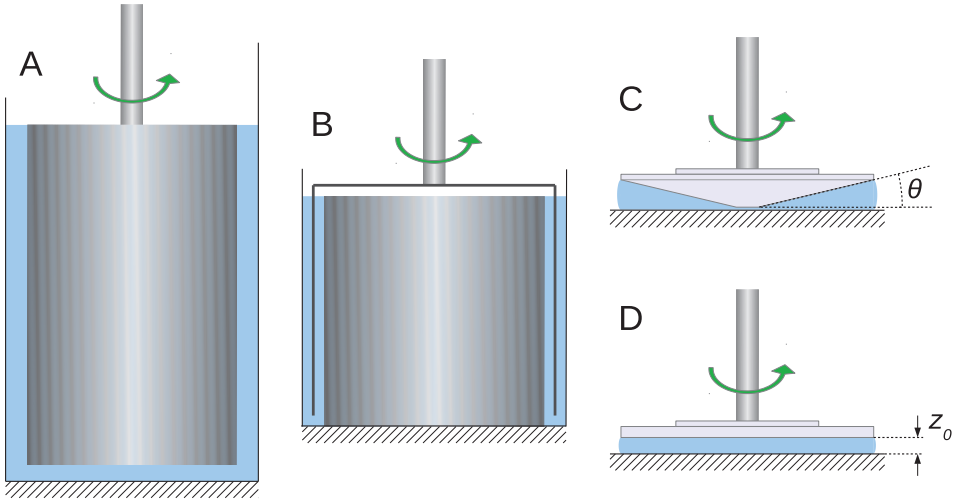

Figure 1.8 – The main types of rotational rheometers

Capillary rheometers

The viscosity of a fluid has an influence on the pressure drop along a pipe in which the fluid circulates. Capillary rheometers, also called tube rheometers, have been elaborated on the basis of this principle: a laminar flow of the studied fluid is created (using, for example, compressed air) in a thin tube, the capillary, at the extremities of which the pressure is measured. In the case of Newtonian fluids, the relationship between the pressure drop along the tube and the viscosity of the fluid is formulated by the Hagen-Poiseuille equation. In the case of non-Newtonian fluids mathematical corrections, dependent on the behaviour of the fluid studied, have to be applied.

Such devices are often used in fluid mechanics experiments due to their convenient principle. However, they are not suitable for every situation. Slatter (1997) used a tube rheometer in order to investigate the behaviour of activated sludge in pipes. In this particular case, the principle of the capillary rheometer fits the operational conditions studied. However, the sludge particles contained in the sample may be too large as compared to the tube diameter, resulting in perturbations in the measurements. Furthermore, due to the existence of velocity gradients over the cross-section of the capillary, the shear rate is not homogeneous in the fluid sample (N.B. this issue is common with the rotational double-plate rheometer). Mathematical corrections thus have to be applied in order to obtain the actual viscosity values from the measured data. Correction factors also have to be applied in order to account for the fact that both extremities of the tube have to be equipped

with cavities in order to connect the pressure gauge. The presence of those cavities induces transitions regions in the velocity profile at both ends of the capillary.

Conclusion

Given the complex properties of activated sludge, particularly in terms of particle size, and the characteristics of the different models of rheometers, a parallel-plate rheometer was chosen. This type of device seemed the most adapted to the objectives of the study.

1.3.2 Experimental methods for the study of batch settling

Classically, batch settling tests are performed ex situ and monitored visually in order to establish the Sludge Volume Index (Dick and Vesilind, 1969). The SVI test is useful to provide extensive data in order to confront settling models to experimental settling curves (Daigger and Roper, 1985; Giokas et al., 2003). However, it does not provide insight into the internal behaviour of activated sludge suspensions.

Optical sensors can be used to perform concentration measurements (Vanrolleghem and Lee, 2003). However these sensors are efficient in a limited range of sludge concentration (Wren et al., 2000; Vanrolleghem and Lee, 2003; De Clercq, 2003), which makes their application to activated sludge suspensions delicate.

De Clercq et al. (2005) used a radioactive tracer in order to measure the complete concentration profiles of activated sludge suspensions during laboratory batch settling tests. This method provides extremely precise results. However, its use in actual wastewater treatment plants is compromised by the complexity of the required equipment.

Acoustic Doppler Current Profilers (ADCPs) have been used to measure velocity fields in settling tanks by De Clercq et al. (2002). ACDPs use ultrasonic signals to measure the velocity of suspended particles. Ultrasonic Doppler methods are robust and can be applied to field measurements. Therefore, they are well suited to the study of activated sludge settling, both in- and ex situ (De Clercq, 2003). Ultrasonic Doppler measurement techniques have been widely applied for medical purposes, particularly as heart motion sensors (Yoshida et al., 1961; Joyner Jr. and Reid, 1963). The interest of such techniques stems from the ability of ultrasounds to travel through several layers of different media (e.g. skin and internal organs in the case of medical applications) and generate an echo which can be analysed in order to gather information on the structure and velocity of internal components that cannot be obtained by the means of optical methods. The intensity of the backscattered signal is related to the properties (such as density, size or rigidity) of the obstacles encountered along the path of the

ultrasound burst (Harker and Temple, 1988). If the medium travelled, or part of it, is in motion, the signal reflected by the moving matter returns with a frequency offset called the Doppler frequency shift, the value of which is a function of the velocity of the medium. In order to deduce velocity values from the echo, it is however necessary to implement a post-processing method tailored to the characteristics of the system studied.

Application of ultrasonic measurement methods to settling tanks

In the field of wastewater systems, ultrasonic techniques are commonly applied to sewage velocity (Abda et al., 2009) or water level monitoring. Commercially available sensors can be used to obtain a precise measurement of the velocity field in one point in space (acoustic Doppler velocimeters), or to obtain the average velocity field over a profile (acoustic Doppler current profilers). In any case, one has to keep in mind that these devices measure the velocity of the particles, not of the flow itself (De Clercq, 2003).

Acoustic Doppler velocimeter are useful to precisely measure the velocity field of the fluid in a specific location (e.g. inlets or outlets of hydraulic structures). In the case of settling, the key information is the vertical gradient of settling velocity. Therefore, it will be necessary to measure velocity profiles. De Clercq et al. (2002) used an acoustic Doppler current profiler in a secondary settling tank in order to obtain the velocity field across the radius of the structure. They found that, in a large upper portion of the settling tank, where the velocity is low, settling was too predominant to allow an accurate measurement of the water velocity. However, they were able to measure the velocity field and calculate the Reynolds stress profiles near the bottom of the tank, where water velocities were sufficient to carry the particles completely.

Deininger et al. (1998) also performed velocity profile measurement in a secondary settling tank, using a different technique. They used an ultrasonic velocity profile monitor in order to obtain velocity profiles. Though this technique does not provide the complete velocity field, it requires only one ultrasonic probe, thus avoiding the necessity of averaging the values measured by several sensors associated with acoustic Doppler current profilers.

In the case of batch settling experiment, it was therefore appropriate to use a technique allowing instantaneous velocity profiles measurement. The ultrasonic velocity profile (UVP) method was thus adopted.

Principle of Ultrasonic Velocity Profile (UVP) measurement

In the case of settling velocity profile measurement systems, only one ultrasonic transducer is necessary, since the vertical velocity component alone is of interest. The schematic of figure 1.9 shows the principle of the acoustic Doppler velocity profile measurement as applied to the activated sludge

batch settling experiments performed during this study. The ultrasonic burst is emitted downward through the suspension, and its echo is recorded at regular time intervals. The recording period is chosen so as to sample the desired number of points within the settling column. To each instant t_i corresponds a depth via the following formula:

$$t_\mathrm{i} = \frac{2z_\mathrm{i}}{c}, \tag{1.48}$$

where c is the velocity of sound (m s^{-1}). The backscattered signal is thus recorded for all sampling points. The displacement of the suspension produces on the backscattered signal a Doppler frequency shift f_D (Hz) which can be expressed as follows:

$$f_\mathrm{D} = \frac{2f_0 v_\mathrm{s}}{c}, \tag{1.49}$$

where

- f_0 is the frequency of the initial ultrasound wave (Hz),
- v_s is the particle settling velocity (m·s^{-1}), and
- c is the speed of sound (m·s^{-1}). f_0 and c are known characteristics of the system.

Therefore, measuring the Doppler frequency shift f_D of each echo yields the settling velocity values ($\mathrm{v_{s,1}}$, ..., $\mathrm{v_{s,i}}$, ...) at the corresponding sampling points.

Conclusion of the literature review

The previous sections showed that activated sludge settling can be simulated using several types of modelling approaches. The models involved generally use parameters which cannot be accessed experimentally, or only with difficulty. Therefore, phenomenological functions are developed in order to close the sets of equations solved by the models, namely for the settling velocity and the effective solids stress. In the case of CFD models, rheological functions are also required to calculate the viscosity of the suspension. The aforementioned functions have to be calibrated using extensive experimental data, which are often not available.

In this work, an experimental procedure is thus developed to investigate the rheology of activated sludge as well as the batch settling process and measure the complete settling velocity profiles of activated sludge suspensions using the Ultrasonic Velocity Profile measurement method. This non-invasive technique is applied in a laboratory-scale settling column.

A 1D settling model based on the mechanistic approach proposed by Bürger et al. (2013) is then applied. This model is confronted and completed with the results of the experimental study. A efficient sensitivity analysis method using the automatic differentiation software Tapenade (Hascoët and Pascual, 2004) is proposed and applied to the 1D model. Finally, the parameters of the settling velocity and effective solids stress phenomenological functions used by the latter are then identified on the basis of the experimental data.

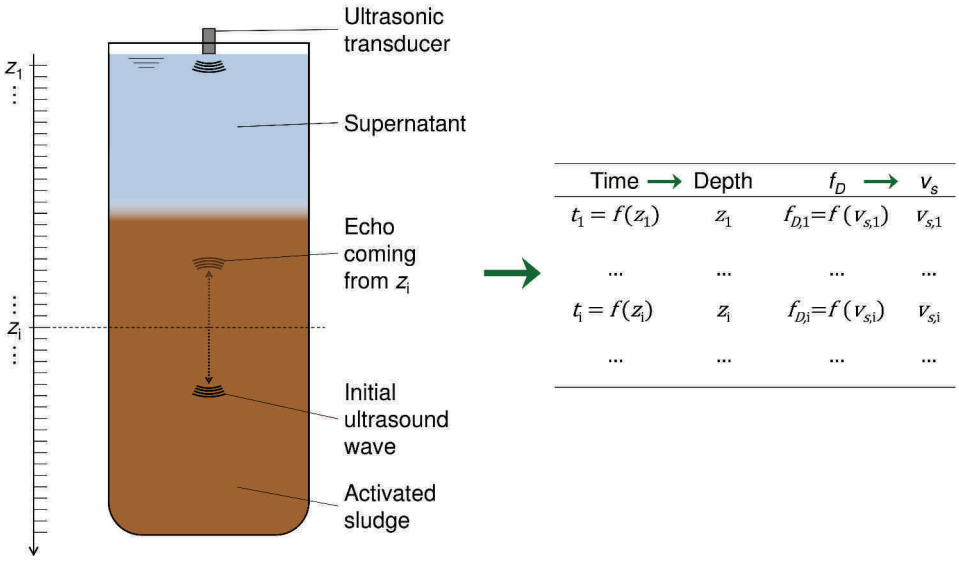

Figure 1.9 – Principle of the acoustic Doppler settling velocity profile measurement.

CHAPTER 2

Experimental study of activated sludge

The conclusions of the previous chapter point to the need for precise and extensive experimental data in the process of model development. This chapter presents the experimental methodology which was developed in order to gain insight into the internal behaviour of activated sludge suspensions and discusses the obtained results. The rheological behaviour of the sludge is studied, and the batch settling process is investigated in detail. This experimental method is also designed to provide data which can be used to calibrate a settling model. The sludge samples used for the experiments have been taken at the wastewater treatment plant managed by the Rosenmeer syndicate (Rosheim, France, Bas-Rhin). Two sampling locations have been used: either in the biological reactor or in the recirculation ditch, where the sludge concentration is generally higher. This methodology allowed obtaining samples of different concentrations. Clear water was also taken at the outlet of the treatment plant in order to perform dilutions of raw sludge samples with a diluent of the same physicochemical nature and widen the concentration range.

2.1 Rheology

2.1.1 Experimental setup

As per the conclusions of the literature review as well as the constraints associated with the properties of activated sludge, the rheological measurements were performed using a double plate geometry. The rheometer model is an AR2000 (TA Instruments, figure 2.10).

Tests were performed in order to determine the appropriate gap. Three gap values were tested: 1.0 mm, 1.5 mm, 2.0 mm. The results obtained with each gap value were in good agreement. Therefore the 2.0 mm gap was

Figure 2.10 – Rheometer used for the rheological measurements.

chosen in order to reduce the risk of friction in case of particle entrapment. The sludge samples were filtered on a 1 mm sieve prior to each experiment so as to reduce this risk further.

Six sludge samples were tested by performing shear rate ramps using the settings presented in table 2.3. Information can be gathered by plotting the shear stress applied to the sample as a function of the strain ϵ, i.e. the sample's relative deformation: such plots are called stress–strain curves. The strain rate $\dot{\epsilon}$ is linked to the shear rate $\dot{\gamma}$ by the theoretical relationship

$$\dot{\epsilon} = \frac{e}{L_0}\dot{\gamma}, \tag{2.50}$$

where

- e is the gap between the measuring geometry and the plate,
- L_0 is the initial dimension of the sample.

Figure 2.11 shows the stress–strain curves obtained with the tested samples. This result shows the existence of a yield stress, above which the sample is no longer plastic, and reached around 100.0 % of strain for all samples. As figure 2.12 shows, the value of this yield stress increases with concentration exponentially (the parameter values are given in table 2.4), which

is consistent with results from the literature (Dick and Ewing, 1967a). For deformations smaller than 100.0 %, the sludge exhibits a plastic behaviour. Once the yield stress has been exceeded, the sludge adopts a transient visco-elasto-plastic state, which corresponds to the plateaus in the stress–strain curves. This state is difficult to describe in terms of rheological functions. No clear tendency can be identified, although this state seems to end for smaller values of deformation as the sludge concentration increases.

These results are obtained with shear rate ramps. Therefore, figure 2.11 also reveals that, in the visco-elasto-plastic domain, the shear stress remains constant for increasing values of shear rate. According to equation (1.42), this means that the viscosity of the samples decreases during the visco-elasto-plastic domain. This, as well as the limit between the visco-elasto-plastic state and the viscous flow, appears clearly on figure 2.13.

Table 2.3 – Settings of the rheological experiments.

Setting	Value
Plate diameter	2 cm
Gap	2 mm
Temperature	15 °C
Pre-shear duration	2 min
Pre-shear rate	5 s^{-1}
Equilibrium	1 min
Acceleration mode	linear
Maximum shear rate	200 s^{-1}

Above a certain value of deformation, the behaviour of the sludge becomes viscous. As discussed in the literature review (section 1.1.3), several rheological models have been applied to the description of activated sludge viscosity. The model of Cross (1965), in particular, was developed to describe the behaviour of flocculated suspensions in which random link chains are formed and disrupted under shear. According to this approach, the viscosity obeys the following equation:

$$\mu\left(\dot{\gamma}\right) = \frac{\mu_0 - \mu_\infty}{1 + k\dot{\gamma}^n} + \mu_\infty, \tag{2.51}$$

where

- $\dot{\gamma}$ is the shear rate (s^{-1}),
- μ_0 is the zero-rate viscosity, i.e. the limit value of the viscosity when the shear rate tends towards zero (Pa·s),
- μ_∞ is the infinite-rate viscosity, i.e. the limit value of the viscosity when the shear rate tends towards $+\infty$ (Pa·s),

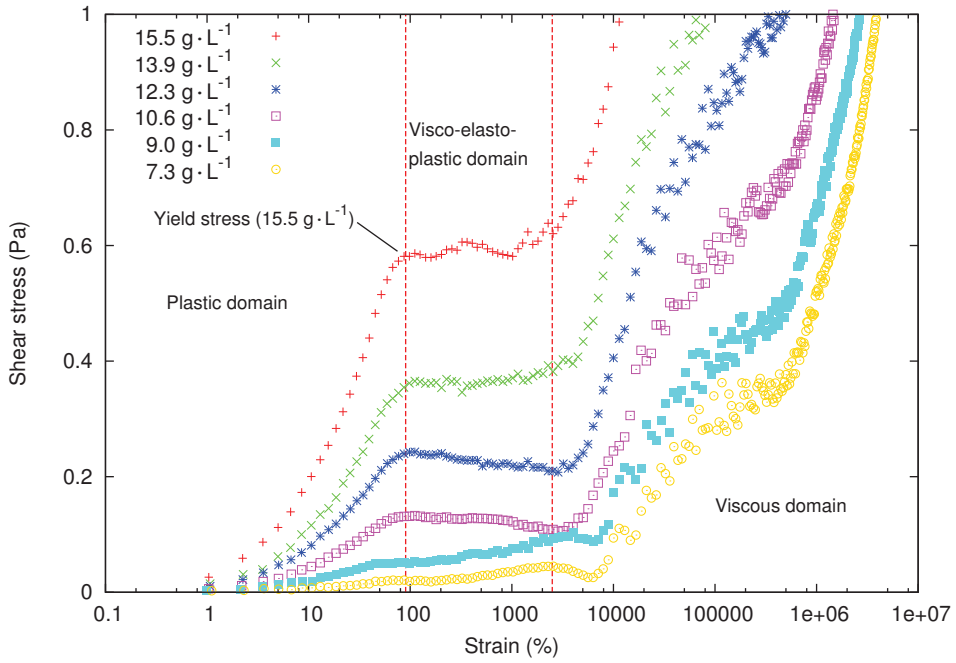

Figure 2.11 – Stress–strain curves obtained with six sludge samples of different concentrations.

- k is the consistency index (s^n),
- n is the rate index (–).

In the case of a double-plate rotational rheometer,

$$\dot{\gamma} = \frac{\omega r}{e}, \tag{2.52}$$

where

- r is the position on the radius of the measuring geometry where the viscosity is calculated (m),
- ω is the angular velocity (s^{-1}) and
- e is the geometry gap (m).

Therefore, equation (2.51) can be rewritten as follows:

$$\mu(\omega) = \frac{\mu_0 - \mu_\infty}{1 + k\left(\frac{\omega r}{e}\right)^n} + \mu_\infty. \tag{2.53}$$

Figure 2.14 shows the evolution of the apparent viscosity with respect to the shear rate obtained with six sludge samples of different concentrations.

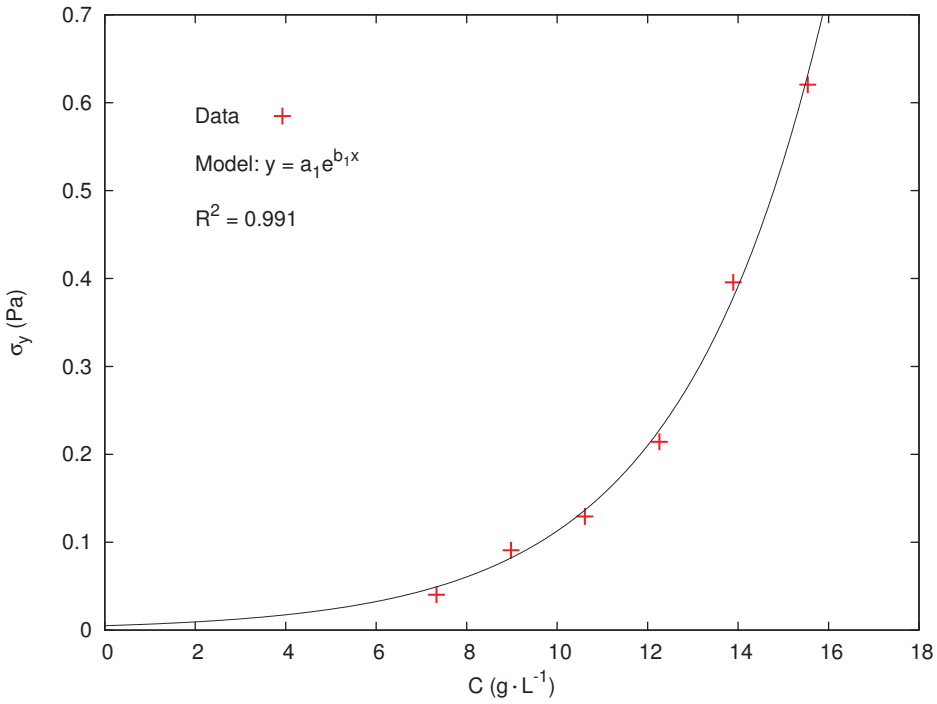

Figure 2.12 – Evolution of the yield stress σ_y with respect to the sludge concentration (the values of parameters a_1 and b_1 are given in table 2.4).

Parameters μ_0 and μ_∞ can be measured experimentally for very low and very high shear rate values respectively.

Figures 2.15 and 2.16 respectively show the evolution of μ_0 and μ_∞ with respect to the concentration. The evolution of μ_0 with respect to the concentration C can be modelled by an exponential function (the values of parameters a_2 and b_2 are given in table 2.4):

$$\mu_0(C) = a_2\left(e^{b_2 C} - 1\right) + \mu_\mathrm{w}, \tag{2.54}$$

where μ_w is the dynamic viscosity of water. The evolution of μ_∞ with respect to the concentration C can be modelled by an affine function (the value of parameter a_3 is given in table 2.4):

$$\mu_\infty(C) = a_3 C + \mu_\mathrm{w}. \tag{2.55}$$

The parameters μ_0 and μ_∞ as modelled by equations (2.54) and (2.55) are both equal to the viscosity of water μ_w when the concentration C is equal to 0 g·L^{-1}. Thus, the apparent dynamic viscosity of the sludge calculated by the Cross function (2.53) is equal to the viscosity of water when the concentration is 0 g·L^{-1}, which was expected. This result also shows that, at low shear

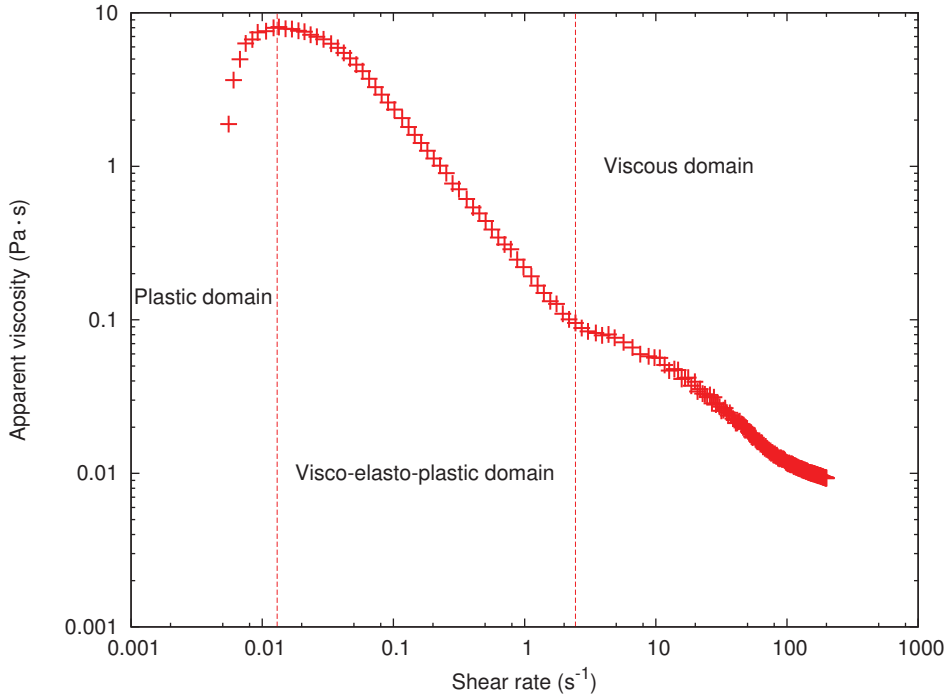

Figure 2.13 – Evolution of the apparent viscosity measured by the rheometer with respect to the shear rate.

rates, the viscosity of the sludge increases quickly with the concentration, while at high shear rates (e.g. in the recirculation), the impact of the sludge concentration is weaker.

Parameters k and n are of delicate identification, for they cannot be measured directly using the experimental data, as opposed to μ_0 and μ_∞, and have to be estimated. In order to do so, the viscosity values calculated by the rheometer software have to be adjusted, for their calculation is based on the hypothesis that the sheared fluid is Newtonian, which introduces a bias. The rheometer software evaluates the viscosity values on the basis of the relationship between the torque applied by the device T and the measured shear stress τ:

$$T(R) = 2\pi \int_0^R \tau(r)\, r^2 dr, \tag{2.56}$$

where R is the radius of the measuring geometry (m). Since $\tau = \mu\dot{\gamma}$, and $\dot{\gamma} = \omega r/e$, equation (2.56) leads to

$$T(R) = 2\pi \int_0^R \frac{\mu\omega r^3}{e} dr. \tag{2.57}$$

In the case of a Newtonian fluid, the dynamic viscosity μ is constant with respect to r, in which case the integral of equation (2.57) can be calculated

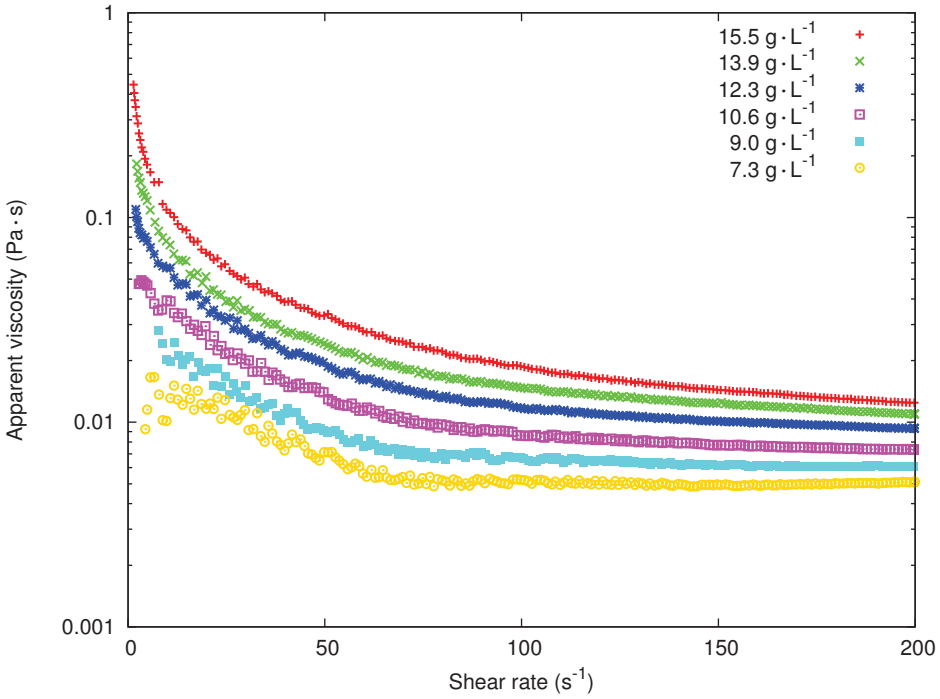

Figure 2.14 – Evolution of the viscosity with respect to the shear rate obtained with six sludge samples of different concentrations.

analytically. This yields

$$T\left(R\right) = \frac{\pi\mu\omega R^4}{2e} \tag{2.58}$$

which, since $\tau(R) = \omega R\mu/e$, can also be written

$$T\left(R\right) = \frac{\pi R^3}{2}\tau(R). \tag{2.59}$$

In the case of a Newtonian fluid, the dynamic viscosity μ can be deduced from the previous equation. However, if the fluid behaves according to a non-Newtonian behaviour law, the latter has to be taken into account when solving equation (2.57), which becomes:

$$T\left(R\right) = 2\pi\int_0^R \frac{\mu\left(\omega\right)\omega r^3}{e}dr. \tag{2.60}$$

The Cross model has been selected. Therefore, combining equations (2.53) and (2.60) leads to

$$T\left(R\right) = 2\pi\int_0^R \left(\frac{\mu_0 - \mu_\infty}{1 + k\left(\omega r/e\right)^n} + \mu_\infty\right)\frac{\omega r}{e}dr. \tag{2.61}$$

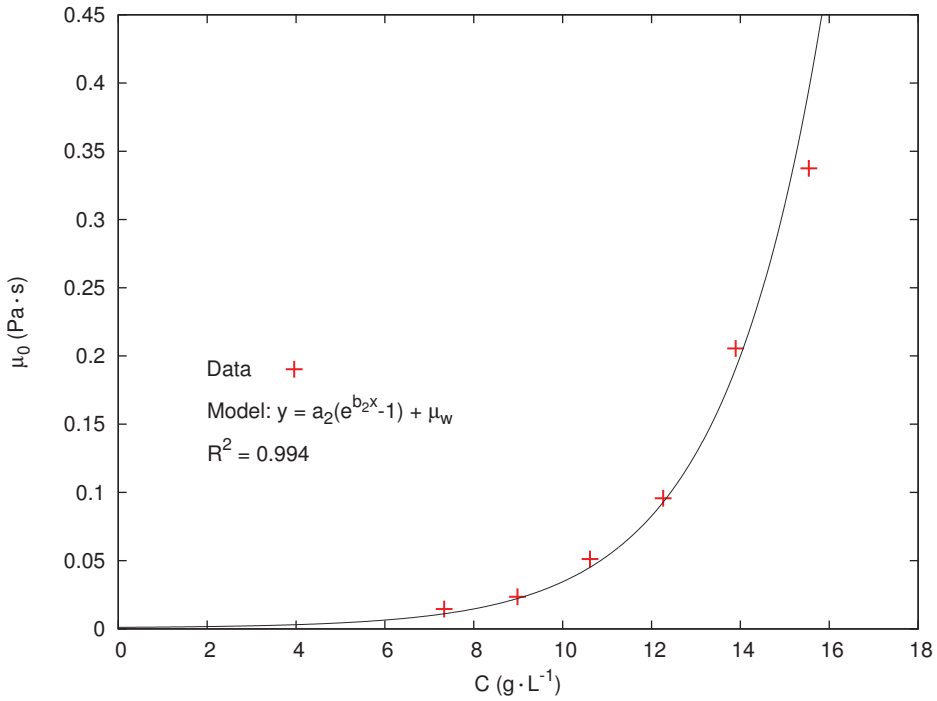

Figure 2.15 – Evolution of the rheological parameter μ_0 with respect to the sludge concentration (the values of parameters a_2 and b_2 are given in table 2.4).

Since n is a positive real number, this equation does not have an analytic solution. This integral is evaluated by using a classical trapezoidal method. In order to evaluate parameters k and n, the automatic differentiation tool Tapenade (Hascoët and Pascual, 2004) was used to obtain the partial derivatives of the state equation 2.61, and a classical identification method using the BFGS algorithm (Byrd et al., 1995) has been applied in order to evaluate the optimal set of parameters by minimising the quadratic cost function

$$\mathcal{J}(k,n) = \sum_{i=1}^{N} \left(T_i(k,n) - T_i^o\right)^2, \tag{2.62}$$

where N is the number of values used for the identification, T_i is a calculated torque value (N·m) and T_i^o is an experimental torque value (N·m).

The obtained results are presented in figure 2.17 for the consistency k, and in figure 2.18 for the rate index n. The evolution of k with the concentration is well modelled by an exponential function (the values of parameters a_4 and b_4 are given in table 2.4),

$$k = a_4 e^{b_4 C}. \tag{2.63}$$

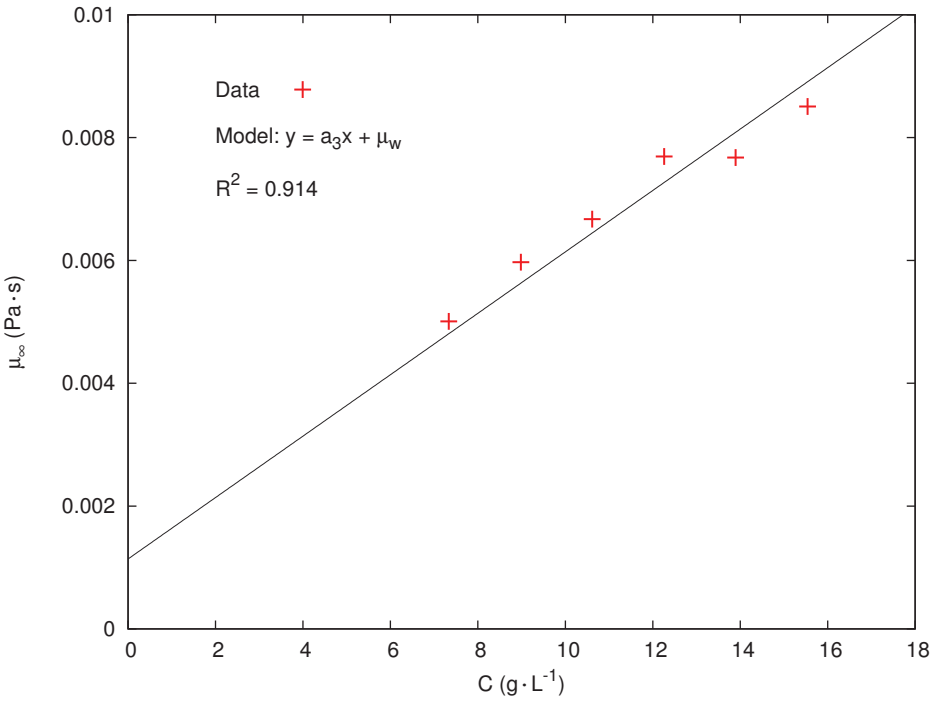

Figure 2.16 – Evolution of the rheological parameter μ_∞ with respect to the sludge concentration (the value of parameter a_3 is given in table 2.4).

Given the form of the Cross function, this means that, when the sludge concentration increases, its viscosity decreases faster with the shear rate. This is consistent with the fact that k is associated by Cross (1965) to the rupture of linkages. Indeed, the higher the concentration, the greater the number of interactions and links between the flocs. Thus, when the concentration of the sludge increases, more interparticle links are destroyed at a given value of shear rate.

The rate index n varies little over the concentration range tested. However, its evolution with the concentration is well modelled by a power function (the values of parameters a_5 and b_5 are given in table 2.4),

$$n = a_5 C^{-b_5} \tag{2.64}$$

It must be notes that relatively large confidence intervals are found for the parameters of the exponential and power functions. This shows that these parameters are strongly correlated. It is therefore delicate to generalise the parameter values presented in table 2.4 to different sludges.

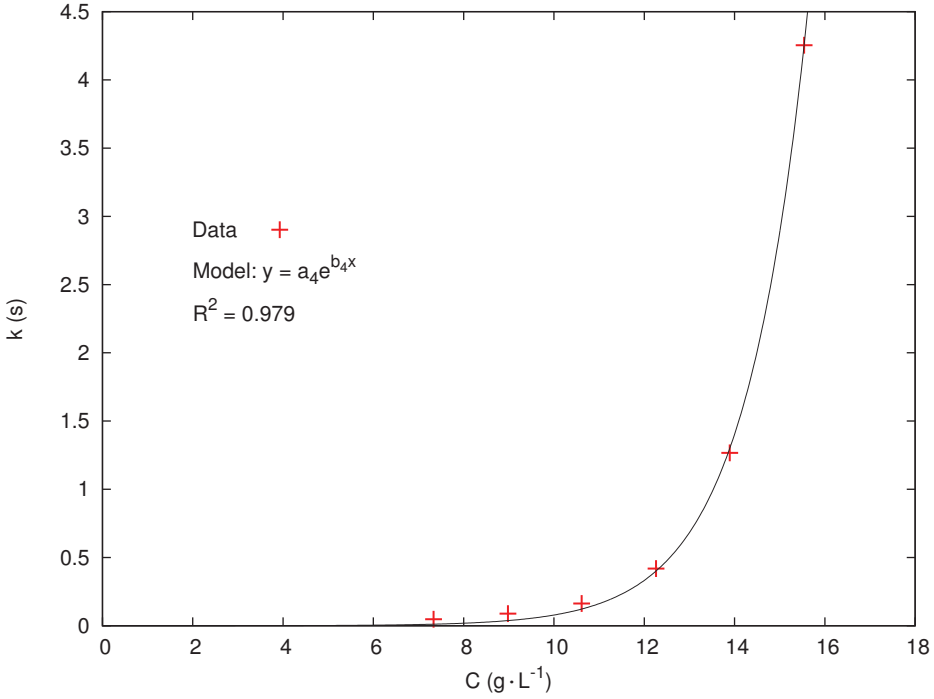

Figure 2.17 – Evolution of the rheological parameter k with respect to the sludge concentration.

Table 2.4 – Values of the rheological parameters. The confidence intervals are calculated according to the method presented by Bolster and Hornberger (2007).

Parameter	Optimal value	95 % confidence interval
a_1 (Pa)	$5.03{\cdot}10^{-3}$	$\pm\ 2.49{\cdot}10^{-3}$
b_1 ($g^{-1}{\cdot}L$)	0.31	$\pm\ 3.36{\cdot}10^{-2}$
a_2 (Pa·s)	$4.00{\cdot}10^{-4}$	$\pm\ 2.50{\cdot}10^{-4}$
b_2 ($g^{-1}{\cdot}L$)	0.44	$\pm\ 4.54{\cdot}10^{-2}$
a_3 (Pa·s)	$5.00{\cdot}10^{-4}$	$\pm\ 3.37{\cdot}10^{-5}$
a_4 (s)	$5.88{\cdot}10^{-5}$	$\pm\ 4.21{\cdot}10^{-5}$
b_4 ($g^{-1}{\cdot}L$)	0.72	$\pm\ 4.64{\cdot}10^{-2}$
a_5 (–)	7.14	$\pm\ 1.50$
b_5 ($g^{-1}{\cdot}L$)	0.89	$\pm\ 9.29{\cdot}10^{-2}$

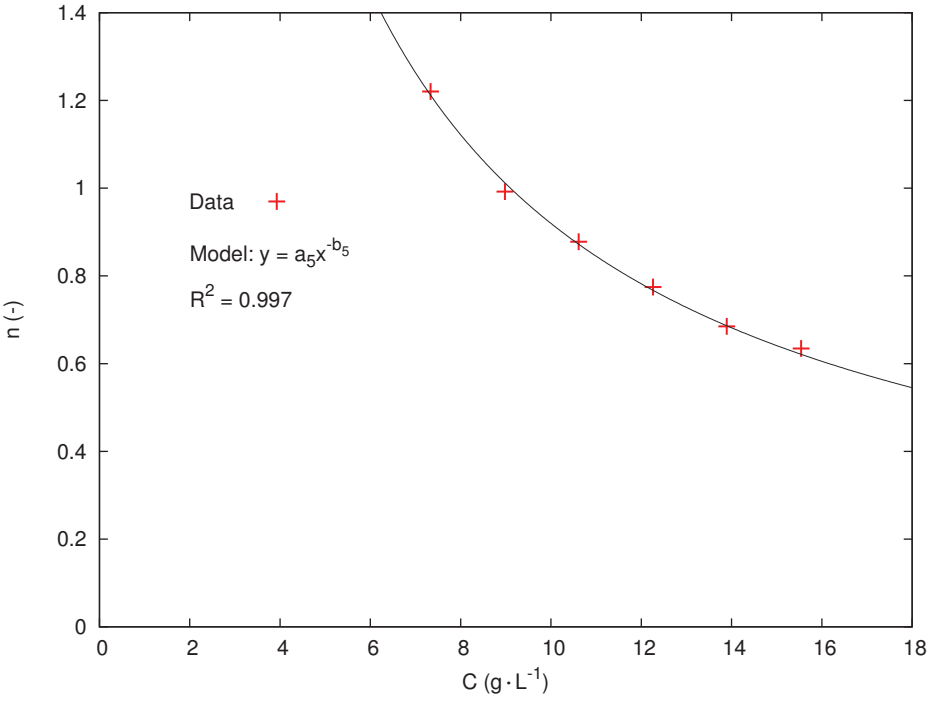

Figure 2.18 – Evolution of the rheological parameter n with respect to the sludge concentration.

2.2 Batch settling

The challenge inherent to the study of activated sludge settling is the necessity of using experimental techniques which disturb the settling process as little as possible. With this requirement in mind, an experimental method was developed that makes use of an ultrasonic transducer. This technique was applied to the detection of the sludge blanket interface and the measurement of the settling velocity inside of the sludge blanket. This section presents the data gathered by the mean of the developed experimental setup and formulates the conclusions deduced from the results obtained.

2.2.1 Experimental process

Equipment

The main body of the experimental setup is a settling column 0.4 m in diameter and 1.0 m high (figure 2.19). The column is transparent in order to allow visual observations. The suspension can be stirred by the mean of a recirculation system equipped with a volumetric pump. The liquid is pumped through four inlets located at the top of the column and injected back through four outlets at the bottom. A homogeneous concentration can thus be achieved. Stirring the suspension is also a mean of simulating the hydrodynamic conditions experienced by activated sludge in an actual treatment plant prior to secondary clarification.

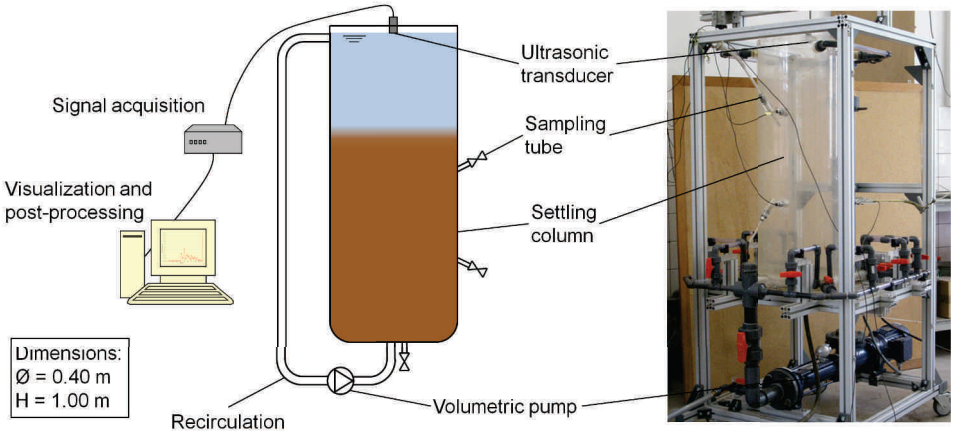

Figure 2.19 – Diagram of the experimental setup.

The settling was monitored and investigated by the mean of an ultrasonic transducer. The transducer was installed above the column to perform vertical measurements. The properties and parameters of the ultrasonic system are presented in table 2.5.

Table 2.5 – Properties and settings of the ultrasonic system.

Sensor diameter	1 cm
Maximum PRF[a]	25 Hz
Maximum PRF_{eff}	15 Hz
Carrier wave frequency	1.92 MHz
Maximum measurable velocity	1.0 $mm \cdot s^{-1}$
Number of points per profile	500

[a] Pulse Repetition Frequency

The PRF is the number of ultrasonic bursts emitted per second. The PRF_{eff} is the effective PRF, i.e. the number of emitted ultrasonic bursts that can be recorded per second. Due to electronics and computing lag times, the PRF_{eff} is smaller than the PRF. The settling velocity is the fastest at the beginning of settling experiments, hence high PRF values are necessary. After some time, when the hindered settling phase is over and settling velocities are lower, the PRF can be decreased in order to avoid an excess of data, since the latter take up large amounts of memory.

A smaller column, 18.5 cm in diameter and 30 cm high, was built in order to be able to produce large variations of the experimental conditions, particularly the non-volatile fraction of the sludge and the temperature of the suspension. This column was fitted with a rotating blade as a stirring system.

Procedure

Once sampled, the sludge was immediately transported to the laboratory and poured into the column. The ultrasonic transducer was installed in such a way that its extremity was submerged in the suspension. Then, the sensor was activated and the suspension stirred for 5 to 10 min at a rate of 10^{-3} m^3 s^{-1}. The intensity of the backscattered signal was monitored during the stirring phase. The attenuation of the signal is dependent on the volume fraction and particle size (Harker and Temple, 1988). The suspension was therefore judged homogeneous when a linear attenuation profile was achieved. Once the sludge was properly stirred according to that criterion, the pump was turned off and the acquisition started.

Data

The experimental process described above provided several kinds of data. The top of the sludge blanket can be precisely localised on the backscattering profile. Activated sludge forms a very sharp and flat interface with

the supernatant when settling in quiescent conditions. When an ultrasound burst reaches this interface, a jump appears in the backscattering profile. By monitoring the position of this jump during the experiments, it was possible to plot the settling curves of the sludge samples studied. Figure 2.20 shows backscattering profiles obtained during a batch settling experiments. It appears that, as the sludge settles, the backscattering profile becomes more and more irregular. These irregularities are a consequence of the complex makeup of activated sludge flocs. It is difficult to correlate these measurements with the concentration of the sludge. Indeed, the strength of the backscattered signal is not influenced only by the density of the medium, but also by the shape of the flocs as well as the orientation of the suspended particles relatively to the trajectory of the ultrasound wave. This last effect is particularly acute with mineral particles, such as clay fragments. Such particles can display highly asymmetrical geometries (e.g. flakes or blades). Therefore, depending on their orientation in space, the surface they oppose to the ultrasound wave can vary considerably, causing significant variations in the intensity of the backscattered signal. During the initial stirring phase preceding each settling experiment, there is considerable randomness in the movement of the particle, thus a much more homogeneous spatial distribution of the particle properties than during the settling phase. This can explain the fact that the irregularity of the backscattering profile increases during the sedimentation, as shown by figure 2.20. Nevertheless, the implemented technique yielded precise measurements of the sludge blanket height.

Using Ultrasonic Velocity Profiling, as discussed in section 1.3.2, the vertical velocity profile of the sludge was measured in both settling columns. The material and settings described earlier allowed measuring the complete settling velocity profiles inside of the activated sludge blanket. Tests were performed in order to select the appropriate frequency of the ultrasounds. On the one hand, when this frequency is increased, the wavelength of the signal is decreased, which allows detecting smaller particles. However, the attenuation is stronger, hence the ultrasound bursts may not be able to reach the bottom of the settling column. On the other hand, when the frequency of the signal is decreased, the ultrasounds are able to travel further down the suspension, but less influenced by small particles, which increases the risk of gaps in the velocity profiles.

2.2.2 Effect of the concentration

According to the literature and Kynch theory, the concentration of the sludge is the main parameter influencing the settling velocity. In order to test different sludge concentrations, several methods were used.

- Some sludge samples were diluted using water taken at the outlet of the treatment plant.

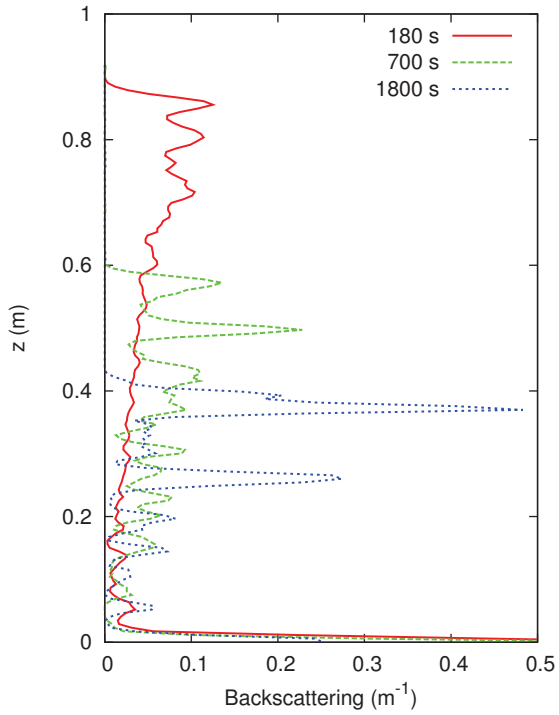

Figure 2.20 – Backscattering profiles measured during a batch settling experiment (initial concentration of the sludge: 3.5 g L^{-1}).

- As explained in the previous section, sludge samples were taken either in the biological reactor, or in the recirculation ditch. In the last case, the concentration of the samples tended to be higher, since the sludge was coming from the thickened sludge blanket in the secondary clarifier.
- Another way of achieving higher initial sludge concentrations was to thicken the samples inside of the settling column: the sludge was left to settle for some time, then the supernatant was extracted and more sludge was poured into the column.

Figure 2.24 shows settling curves obtained with eight different sludge concentrations, varying from 1.5 g·L^{-1} to 7.4 g·L^{-1}. This result reveals very sharp contrasts between the different samples, even though the range of concentration is relatively narrow. The settling curves obtained are comparable to the ones obtained with standard visual methods (e.g. Stricker et al. (2007)). The initial lag stage common to the majority of batch settling experiments (figure 2.21, up to point A) could not be visualised here due to the blind zone of the transducer. However, for all curves except 7.4 g·L^{-1}, the two subsequent regimes are clearly visible:

- a zone settling phase, during which the particle velocity at the interface

is limited by the momentum exchange between the flocs and the water (figure 2.21, from point A to point B),

- a compression phase, during which the velocity of the interface decreases (figure 2.21, after point B); the concentration becomes high enough for the flocs to be in permanent contact with each other and form a compressible matrix (Bürger et al., 2012).

Since the zone settling phase cannot be observed on the settling curve obtained with the 7.4 $g{\cdot}L^{-1}$ sample, this concentration was larger than the critical concentration of the sample, i.e. the concentration above which permanent particle-particle contact and compressive stresses exist. The 7.4 $g{\cdot}L^{-1}$ sample was therefore in compression from the beginning of the experiment.

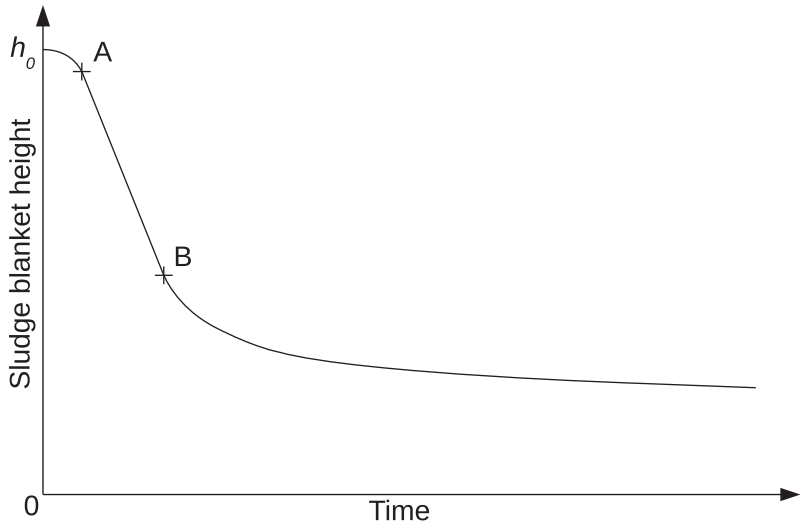

Figure 2.21 – Schematics of a typical batch settling curve (Rushton et al., 2000; De Clercq, 2006).

These results allowed calculating the hindered settling velocities v_{hs} of the sludge samples and calibrating a function of Vesilind (1968) (see section 1.1.4). Figure 2.22 presents the experimental data points and the curve of the calibrated function using a logarithmic scale. This figure indicated that the Vesilind function satisfactorily models the experimental data. Two types of sludges are distinguished according to their Non-Volatile Suspended Solids (NVSS) fraction. Indeed, most of the sludge samples studied have a NVSS fraction lower than 30 % (type 1 sludges), while a few others have a NVSS fraction between 30 and 40 % (type 2 sludges). Though all sludge samples have hindered settling velocities close to the values calculated with the Vesilind function, the type 2 sludges seem to have hindered settling

velocities slightly above the trend materialised by the curve of the Vesilind function. This effect will be discussed in detail in the following subsection.

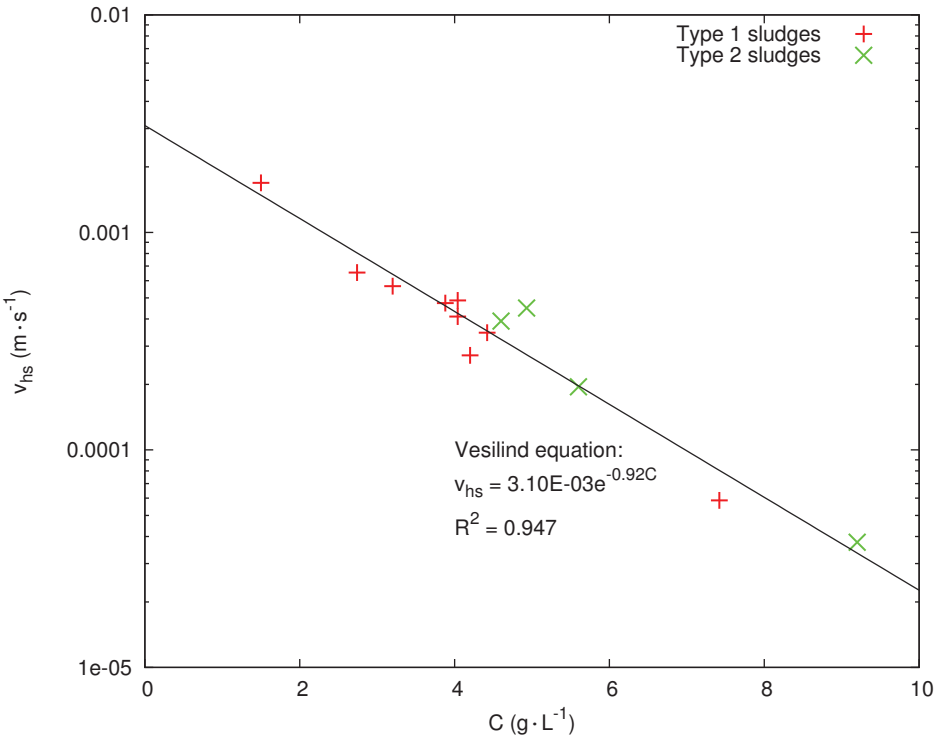

Figure 2.22 – Evolution of the hindered settling velocity with respect to the TSS and the corresponding Vesilind model. Type 1 sludges: NVSS fraction $<$ 30 %, type 2 sludges: NVSS fraction $>$ 30 %.

The initial concentration of the sludge also has an important impact on the settling velocity profile. Figures 2.25 and 2.26 show velocity profiles measured at different instants during the sedimentation of several sludge samples.

- Figure 2.25: At 5 and 10 min, between 1.5 g·L^{-1} and 5.6 g·L^{-1}, the settling velocity inside of the suspension displays fluctuations. Those fluctuations are only visible during the zone settling phase. It can be seen that they dissipate almost immediately at the bottom of the suspension and are followed by the development of a stable velocity profile, which then spreads progressively upward. The disappearance of the fluctuations corresponds to the apparition of a permanent contact between particles. The zone settling phase ends when all particles are in contact up to the top of the sludge blanket, which corresponds to the moment when the stable velocity profile ascending from the bottom of the suspension reaches the interface of the sludge blanket.

- Figure 2.26: The velocity fluctuations have disappeared. On the settling curves of figure 2.24, it can be seen that all the sludge samples are already in compression at 30 min.

Trends can be detected in the time evolution of the settling velocity fluctuations by observing the velocity profiles. Figure 2.23 shows profiles obtained at different times with a sludge of initial concentration 1.5 g·L^{-1}. Above the compression layer, materialised by the orange dashed line, zones of alternatively low and high velocities can be distinguished and followed through the successive profiles. This behaviour suggests the existence of zones of different properties, namely the floc size distribution. Indeed, particles with similar sizes settle with approximately the same velocity, wich can lead to a segregation of the flocs in different size groups within the sludge blanket.

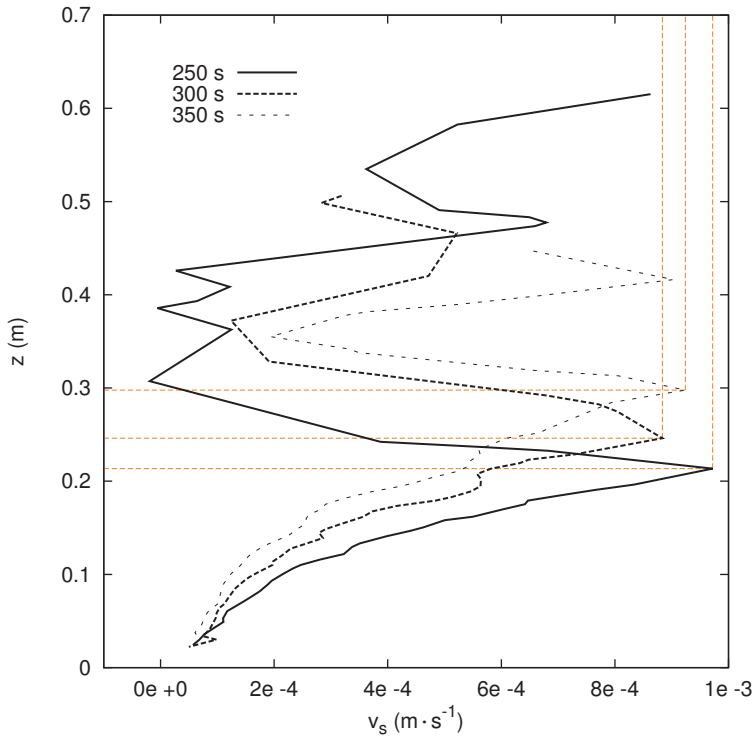

Figure 2.23 – Settling velocity profiles obtained during the settling of a sludge sample of initial concentration 1.5 g·L^{-1}. The orange dashed lines materialise the limit between the compression layer and the hindered settling layer.

On figure 2.25, the intensity of the settling velocity fluctuations in the zone settling layer appears to decrease with increasing concentration. These fluctuations can be quantified by the derivative of the settling velocity with respect to height. Table 2.6 displays the values of the standard deviation

of this derivative for different concentrations and sedimentation times. This result shows that, at a given time, the amplitude of the velocity fluctuations decreases when the concentration increases. Higher concentrations thus favour the dissipation of momentum through particle-particle interactions. Additionally, it impedes the formation of distinct zones of different particle sizes, as observed earlier.

Table 2.6 – Standard deviation values (s^{-1}) of the derivative of the settling velocity with respect to height in the zone settling layer.

Time	Concentration			
	1.5 g·L^{-1}	2.7 g·L^{-1}	3.2 g·L^{-1}	4.6 g·L^{-1}
250 s	1.3E-02	7.8E-03	5.2E-03	1.7E-03
300 s	1.2E-02	7.0E-03	3.9E-03	1.4E-03
350 s	8.4E-02	5.1E-03	2.8E-03	1.2E-03

Even though the initial concentration of the sludge is the main parameter affecting the settling velocity, other effects are brought to attention by comparing the 4.2 g·L^{-1} and 4.6 g·L^{-1} settling curves on figure 2.24. Despite the higher concentration, the sludge blanket at 4.6 g·L^{-1} is lower during the entire experiment. It appears that this sludge contains a higher percentage of non-volatile suspended solids (NVSS). This fraction of the suspended matter often contains mineral components of high density, such as clay. Rainwater runoffs can increase the percentage of NVSS in the sludge by transporting inorganic soil elements to the wastewater treatment plant. In addition, the temperature of the experiment with the 4.6 g·L^{-1} sludge is 4 °C higher than that of the other experiment. This can have a positive effect on the settling velocity by decreasing the viscosity of water, thus reducing the drag on the flocs. In order to have a better insight into the influence of the NVSS and the temperature on the sedimentation of the sludge, further experiments were performed.

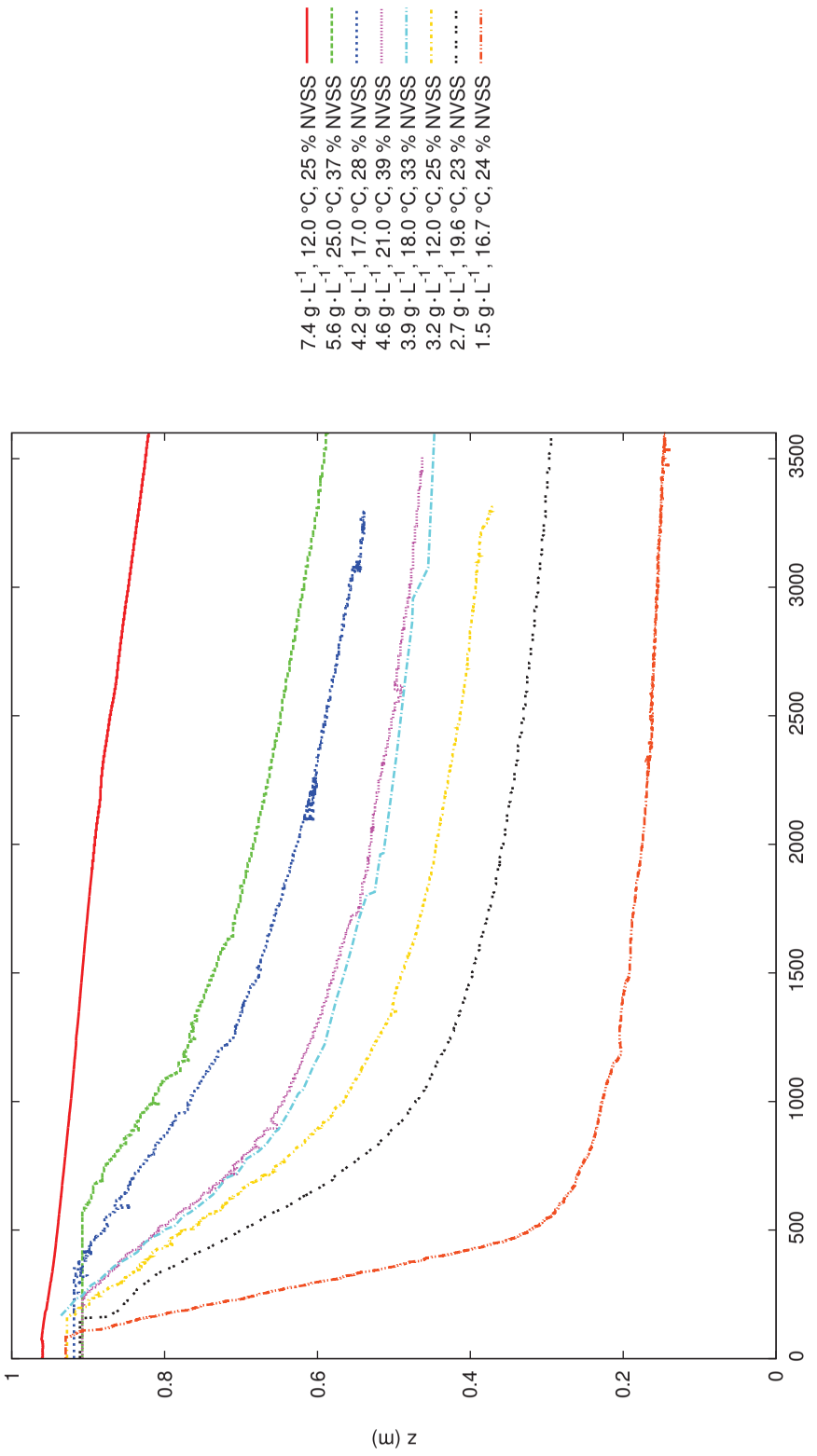

Figure 2.24 – Settling curves obtained with sludge samples of different concentrations.

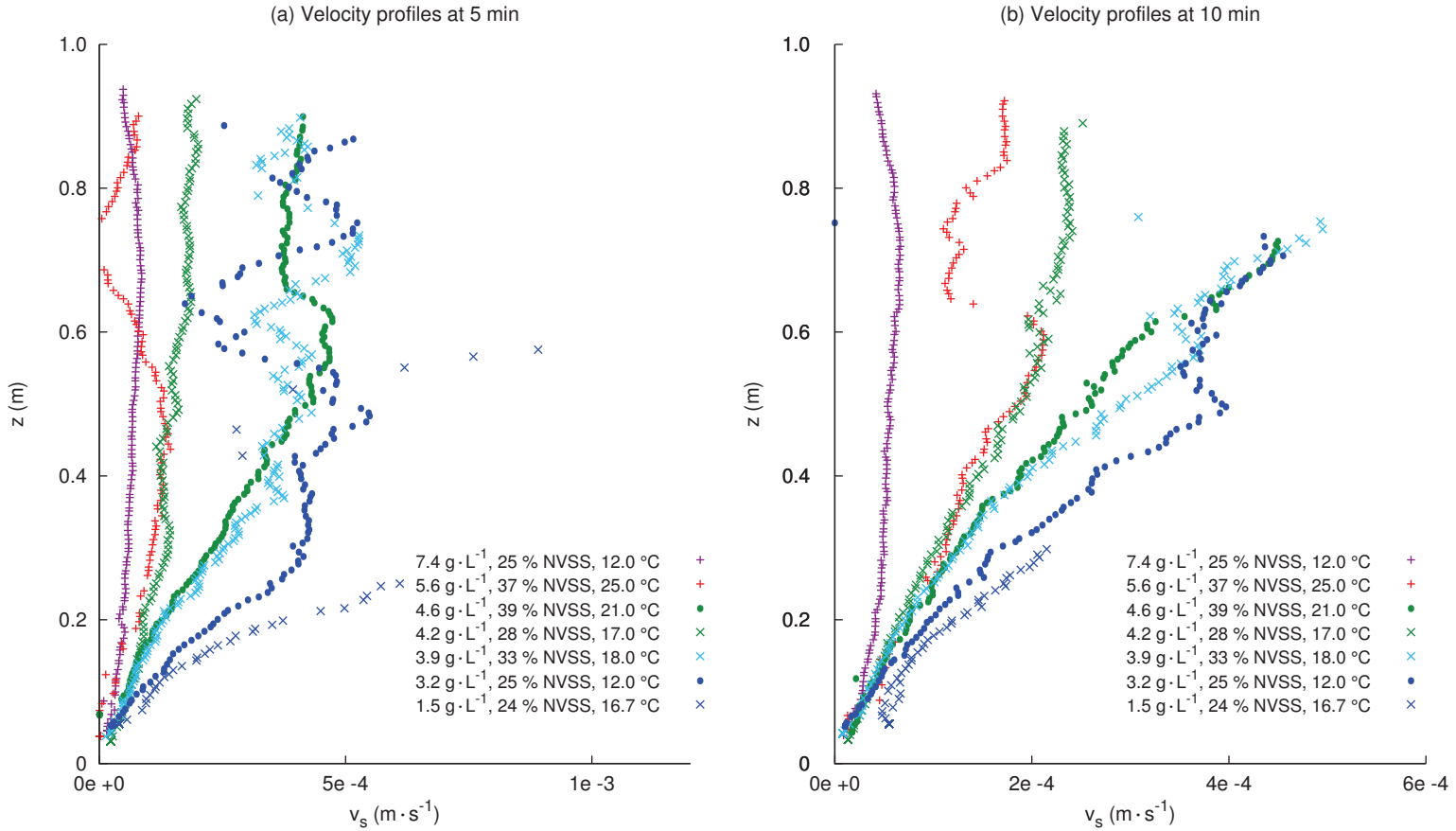

Figure 2.25 – Settling velocity profiles obtained with sludge samples of different concentrations at (a) 5 min and (b) 10 min of sedimentation.

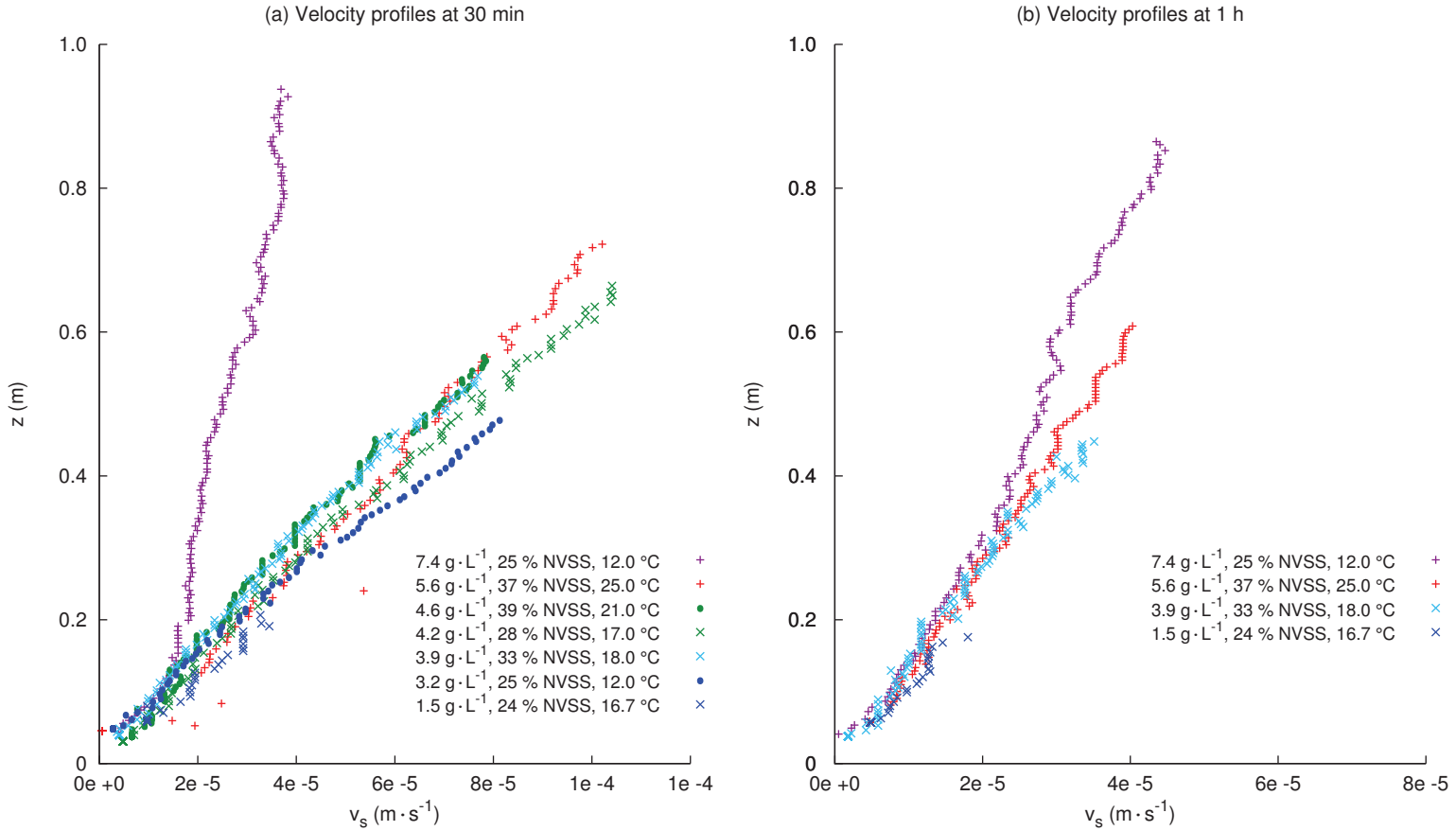

Figure 2.26 – Settling velocity profiles obtained with sludge samples of different concentrations at (a) 30 min (left) and (b) 60 min (right) of sedimentation.

2.2.3 Influence of the non-volatile suspended solids

Influence on the settling

Different NVSS fractions were achieved by adding loess to the sludge. Since loess is an abundant sediment in nature, it is easy to obtain and represents a realistic testing material. The raw, dry loess was first mixed to water in order to obtain a mineral suspension of known concentration. This suspension was used to artificially increase the NVSS fraction of several sludge samples.

Figure 2.27 shows settling curves obtained with different concentrations of additional loess in the large and the small settling columns. In figure 2.27.a, settling curves obtained in the large settling column by progressively increasing the amount of NVSS in a raw sludge sample of initial concentration 4.9 g·L^{-1} are displayed. Two observations can be made.

- Even though the addition of loess results in an increase of the total concentration of the suspension, it yields lower sludge blanket heights.
- Small amounts of additional NVSS produce sizeable impacts on the settling curve.

In order to emphasise the influence of the NVSS fraction of the sludge, larger loess concentrations were added to a sludge sample of initial concentration 4.0 g·L^{-1} in the small settling column. The settling curves thus obtained are shown in figure 2.27–(b). It appears that the addition of loess consistently lowers the sludge blanket, but does so less and less as the additional loess concentration increases. Nevertheless, in the context of this experiment, sludge suspensions with increased NVSS fractions do not appear to reach an earlier state of equilibrium, which indicates that adding loess to the sludge increases its compressibility.

The hindered settling velocity v_{hs} was evaluated for each experiment by measuring the slope of the linear portion of the settling curves. Figure 2.28 shows the percentage of increase of v_{hs} with respect to the percentage of additional loess concentration. This result shows a strong linear increase of the hindered settling velocity.

On the other hand, the impact of the NVSS on the velocity in the compression region is weaker. Figure 2.29 juxtaposes velocity profiles obtained in the small settling column with a raw sludge sample of concentration 4.0 g·L^{-1} and with the same sludge mixed with 12.0 g·L^{-1} of loess. Despite the lower sludge blanket of the loess-densified sludge, the velocity profiles are remarkably similar. This observation is confirmed by the velocity contours of figures 2.30 and 2.31. In both cases, the hindered settling phase ends around 200 s, after which the velocity contours are comparable. Only the position of the sludge blanket interface changes significantly.

In order to quantify the impact of loess on the density of the sludge, further experiments were carried out.

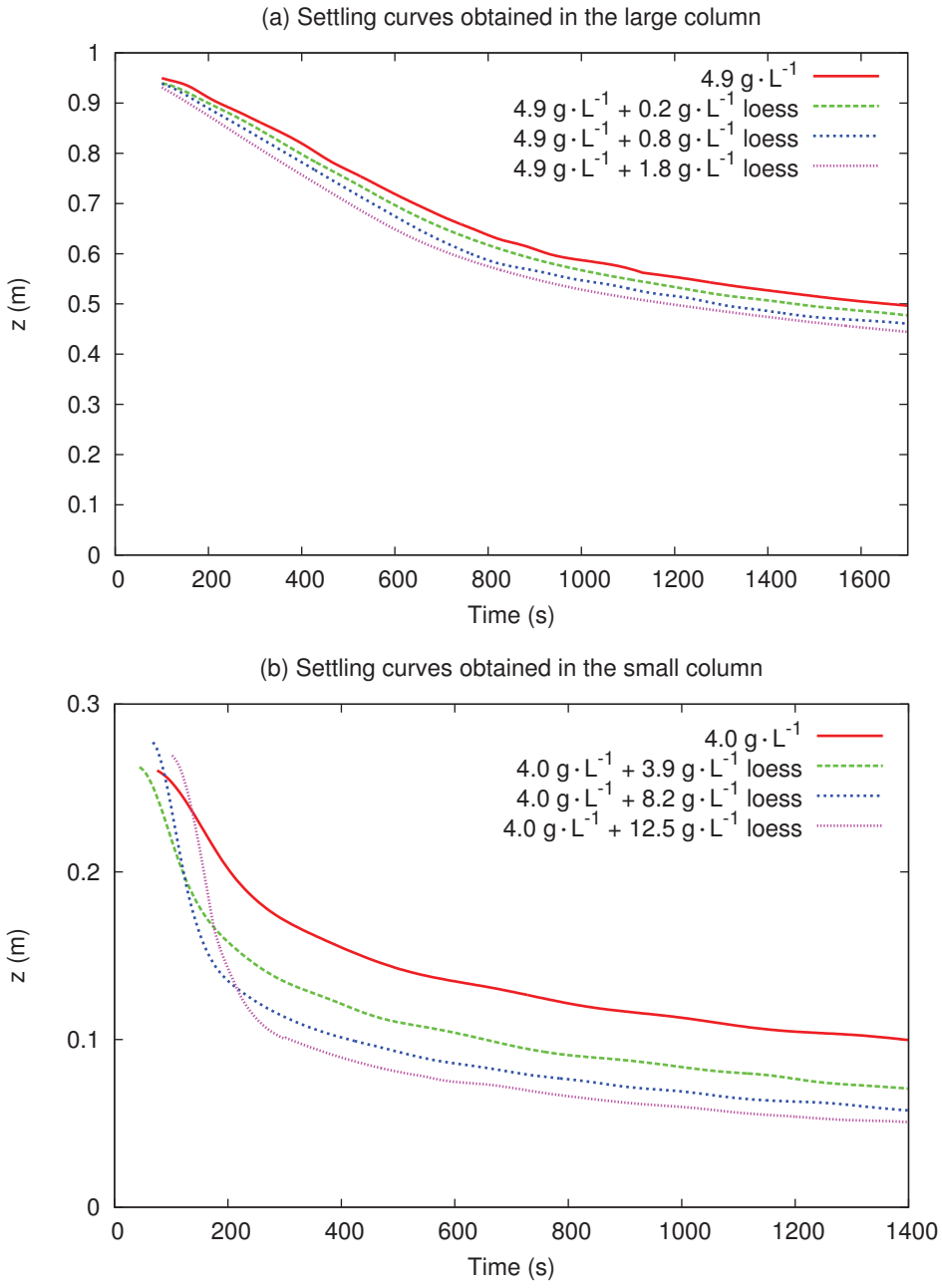

Figure 2.27 – Settling curves obtained by adding loess to a sludge sample in (a) the large settling column and (b) the small settling column.

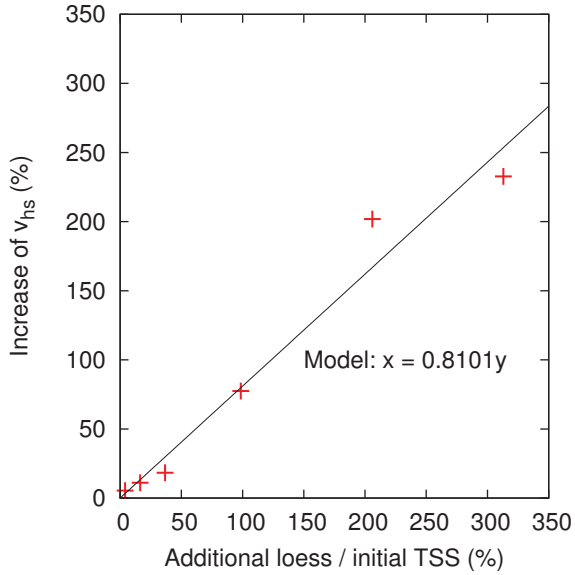

Figure 2.28 – Evolution of the hindered settling velocity as a function of the percentage of NVSS added to the initial concentration.

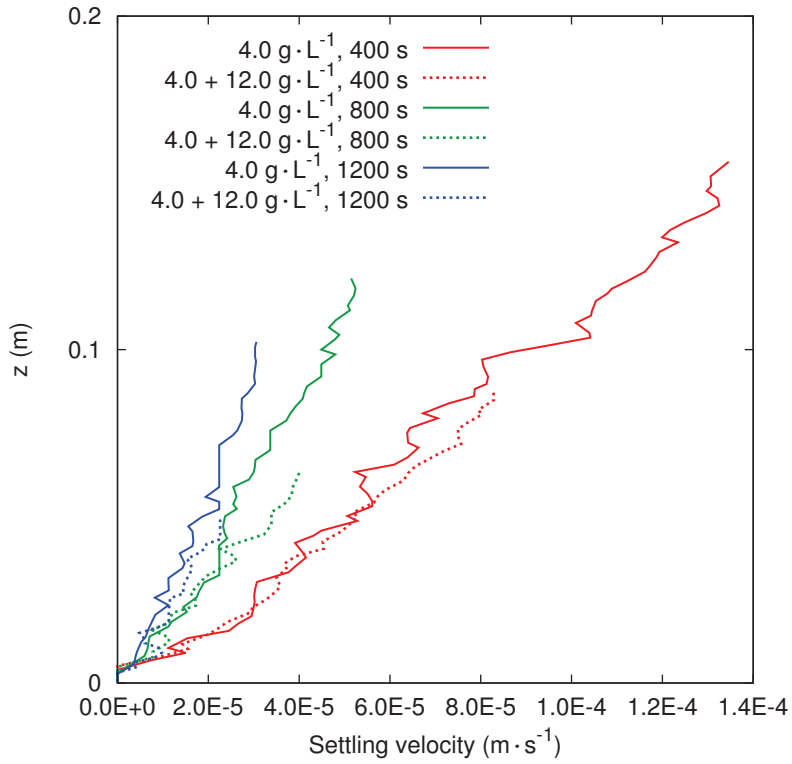

Figure 2.29 – Velocity profiles obtained with the 4.0 g·L^{-1} sludge and the 4.0 + 12.0 g·L^{-1} sludge in the small settling column.

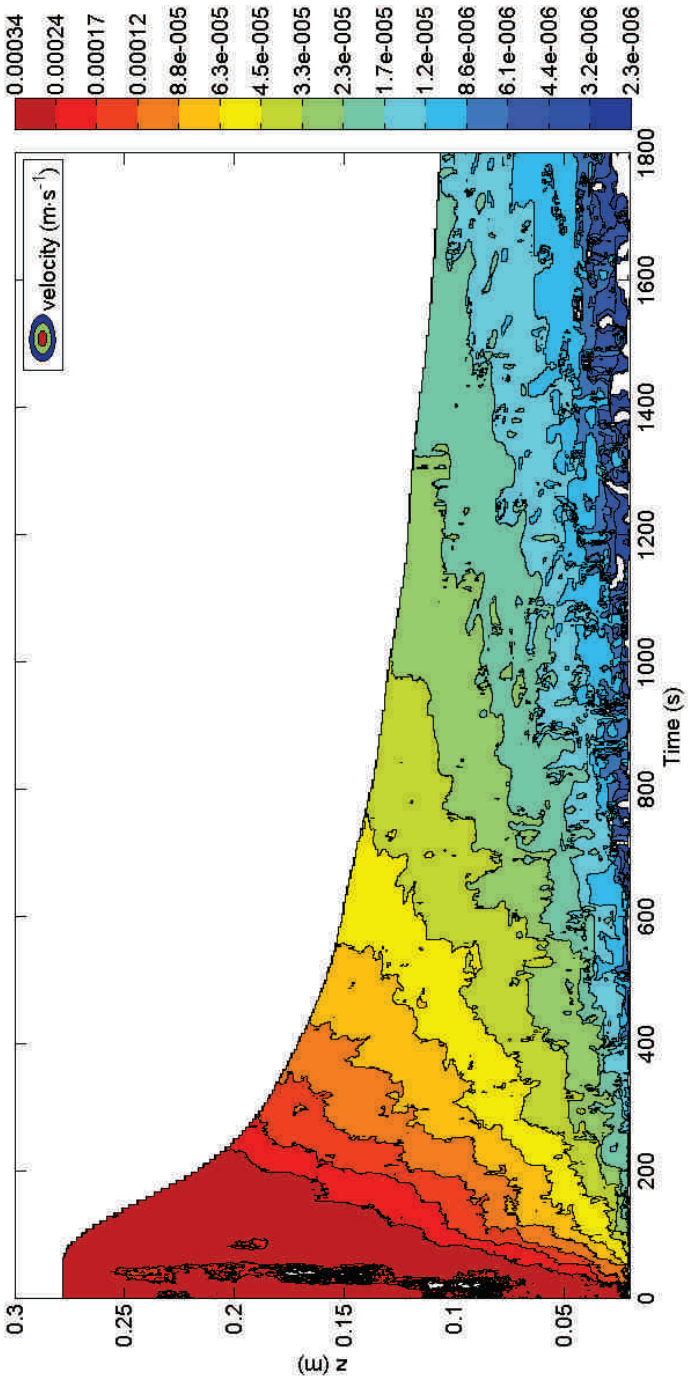

Figure 2.30 – Velocity contours obtained with a 4 g·L^{-1} sludge in the small settling column.

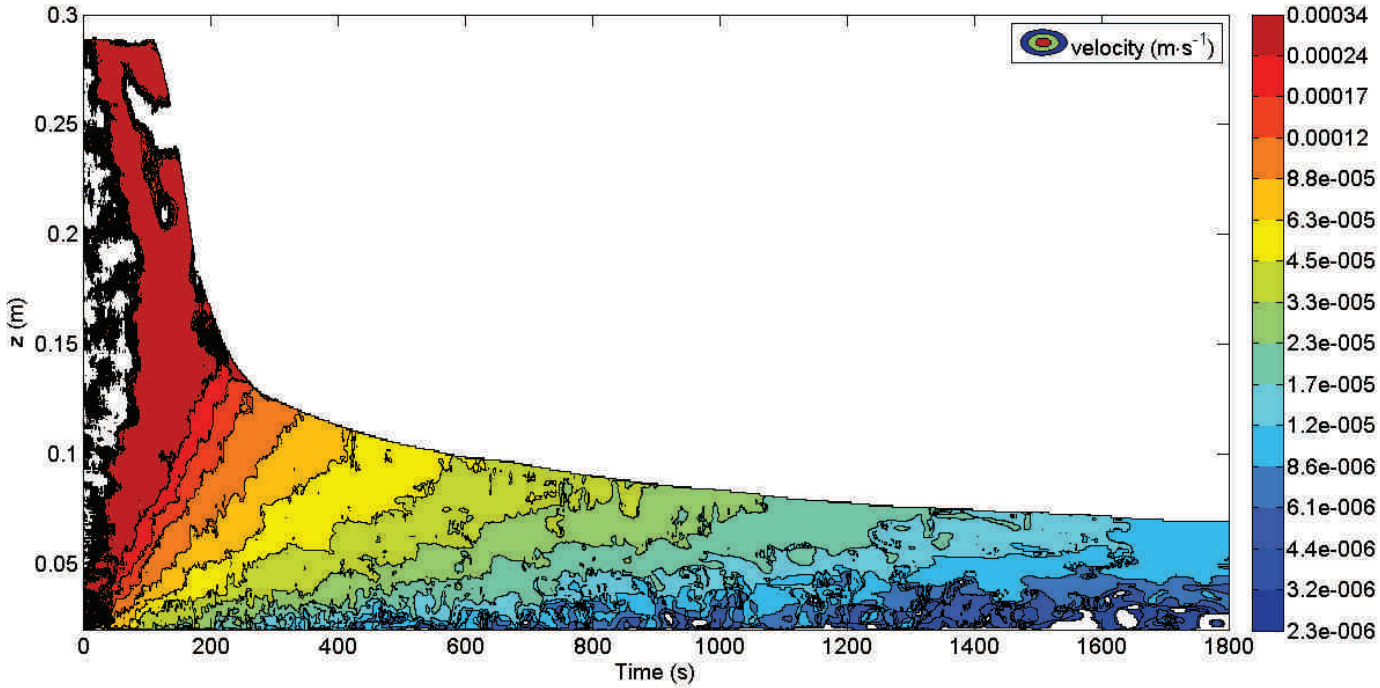

Figure 2.31 – Velocity contours obtained with a 4 g·L^{-1} sludge mixed with 12 g·L^{-1} of loess in the small settling column.

Influence on the density of activated sludge

Pycnometry experiments were performed in order to determine the density of activated sludge samples mixed with different amounts of additional loess. In order to measure the density of a sample, it has to be centrifuged in order to separate flocs and water. Therefore, tests were first carried out in order to evaluate the influence of the centrifuging time at the maximum rate of centrifuging (4200 RPM) on the density measurements. Three centrifuging times were tested: 20 min, 30 min and 40 min. The measured density was the same for each centrifuging time: approximately 1.04.

The pycnometry procedure is the following:

- the pycnometer is filled with distilled water up to the line of reference using a Pasteur pipette, then weighed, which gives a mass m_1,
- a sludge sample is centrifuged at 4200 RPM for 20 min in a sample tube of known mass m_t,
- the water is extracted from the centrifuged sample,
- the pycnometer filled with distilled water and the sample tube containing the centrifuged sludge are weighed together, which gives a mass m_2,
- the sample is placed in the pycnometer, and distilled water is added up to the line of reference,
- the pycnometer containing the sample and distilled water is weighed, which gives a mass m_3.

The density of the sludge d_s is obtained by virtue of the following relationship:

$$d_\mathrm{s} = \frac{m_2 - m_\mathrm{t} - m_1}{m_2 - m_\mathrm{t} - m_3}. \tag{2.65}$$

The sludge sample used for this experiment had an initial concentration of 3.7 g·L^{-1}. Figure 2.34 shows the increase of the density of this sample with respect to the percentage of loess added to the initial concentration. The density of the raw sample, 1.01, was less than that of the sample used for the centrifuging velocity tests. Despite some irregularities in the measurements, the result obtained shows a clear linear increase of the sludge density. By comparing this result to figure 2.28, it seems that the hindered settling velocity v_hs is very sensitive to small variations of the sludge density.

Conclusion

The NVSS fraction of the sludge mainly impacts the velocity in the hindered settling phase. When loess is added to the sludge, the usual effects

of increasing the concentration (lower settling velocities, higher sludge blanket) are outbalanced by the increased density of the suspension. Since the sludge blanket is lower at a given time, the concentration of the sludge is higher. However, the settling velocity profiles and contours showed that the settling velocity in the compression phase was not significantly modified by an increase of the NVSS fraction of the sludge.

Figure 2.32 – Pycnometer containing an activated sludge sample.

Figure 2.33 – Clay suspension used to modify the NVSS fraction of the sludge samples.

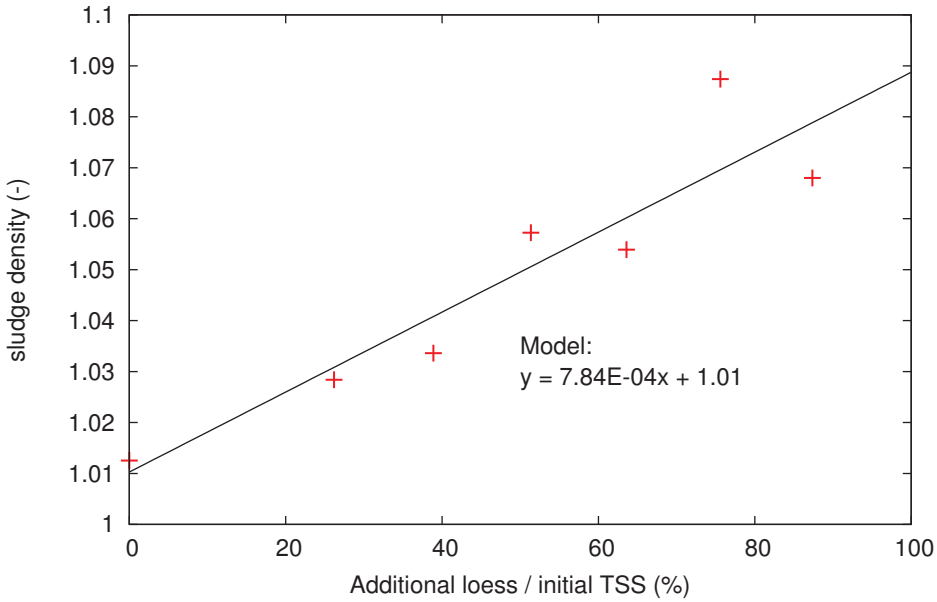

Figure 2.34 – Evolution of the sludge density with respect to the percentage of loess added to the initial concentration (3.7 $g \cdot L^{-1}$).

Since secondary clarifiers may also be subject to large variations of temperature, the effect of the latter was subsequently investigated.

2.2.4 Influence of the temperature

Wastewater treatment plants are exposed to large seasonal changes of temperature, particularly in Alsace, were this study was carried out. Figure 2.35 shows settling curves obtained in the large settling column with raw sludge samples at different temperatures. This result suggests that the sludge blanket height decreases when the temperature increases. However, since the concentration and NVSS fraction are different from one sample to another, it is difficult to pinpoint the influence of the temperature. Experiments were thus carried out to this end. Since controlling the temperature of the suspension in the large settling column is not feasible, the small settling column was used.

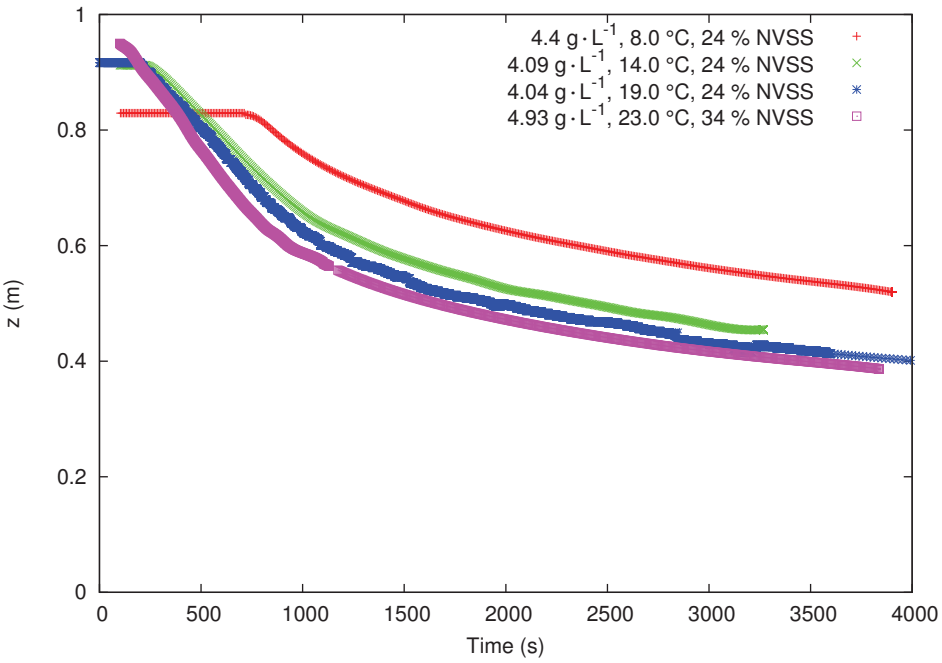

Figure 2.35 – Settling curves obtained at different temperatures in the large settling column.

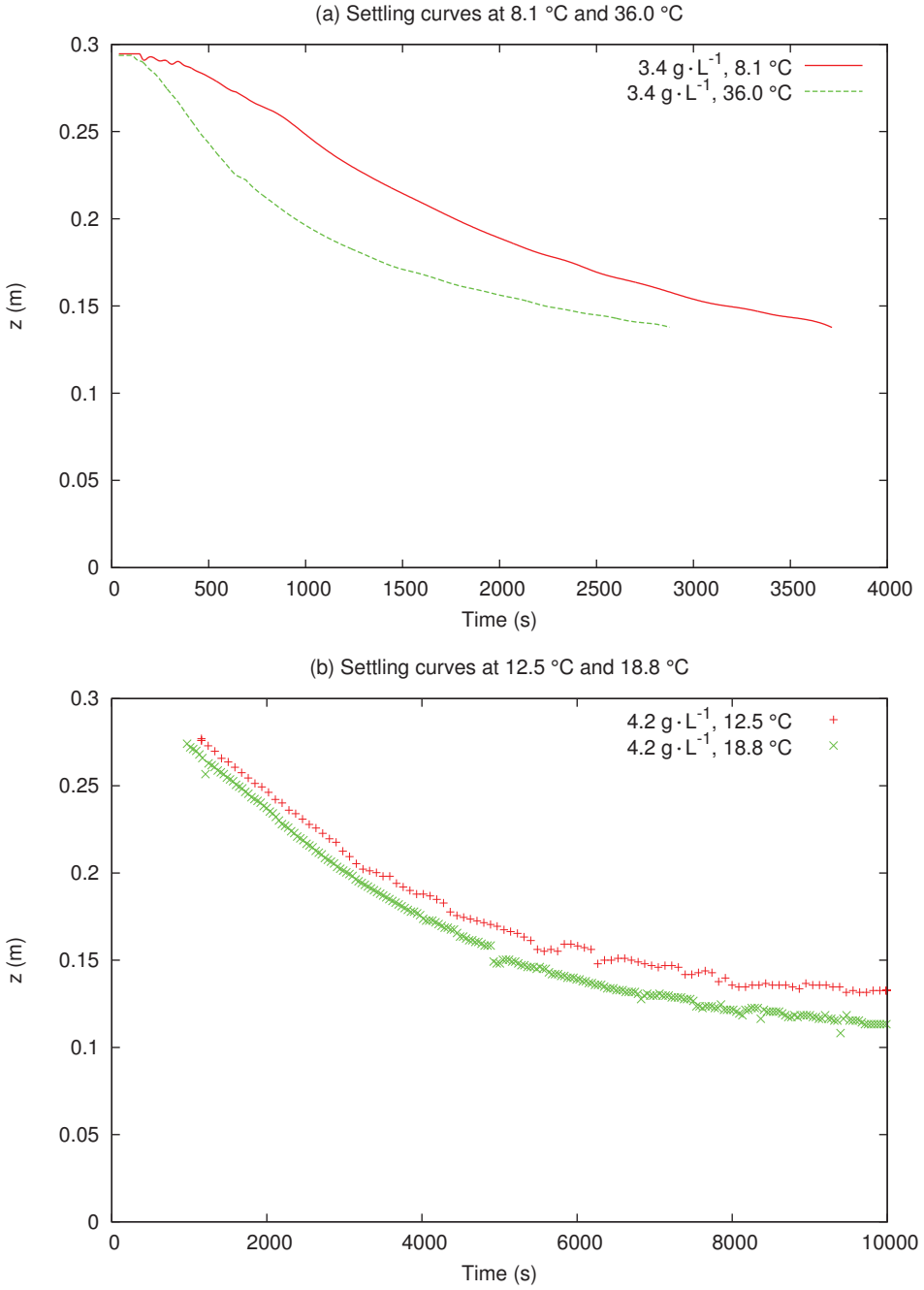

Figure 2.36 – Settling curves obtained at different temperatures in the small settling column.

Figure 2.36.a shows settling curves obtained in the small settling column with the same sludge sample at two different temperatures: 8.1 °C and 36.0 °C. The sludge blanket height is clearly lower at the hotter temperature.

A higher temperature may increase the settling velocity by reducing the viscosity of water, thus the drag exerted on the flocs. The effect of the temperature persists with time, as appears on the two settling curves of figure 2.36–b, both obtained with the same sludge sample during approximately 3 h of sedimentation at different temperatures. As well as reducing the viscosity of water, a higher temperature may also reduce the viscosity of the sludge blanket in compression, which can thus thicken more easily under its own weight.

Conclusion

Although the temperature of the sludge suspension is difficult to control and its influence not easily distinguishable from that of other parameters, the experimental results obtained clearly show that an increase of temperature lowers the sludge blanket. This can be linked to the decreased water viscosity: since the flow properties of water are improved, it exerts less drag on the flocs and can circulate more easily inside of the sludge blanket in compression. Furthermore, since the sludge contains an important amount of water, it also becomes less viscous at higher temperature and thus deforms more easily during the compression phase. This effect is not taken into account in most of the current modelling frameworks and requires further investigation.

2.2.5 Long term effects

The previous sections highlighted the sensitivity of activated sludge settling to such parameters as the concentration, the non-volatile fraction of the sludge and the temperature. They also showed that activated sludge suspensions in batch settling evolve over long periods of time. The changes experienced by the sludge during its settling will be presented and discussed hereafter. Particular attention will be paid to the development of compression.

Settling velocity

As observed in section 2.2.3, the settling velocity during the compression phase is not very sensitive to variations of the non-volatile fraction of the sludge, and the velocity contours display a regular evolution with time. Figure 2.37 shows velocity contours obtained during 2 h of sedimentation of a sludge of initial concentration 3.9 g·L^{-1}. It appears that the velocity isolines, which separate the different levels of the contours, are fairly linear, which can be related to the theory of Kynch (1952). It can thus be inferred that the velocity isolines are straight lines, the equation of which links the height z (m) and the time t (s),

$$z = \lambda v_s t, \tag{2.66}$$

where v_s is the settling velocity along an isoline ($\mathrm{m{\cdot}s^{-1}}$) and λ is a constant (–). Therefore, while the previous equation is valid, the settling velocity inside of the sludge blanket can be written

$$v_s = \frac{z}{\lambda t}. \tag{2.67}$$

This observation suggests that the internal behaviour of an activated sludge blanket is similar to that of an emulsion. This implies that the floc matrix behaves as a primary continuous phase through which dispersed water bubbles of inferior density ascend. It appears that, when equation (2.67) applies, the settling velocity is independent of the sludge concentration. In order to evaluate the value of the coefficient λ, linear regressions have been performed on settling velocity profiles at different times of sedimentation and with different sludges. Table 2.7 shows the results thus obtained. In order to assess the behaviour of the settling velocity over all the sludges tested, the average value of λ was calculated and used to plot the trend line appearing in the velocity profiles of figures 2.38 to 2.41.

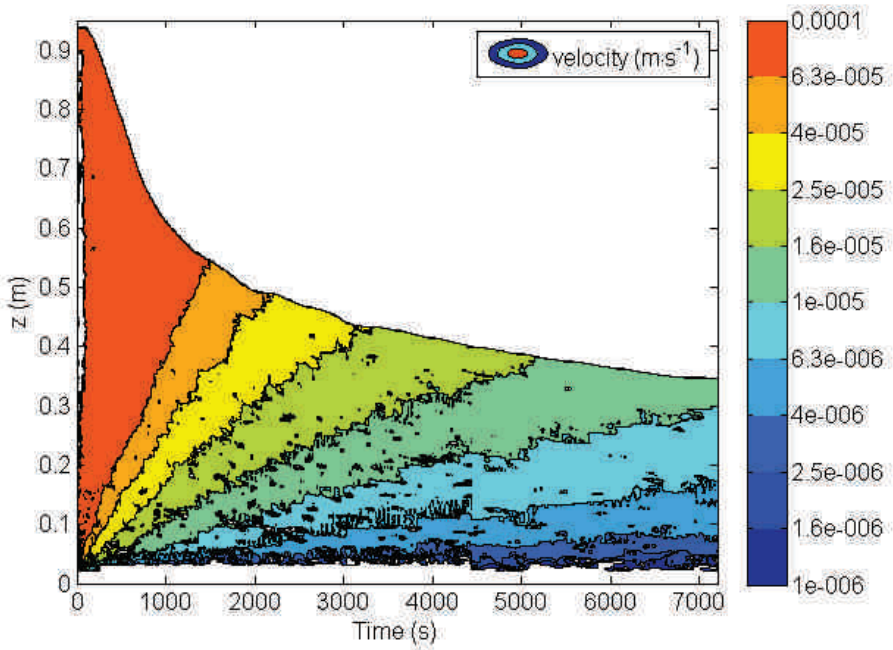

Figure 2.37 – Evolution of the settling velocity profile of an activated sludge suspension as a function of time during 7200 s (initial concentration: 3.9 $\mathrm{g{\cdot}L^{-1}}$).

On figure 2.38–b, it can be seen that, in the region of the suspension where the velocity fluctuations predominant in figure 2.38.a have disappeared, the

Table 2.7 – Values of the coefficient λ (2.67) obtained by linear regressions carried out on velocity profiles obtained with different sludge samples at different times.

Sludge properties	λ (1800 s)	λ (3600 s)	λ (7200 s)	λ (10800 s)
5.6 g·L^{-1}, 38 % NVSS, 25 °C	3.90	4.03	3.29	3.01
5.0 g·L^{-1}, 40 % NVSS, 17 °C	3.79	3.57	3.54	2.96
4.9 g·L^{-1}, 34 % NVSS, 23 °C	3.39	3.46	2.71	2.39
4.4 g·L^{-1}, 24 % NVSS, 8 °C	4.05	3.67	3.29	2.99
3.9 g·L^{-1}, 33 % NVSS, 18 °C	4.18	3.74	3.30	2.77
Average		3.40 ± 0.49		

velocity profiles are already close to the general trend line expressed by equation 2.67. Where the fluctuations have disappeared, the velocity profiles assume a slightly concave shape.

In figure 2.39, it appears that the model fits the different velocity profiles fairly well, except at 7.4 g·L^{-1}. In figure 2.39.a, the lower part of the velocity profile at 7.4 g·L^{-1} is nonetheless aligned with the other velocity profiles. At 1 h, in figure 2.39.b, The 7.4 g·L^{-1} profile has moved closer to the other profiles. It thus appears that, though the 7.4 g·L^{-1} sludge initially has a behaviour different from the other samples, this behaviour tends to change and become close to the general trend.

In figure 2.40.a, all the profiles are well aligned with the model line. Equation (2.67) is therefore still valid. This equation can therefore be applied during sedimentation times consistent with the duration of industrial processes and classical batch settling experiments. In figure 2.40.b, however, the velocity profile diverge from the model line and exhibit a slightly convex shape in the upper part of the sludge blanket. This indicates that the velocity gradient decreases near the top of the latter.

The decrease of the velocity gradient observed in the upper layers of the sludge blanket is confirmed in figure 2.41. This result indicates that, in the vicinity of the sludge blanket interface, the sludge settles at homogeneous velocity and concentration. In this region, the resistance of the sludge to deformation and, to a certain extent, the hydraulic gradient due to the circulation of water inside of the floc matrix compensate the effect of gravity. This behaviour can also be observed on the shape of the velocity isolines. Figures 2.42 and 2.43 show settling velocity contours measured during long batch settling experiments in the large settling column. It appears that, after 2 h, the velocity isolines tend to curve upward in the upper part of the suspension, which corroborates the previous observations. In order to

emphasise this effect, extended batch settling experiment were carried out in the small settling column. Figure 2.44 displays the settling velocity contours thus obtained with a sludge of initial concentration 4.2 $g{\cdot}L^{-1}$. This result shows that the effect discussed is proportionally more important in a settling column of smaller dimensions.

The previous observations show that, despite varying properties, the different sludges studied show common behaviours, particularly in terms of settling velocity during the compression phase. Given the quality and quantity of the velocity data obtained, they can be used to evaluate the evolution of the concentration inside of the settling column, which will be discussed hereafter.

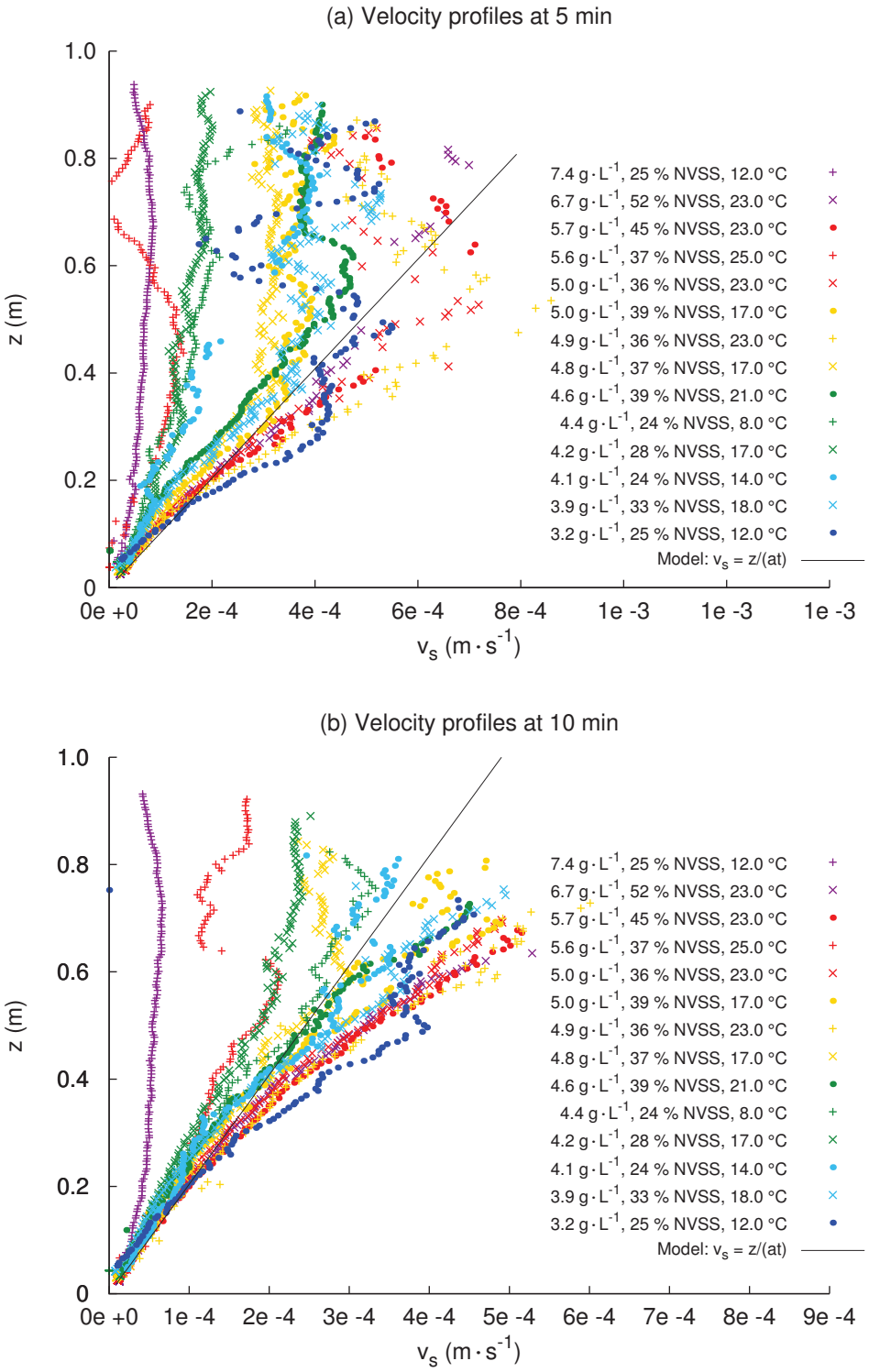

Figure 2.38 – Velocity profiles obtained with different sludge samples in the large settling column after (a) 5 and (b) 10 min of sedimentation.

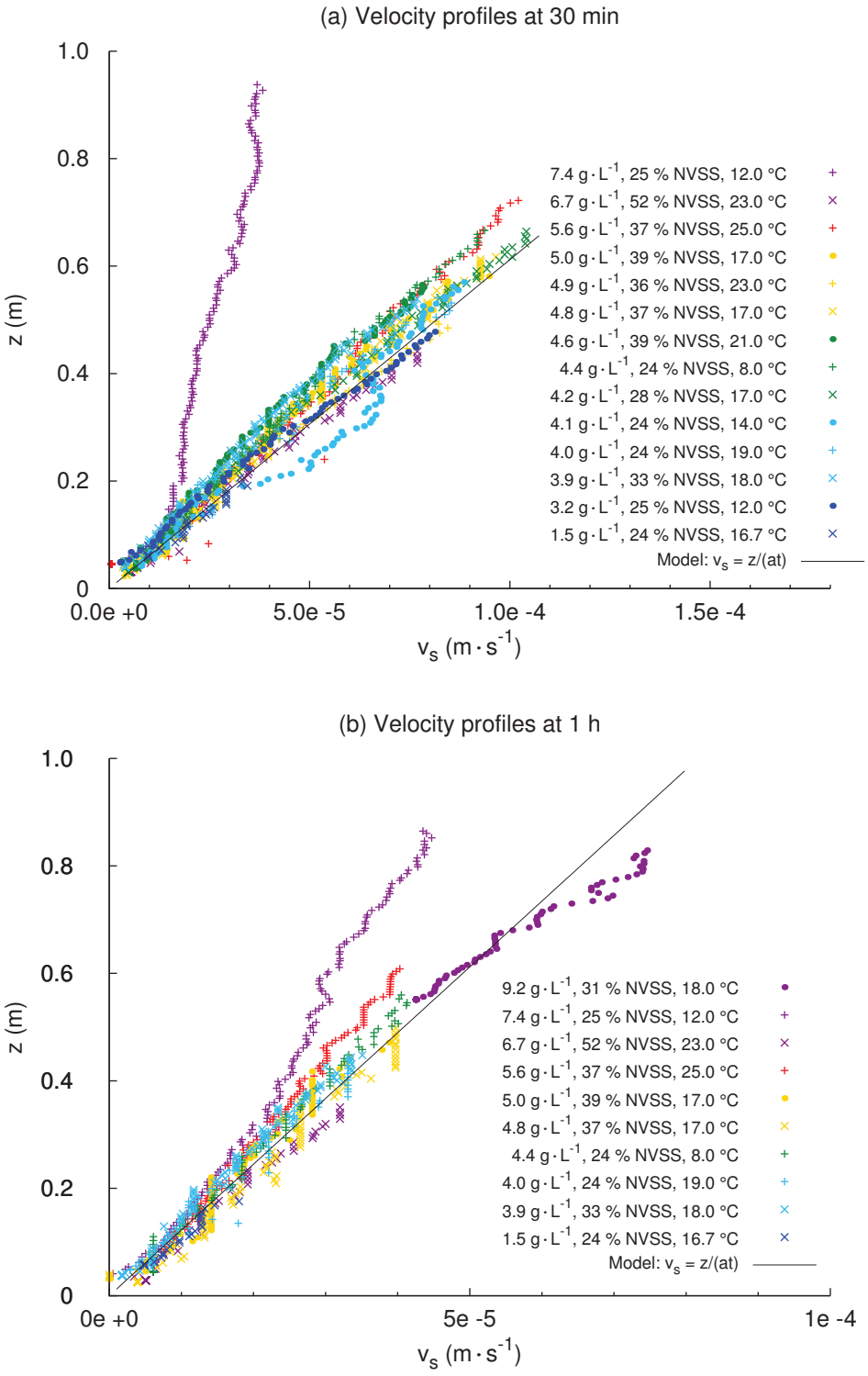

Figure 2.39 – Velocity profiles obtained with different sludge samples in the large settling column after (a) 30 min and (b) 1h of sedimentation.

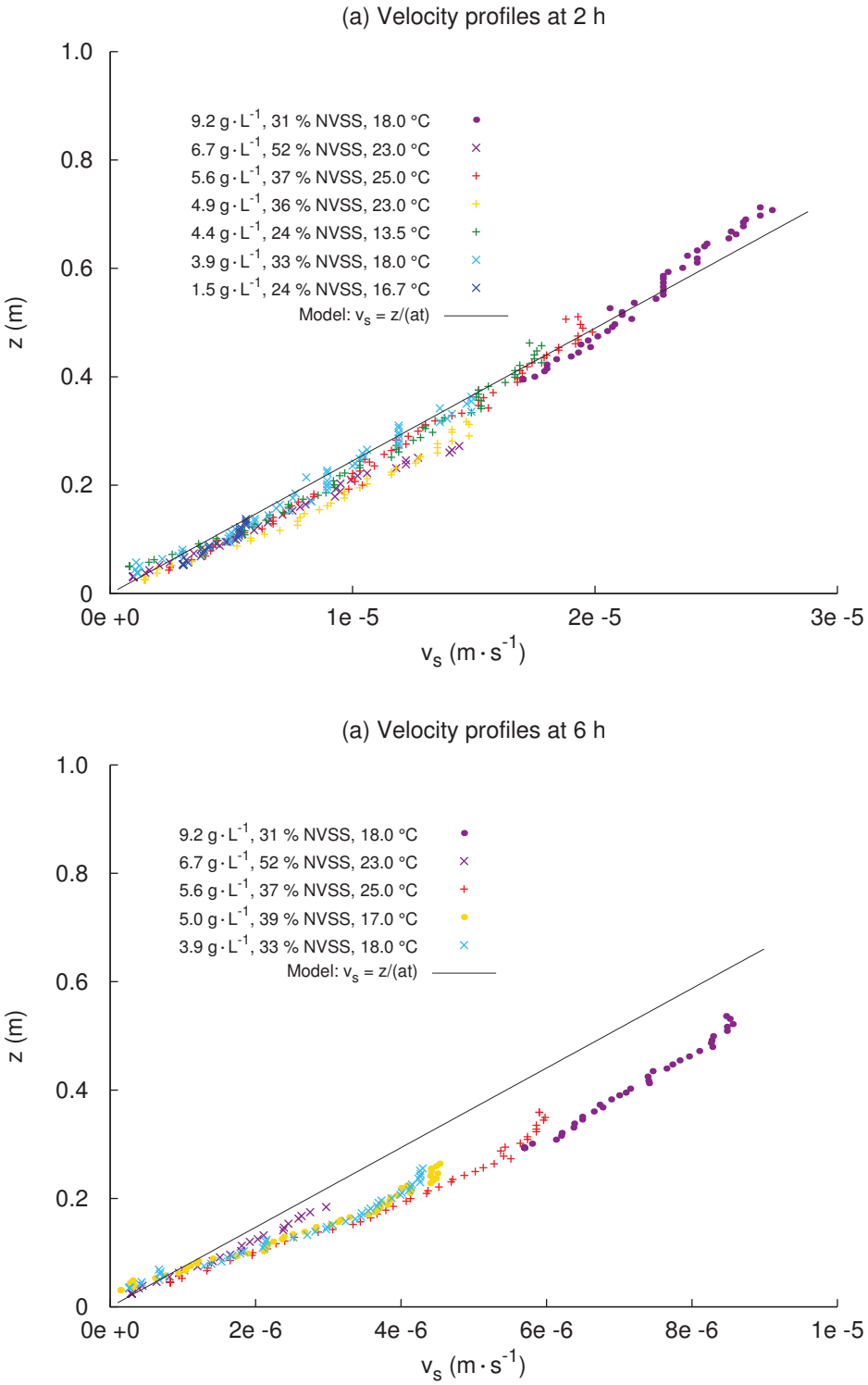

Figure 2.40 – Velocity profiles obtained with different sludge samples in the large settling column after (a) 2 h and (b) 6 h of sedimentation.

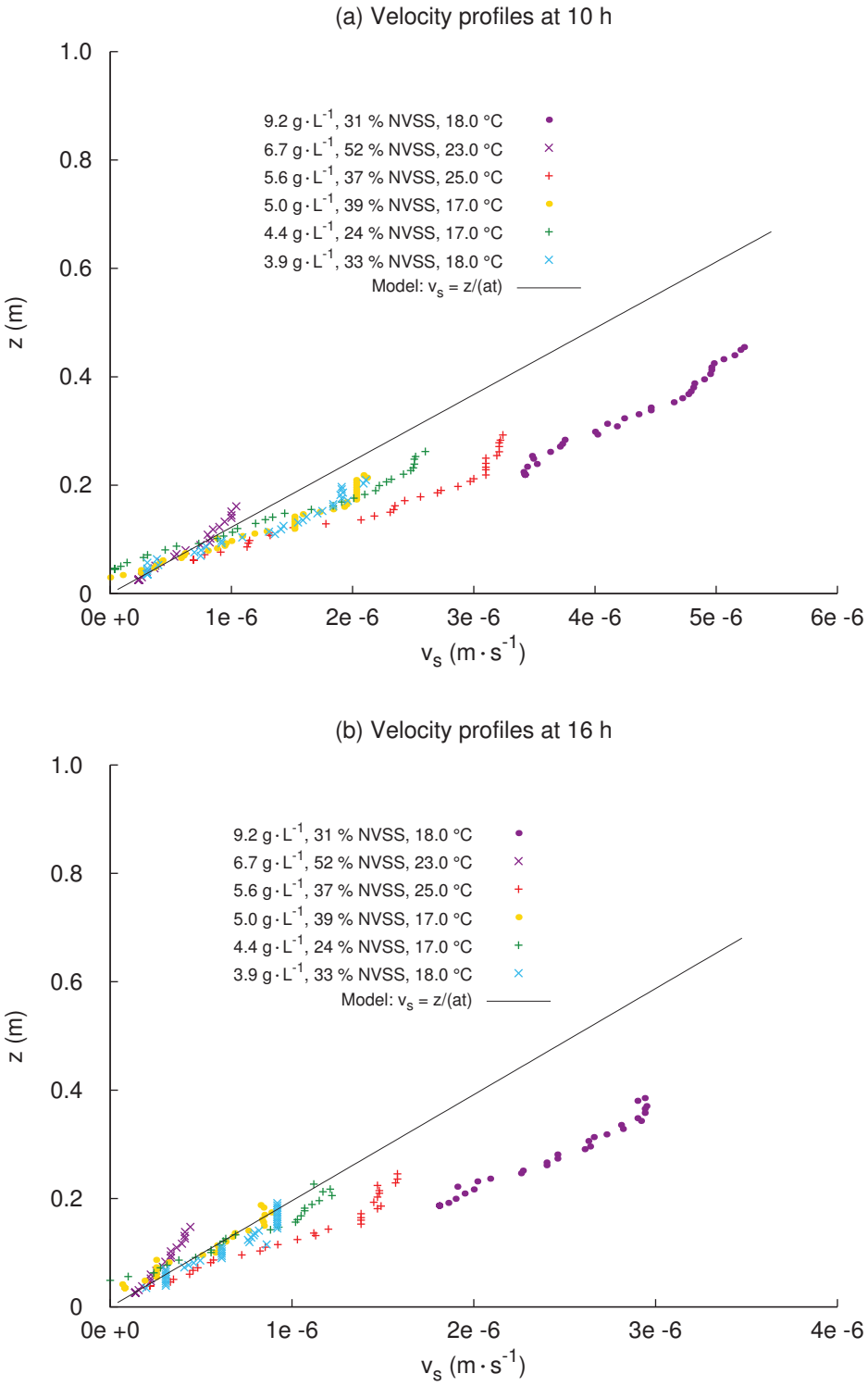

Figure 2.41 – Velocity profiles obtained with different sludge samples in the large settling column after (a) 10 h and (b) 16 h of sedimentation.

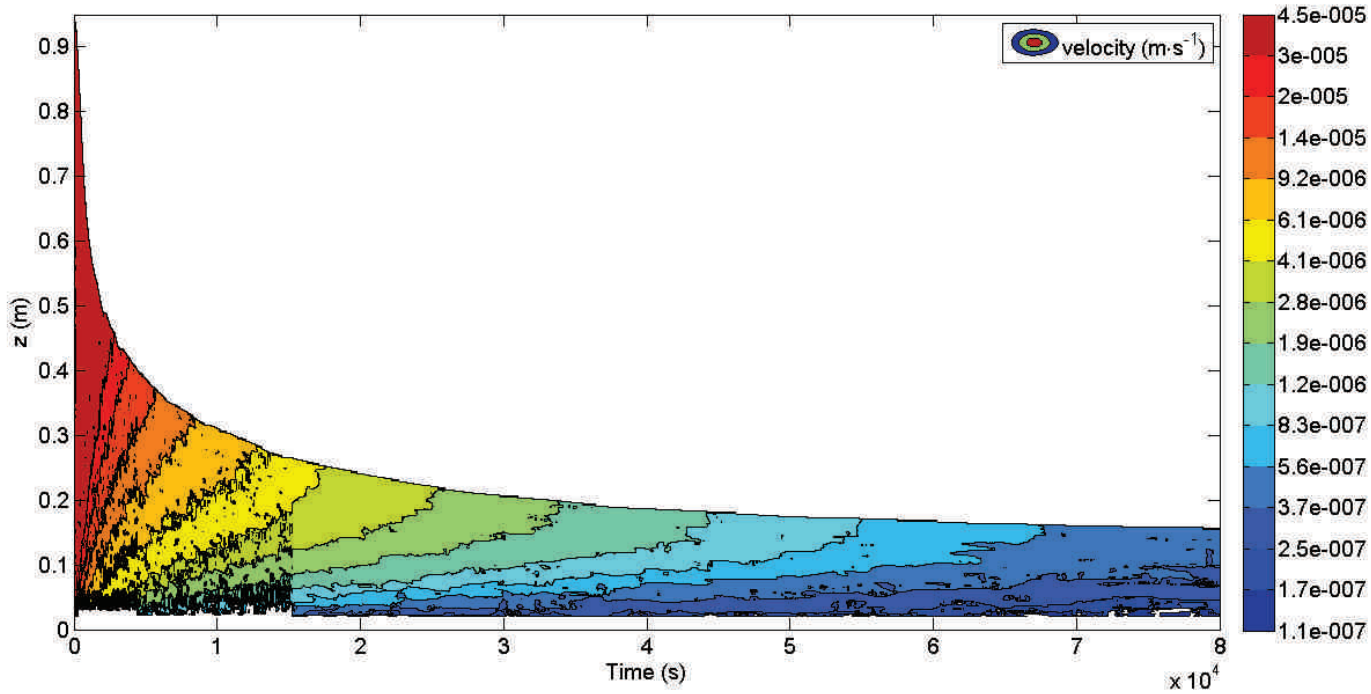

Figure 2.42 – Velocity contours obtained with a 3.9 g·L^{-1} sludge during 22 h of sedimentation in the large settling column.

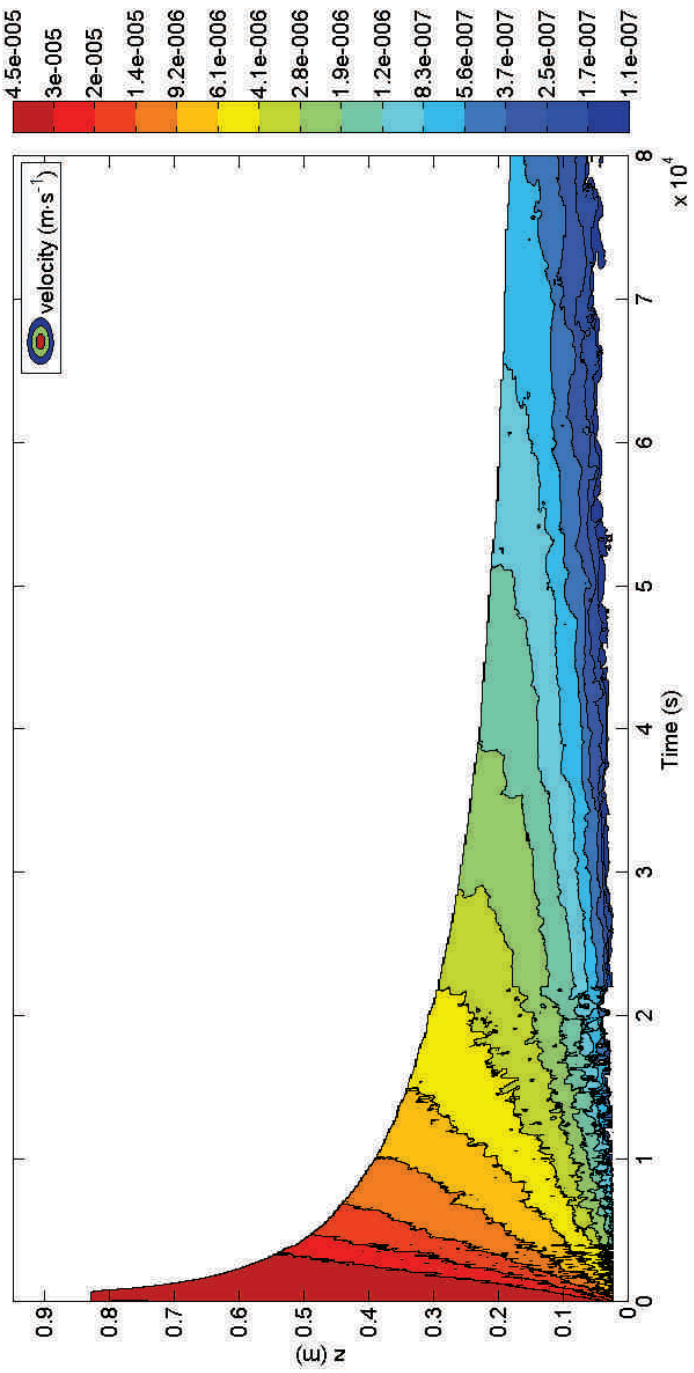

Figure 2.43 – Velocity contours obtained with a 4.4 $g{\cdot}L^{-1}$ sludge during 22 h of sedimentation in the large settling column.

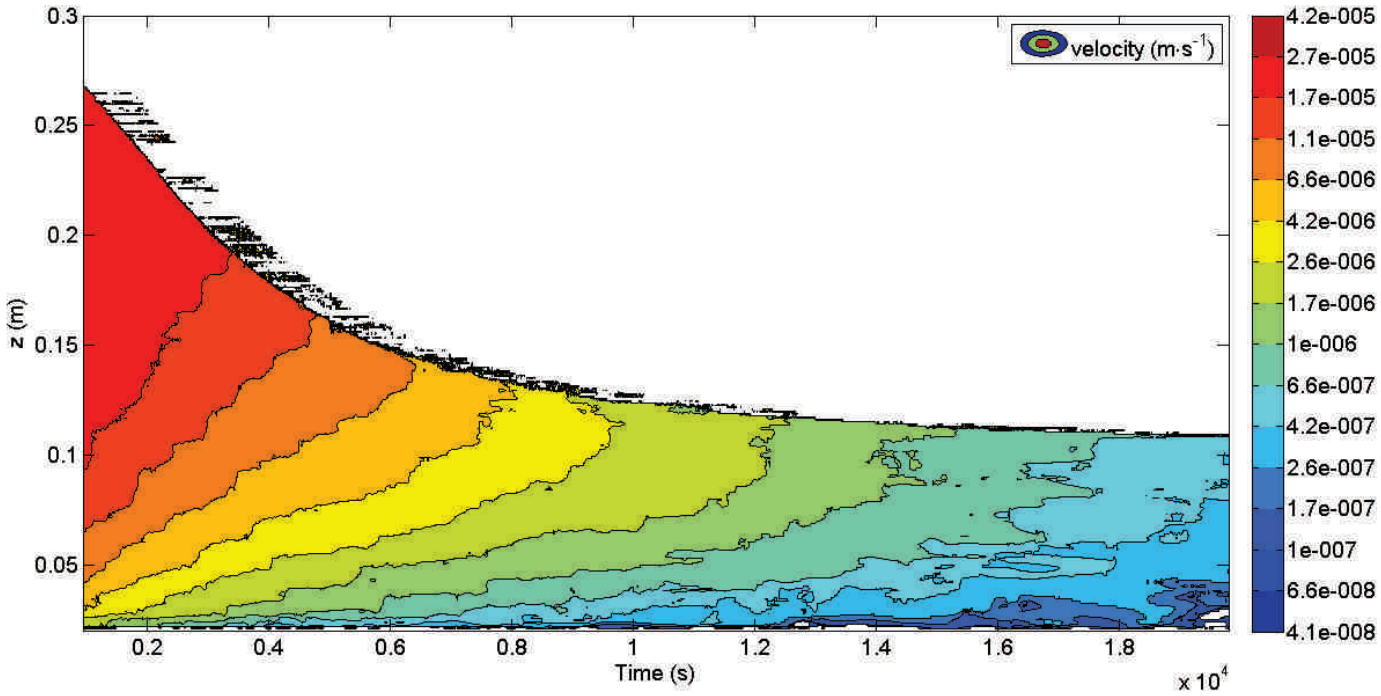

Figure 2.44 – Velocity contours obtained with a 4.2 g·L^{-1} sludge during 5 h 30 min of sedimentation in the small settling column.

Concentration

It is possible to evaluate the evolution of the concentration within the sludge blanket using the velocity data obtained. In order to do so, the continuity equation is used:

$$\frac{\partial C}{\partial t} = \frac{\partial C v_\mathrm{s}}{\partial z}, \tag{2.68}$$

where C is the sludge concentration ($\mathrm{g{\cdot}L^{-1}}$), t is the time (s), v_s is the settling velocity ($\mathrm{m{\cdot}s^{-1}}$) and z is the height inside of the settling column. This equation is discretised on a regular mesh representing the settling column. Supposing a homogeneous initial concentration, and knowing the values of the settling velocity in each cell of the mesh thanks to the experimental data, the evolution of the concentration can thus be evaluated. The experimental velocity profiles were fitted to polynomial regressions in order to filter out the irregularities. Figures 2.45 and 2.46 show concentration contours thus obtained.

These results show that, for approximately 2 h, the vertical variations of concentration are marginal, except in the lower layers of the sludge blanket. The vertical concentration gradient increases afterwards, while the concentration near the top of the sludge blanket remains fairly constant. This observation is confirmed by figure 2.47. Furthermore, this result allows calculating the sludge critical concentration C_c by applying to the hypothesis of De Clercq et al. (2008) stating that C_c is the concentration just below the sludge blanket interface. The experimental evolution of the critical concentration with time was found to be satisfyingly modelled using the function

$$\frac{dC_\mathrm{c}}{dt} = a\left(\frac{1}{C_\mathrm{c}^2} - \frac{1}{C_\mathrm{m}^2}\right), \tag{2.69}$$

where C_m is the maximum critical concentration ($\mathrm{g{\cdot}L^{-1}}$) and a is a parameter ($\mathrm{g^3{\cdot}L^{-3}{\cdot}s^{-1}}$). This function is materialised by the green curve in figure 2.47. The values of parameters a and C_m are given in table 2.8. These values were obtained by fitting the values of critical concentration derivative calculated by equation (2.69) to the experimental values of this derivative. The fitting was achieved by minimising the sum of the squared differences between calculated and experimental values. Despite variations, this result can be observed with other raw sludges. The maximum critical concentration is always close to 13 $\mathrm{g{\cdot}L^{-1}}$. The function thus obtained can be used in a settling model to calculate the time evolution of the critical concentration.

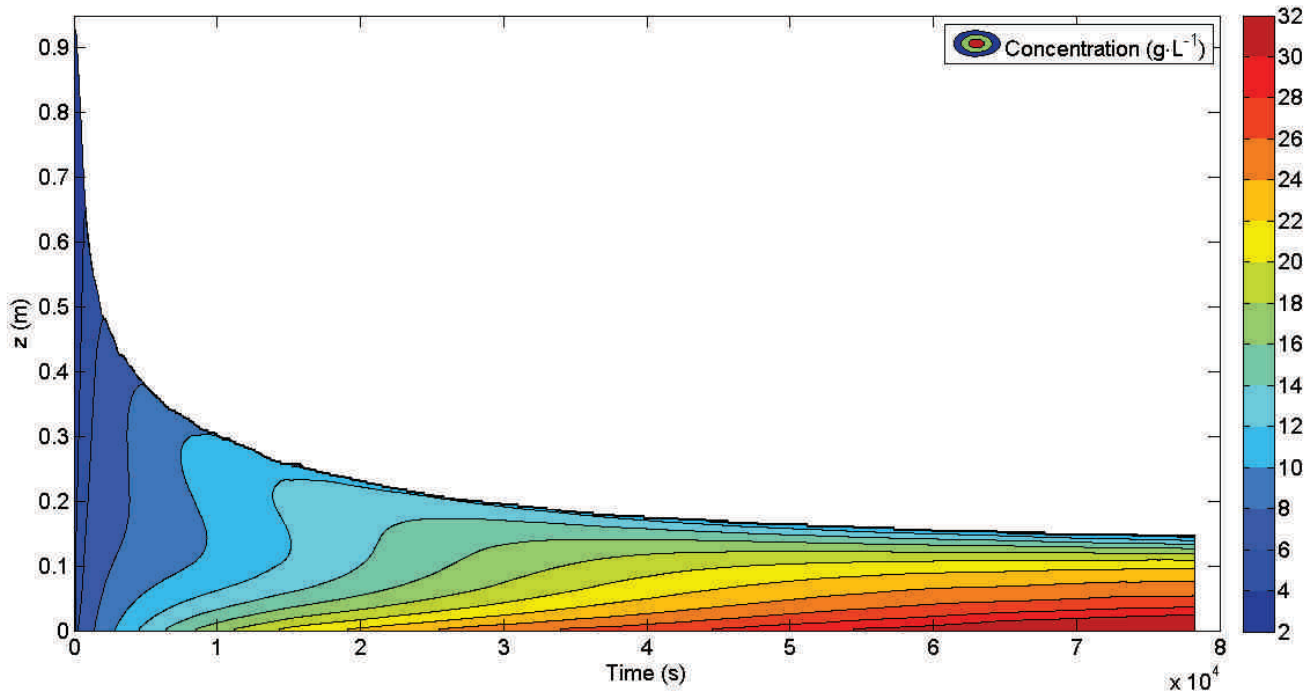

Figure 2.45 – Concentration contours obtained with a 3.9 g·L^{-1} sludge during 22 h of sedimentation in the large settling column.

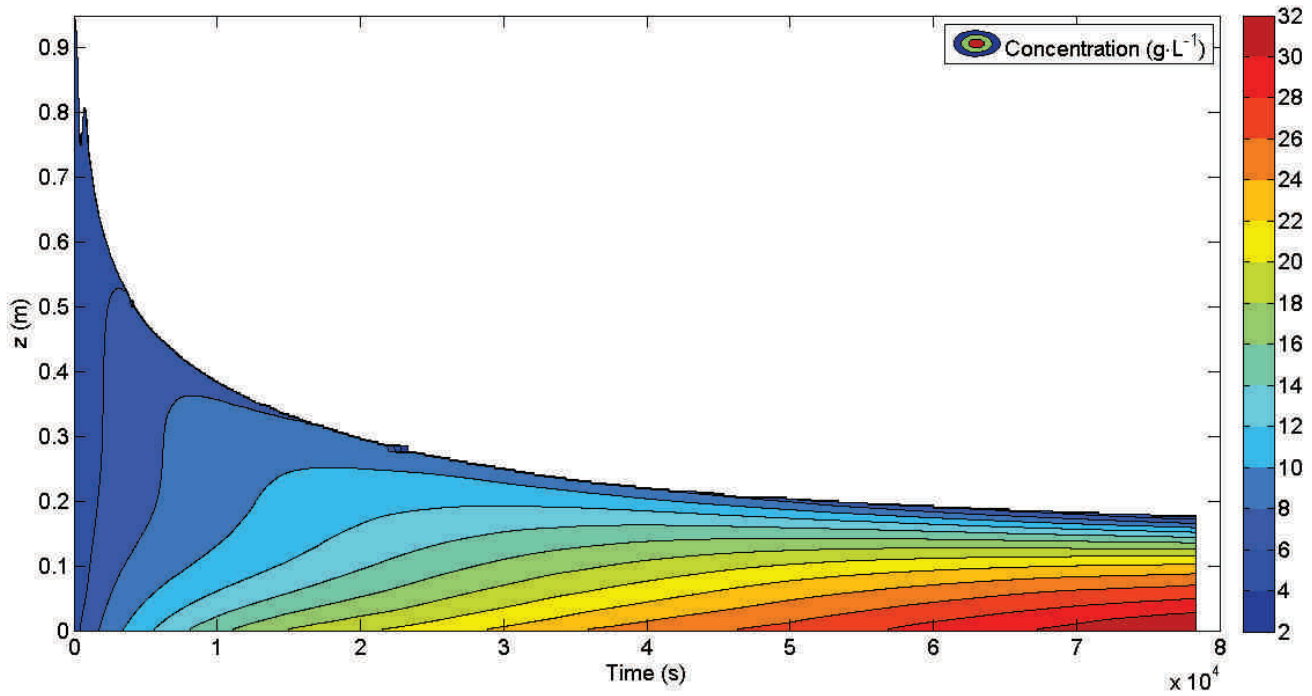

Figure 2.46 – Concentration contours obtained with a 4.4 g·L^{-1} sludge during 22 h of sedimentation in the large settling column.

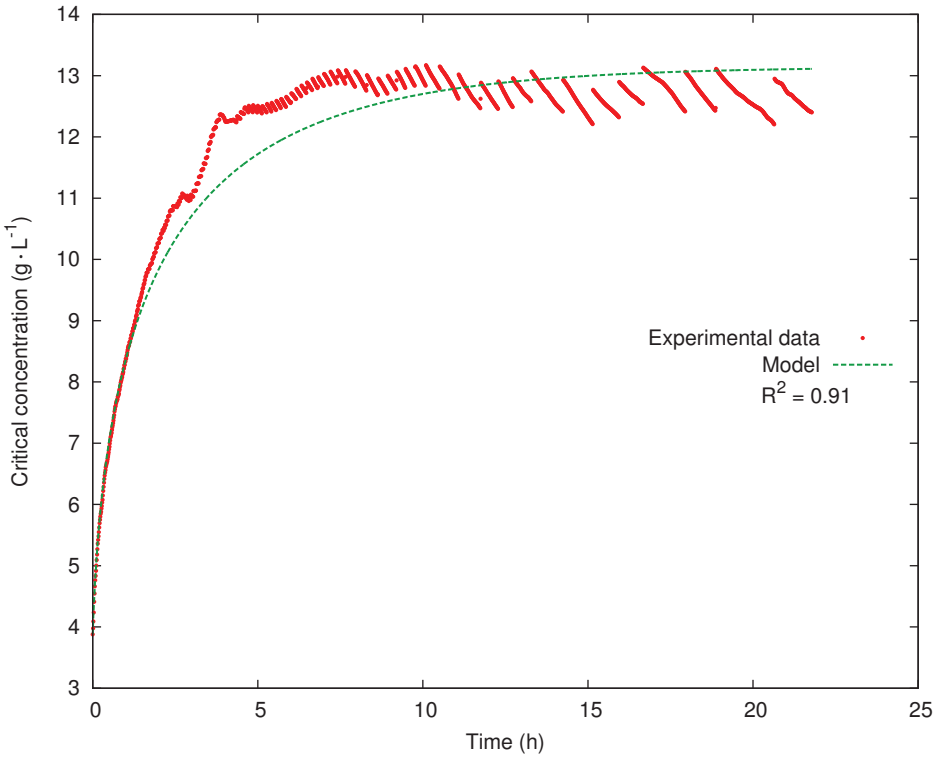

Figure 2.47 – Evolution of the concentration near the top of the sludge blanket obtained with a sludge of initial concentration 3.9 g·L^{-1}.

Table 2.8 – Values of the parameters of equation (2.69).

Parameter	Optimal value	95 % confidence interval
a (g^3·L^{-3}·s^{-1})	$6.64{\cdot}10^{-2}$	$1.23{\cdot}10^{-2}$
C_m (g·L^{-1})	13.15	1.02

Calculation of the sludge blanket height The results obtained show that, as opposed to the settling velocity, the sludge concentration does not display significant vertical variations during approximately 2 h of sedimentation. Supposing a homogeneous concentration in the sludge blanket, the continuity equation (2.68) can be written

$$\frac{\partial C}{\partial t} = C\frac{\partial v_{\mathrm{s}}}{\partial z}. \tag{2.70}$$

Combining this equation and equation (2.67) yield

$$\frac{dC}{dt} = \frac{C}{\lambda t}. \tag{2.71}$$

Solving this differential equation leads to:

$$C = C_0 \left(\frac{t}{t_0}\right)^{\frac{1}{\lambda}}, \tag{2.72}$$

where C_0 is the homogeneous concentration of the sludge blanket ($\mathrm{g{\cdot}L^{-1}}$) at the initial time t_0 (s). Furthermore, the conservation of mass principle yields

$$h(t)C(t) = h_0 C_0, \tag{2.73}$$

where h is the height of the sludge blanket at time t, and h_0 is the height of the sludge blanket at time t_0. Combining equation (2.72) and (2.73) leads to

$$h(t) = h_0 \left(\frac{t}{t_0}\right)^{-\frac{1}{\lambda}}. \tag{2.74}$$

According to this equation, the sludge blanket height follows a power law. Figure 2.48 shows settling curves obtained during extended batch settling experiments. These curves are plotted in log-log plot in figure 2.49. In this figure, the settling curves display a clear linear behaviour during several hours of sedimentation. This linear aspect in log–log scale is consistent with a power law and confirms the previous reasoning. In order to fit equation (2.74) to the experimental settling curves of figure 2.49, the average value of λ calculated earlier (table 2.7) was used, except for the 6.7 $\mathrm{g{\cdot}L^{-1}}$ sludge, which settles noticeably faster in figure 2.49. For this sludge, the value of λ = 2.8 was used. The values of h_0 and t_0 used were those of the sludge blanket height and time at the end of the hindered settling phase for the experiment considered. Figure 2.49 shows the lines corresponding to the power law associated to each experiment. This result shows that the experimental settling curves are fairly well correlated to the calculated power law models during several hours of sedimentation.

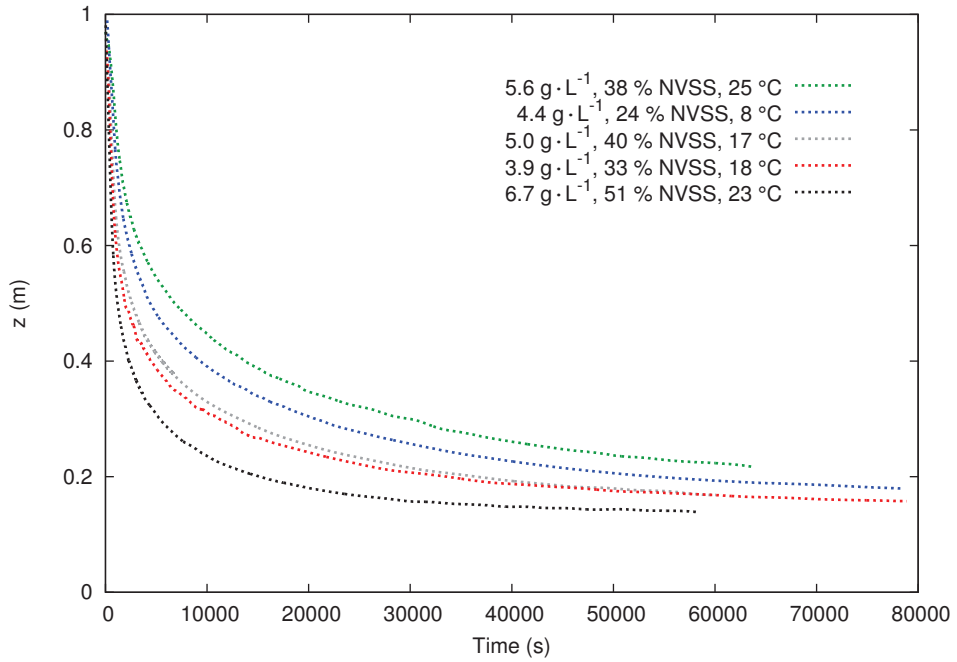

Figure 2.48 – Settling curves obtained during extended batch settling experiments.

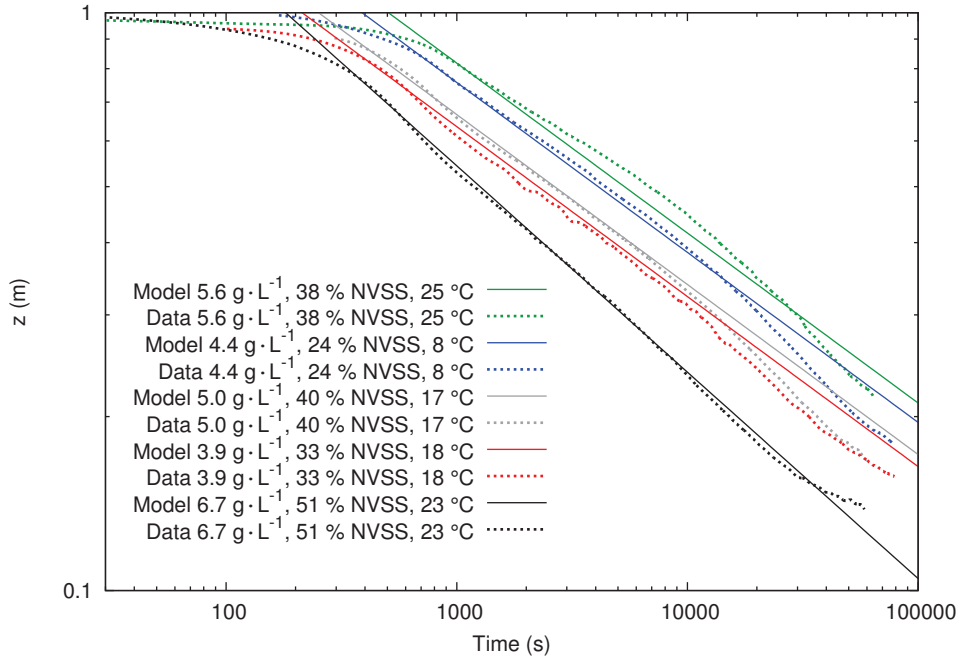

Figure 2.49 – Settling curves obtained during extended batch settling experiments and power-law models plotted in log-log scale.

Conclusion of the experimental study

This study allowed proposing a rheological model adapted to the behaviour of activated sludge, and functions to model the influence of the concentration on the parameters of this model. The investigation of the batch settling process provided detailed results, bringing new insights into the internal behaviour of activated sludge suspensions. The similarity between the behaviour of an activated sludge suspension and that of an emulsion was noted. This comparison was established on the basis of the assumption that, during the thickening of an activated sludge suspension, the sludge is the primary continuous phase, and the water, the secondary phase ascending through it. This has implications regarding the configuration of models, particularly the choice of phase hierarchy. The batch settling study also led to the proposition of relations for the influence of the NVSS on the hindered settling velocity v_{hs} and for the time evolution of the critical concentration C_{c}. The UVP method, used in this work, can be applied in actual wastewater treatment plants and thus allow investigating the influence of the process design on the behaviour of activated sludge suspensions.

The experimental results and proposed functions can be used to test and calibrate models. The next chapter will thus present a 1D settling model and detail a sensitivity analysis procedure as well as an identification method based on the experimental data.

CHAPTER 3

Modelling activated sludge settling

The previous chapter described the data obtained using the developed experimental methodology. These data bring further insight into the mechanisms of the batch settling process, especially the compression phase. The obtained results allowed to propose a function describing the critical concentration variation with time. The comprehensive datasets generated were therefore used to calibrate a 1D model. The latter was devised according to the method proposed by Bürger et al. (2013) and accounts for a variable critical concentration. It is based on a mechanistic approach, as described in section 1.1.2. This approach consists in applying the equations of conservation of mass and momentum to the relative motions of particles and water. This yields equations based on the fundamental physical parameters of activated sludge suspensions. However, since some of these parameters, such as the drag coefficient of flocs or the pore pressure inside of the sludge blanket, cannot be measured, phenomenological functions have been introduced in order to account for the behaviours depending on such unknown parameters. The implemented modelling approach includes two phenomenological functions reported in the literature:

- the hindered settling velocity function of Vesilind (1968),

$$v_{\mathrm{hs}}(C) = v_0 e^{-r_{\mathrm{V}} C}, \tag{3.75}$$

where v_{hs} is the hindered settling velocity ($\mathrm{m{\cdot}s^{-1}}$), C is the sludge concentration, v_0 is the maximum theoretical settling velocity ($\mathrm{m{\cdot}s^{-1}}$) and r_{V} is the Vesilind settling parameter ($\mathrm{g^{-1}{\cdot}L}$),

- and the effective solids stress function σ_{e} of De Clercq et al. (2008),

$$\sigma_{\mathrm{e}} = \begin{cases} 0, & \text{if } 0 \leq C < C_{\mathrm{c}}, \\ \alpha \ln\left(1 + \dfrac{C - C_{\mathrm{c}}}{\beta}\right), & \text{if } C \geq C_{\mathrm{c}}, \end{cases} \tag{3.76}$$

where α (Pa) and β ($\mathrm{g{\cdot}L^{-1}}$) are parameters, and C_{c} is the critical concentration above which an effective solids stress exists.

The two following articles focus on two aspects of the modelling process. The first article deals with the sensitivity analysis of the model using the automatic differentiation engine Tapenade (Hascoët and Pascual, 2004). The second article, building on the sensitivity analysis performed in the first one, proposes an identification process using an inverse approach to calibrate the values of the phenomenological parameters of the model.

Modelling the settling of flocculated suspensions and sensitivity analysis through automatic differentiation

For submission in Computers & Chemical Engineering

Florent Locatelli[a], Isabelle Charpentier[a], Pierre François[a], Robert Mose[a]

Icube UMR 7357, Université de Strasbourg, CNRS, ENGEES, 2 rue Boussingault, 67000, Strasbourg, France

Abstract

The development of activated sludge settling models requires a detailed understanding of the influence of the phenomenological parameters on their solution. Sensitivity analysis is a key tool in the study of the relationships between the input parameters of a model and the output solution. Even thought the respective roles of each parameter may be apparent given the form of the involved functions, their precise influences on the model solution may be difficult to pinpoint, particularly when different behaviours interact, as is the case of activated sludge settling.

This paper first describes a 1D model using well-known settling and compression functions and introduces a new equation for the evolution of the critical concentration with respect to time. This equation is proposed on the basis of a detailed experimental investigation of the settling process. Secondly, a sensitivity analysis is performed. The results obtained allow precisely describing and understanding the respective impacts of each parameter on the model results. Two sets of parameters, corresponding to activated sludge suspensions of distinct behaviours, were tested. The proposed method appears to fit a critical study of the model parameters, and makes up a powerful tool for identification. Furthermore, it can be applied to other functions than the ones used in the present paper.

1 Introduction

The field of wastewater treatment processes is in constant need for optimisation. The requirements defined by the European Water Framework Directive in response to environmental issues as well as the intensifying pressure of population growth on water resources (Willuweit and O'Sullivan, 2013) call

for increasingly accurate prediction tools, such as numerical models. Their enhancement depends on thorough experimental and numerical studies of the underlying physical phenomena. Activated sludge wastewater treatment is a widespread method that broadly consists in mixing the wastewater to a bacterial suspension in a biological reactor. The bacteria degradation of the pollution results in the formation of particle aggregates (flocs), mainly composed of bacteria, mineral matter, residual organic matter, and water. The resulting suspension (mixed liquor) is sent to a secondary settling tank in which the flocs can settle in quiescent conditions while the clarified supernatant overflows at the top. Several models have been developed in order to describe the settling on the basis of a mechanistic approach (Bürger, 2000; De Clercq, 2006). Phenomenological functions have been introduced (Vesilind, 1968; Takács et al., 1991; Cacossa and Vaccari, 1994; Kinnear, 2002; Bürger et al., 2011) due to either the difficulty or impossibility of measuring fundamental physical parameters, such as the effective solids stress or the drag coefficient of flocs.

Sensitivity analysis is a powerful tool for the understanding of the relationships between the model inputs (modelling parameters or initial conditions, for instance) and the model solution. Usages are concerned with uncertainty measurements or parameter identification. Sensitivity analysis is thus extensively addressed in the literature. Nevertheless, to date, little attention has been brought to the methodological study of the sensitivity of activated sludge settling models to the parameters of the phenomenological functions. In other words, the sensitivity analysis to a perturbation in the modelling parameter is often addressed qualitatively only, by plotting simulation results obtained with different values of the parameters.

This paper discusses quantitative sensitivity analysis applied to the modelling of the batch settling of a flocculated suspension. The implementation relies on the automatic differentiation software Tapenade (Hascoët and Pascual, 2004) that provides a user interface for an interactive differentiation. Sensitivity results are proposed for concentration and velocity calculated by a 1D activated sludge settling and compression model. Section 2 presents the model equations and the numerical method applied. Section 3 presents the structure of the model and the differentiation method used. Section 4 presents the results of the model and the analysis of their sensitivity to the parameters of the latter. Section 5 details the conclusions of the study.

2 Modelling the settling process

Table 1 – Nomenclature

a	Parameter of the critical concentration equation ($g^3 \cdot L^{-3} \cdot s^{-1}$)
C	Solids concentration ($kg \cdot m^{-3}$)
C_0	Initial sludge concentration ($kg \cdot m^{-3}$)
C_c	Critical solids concentration ($kg \cdot m^{-3}$)
C_d	Sensitivity of C ($kg \cdot m^{-3}$)
C_m	Maximum critical solids concentration ($kg \cdot m^{-3}$)
d_{comp}	Compression function ($m^2 \cdot s^{-1}$)
f_{bk}	Kynch batch flux density function ($kg \cdot m^{-2} \cdot s^{-1}$)
g	Gravitational acceleration ($m \cdot s^{-2}$)
r	Resistance coefficient ($kg \cdot m^{-3} \cdot s^{-1}$)
r_V	Vesilind parameter ($m^3 \cdot kg^{-1}$)
t	Time (s)
v_d	Drift velocity ($m \cdot s^{-1}$)
v_{hs}	hindered settling velocity function ($m \cdot s^{-1}$)
v_s	Settling velocity ($m \cdot s^{-1}$)
vs_d	Sensitivity of v_s ($m \cdot s^{-1}$)
v_w	Water velocity ($m \cdot s^{-1}$)
v_0	Maximum theoretical settling velocity ($m \cdot s^{-1}$)
$\tilde{p}$	Pore pressure (Pa)
$\overline{\overline{T_s^E}}$	Solids component viscous stress tensor (Pa)
$\overline{\overline{T_w^E}}$	Water component viscous stress tensor (Pa)
$\overrightarrow{k}$	Downward-pointing vertical unit vector
$\overrightarrow{m}$	Solid-fluid interaction force per unit volume ($N \cdot m^{-3}$)
z	Coordinate along the upward-pointing vertical axis (m)
α	Effective solids stress parameter (Pa)
β	Effective solids stress parameter ($kg \cdot m^{-3}$)
γ	Virtual mass ($kg \cdot m^{-3}$)
ϕ	Solids volume fraction (–)
ρ_s	Solids density ($kg \cdot m^{-3}$)
ρ_w	Water density ($kg \cdot m^{-3}$)
σ_e	Effective solids stress (Pa)

Classically, experiments (De Clercq, 2003; De Clercq et al., 2005) are developed to observe the settling process and deduce the internal behaviour of activated sludge suspensions. The main bodies of these experimental procedures are settling columns, in which the suspension can be stirred by the mean, for example, of a recirculation system, the liquid being pumped at the

top of the column and injected back at the bottom (figure 1).

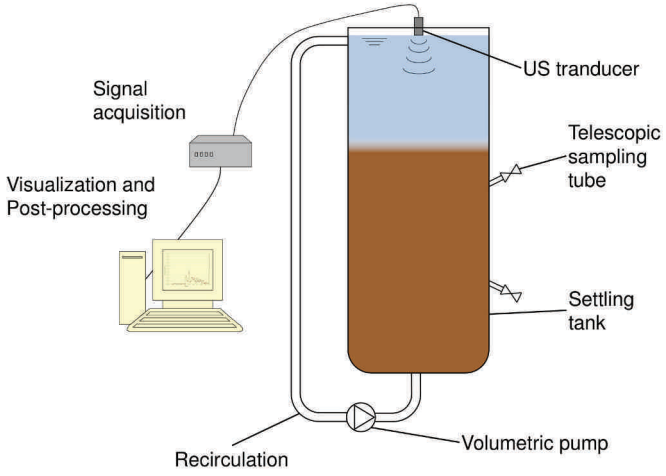

Figure 1 – Diagram of the experimental setup

In many procedures, ultrasonic (US) transducers are used in order to measure the velocity of particles in fluid flows by Doppler methods (Takeda, 1986, 1995, 1999; Eckert and Gerbeth, 2002; Wang et al., 2003b; Manneville et al., 2004; Wiklund et al., 2007; Abda et al., 2009).

This section describes the physical model under study. Mainly based on Bürger et al. (2013), it moreover considers the critical concentration C_c as variable, as proposed by Kinnear (2002). The variation of C_c is described using a new creep-based mechanical equation.

2.1 Mechanistic model

The development of an activated sludge settling model stems from the application of the equations of conservation of mass, momentum and energy to the relative motions of particles and water (Karl and Wells, 1999; Bürger et al., 2000c; Bürger, 2000; Bürger et al., 2013). These are completed with phenomenological functions for the Kynch batch flux density function, the compression function and the critical concentration, which will be detailed in a subsequent paragraph. The definitions of the terms of the equations are indicated in table 1.

Conservation laws The one dimensional continuity equation for the flocs is

$$\frac{\partial \phi}{\partial t} + \frac{\partial \phi v_s}{\partial z} = 0. \tag{1}$$

The momentum conservation equation for the flocs is

$$\begin{aligned}\rho_{\mathrm{s}}\phi\left(\frac{\partial v_{\mathrm{s}}}{\partial t}+v_{\mathrm{s}}\frac{\partial v_{\mathrm{s}}}{\partial z}\right)=\\ =-\frac{\partial\phi\tilde{p}}{\partial z}-\frac{\partial\sigma_{\mathrm{e}}}{\partial z}+\left(\nabla\cdot\overline{\overline{T_{\mathrm{s}}^{E}}}\right)\cdot\overrightarrow{k}+\rho_{\mathrm{s}}\phi g+\overrightarrow{m}\cdot\overrightarrow{k}.\end{aligned} \tag{2}$$

In equation (2), the effective solid stress σ_{e} models the solid-like properties developed by the concentrated activated sludge in compression. The momentum conservation equation for water is

$$\begin{aligned}\rho_{\mathrm{w}}\left(1-\phi\right)\left(\frac{\partial v_{\mathrm{w}}}{\partial t}+v_{\mathrm{w}}\frac{\partial v_{\mathrm{w}}}{\partial z}\right)=\\ =-\frac{\partial\left(1-\phi\right)\tilde{p}}{\partial z}+\left(\nabla\cdot\overline{\overline{T_{\mathrm{w}}^{E}}}\right)\cdot\overrightarrow{k}+\rho_{\mathrm{w}}\left(1-\phi\right)g-\\ -\overrightarrow{m}\cdot\overrightarrow{k},\end{aligned} \tag{3}$$

where the vector $\overrightarrow{m}$ describes the interaction force per unit volume between the flocs and the water, that is

$$\overrightarrow{m}=\tilde{p}\nabla\phi-r\left(\phi\right)\overrightarrow{v_{\mathrm{d}}}+\gamma\left(\phi\right)\left(\frac{\partial\overrightarrow{v_{\mathrm{d}}}}{\partial t}+\left(\overrightarrow{v_{\mathrm{d}}}\cdot\nabla\right)\overrightarrow{v_{\mathrm{d}}}\right). \tag{4}$$

The drift velocity v_{d},

$$v_{\mathrm{d}}=v_{\mathrm{s}}-v_{\mathrm{w}}, \tag{5}$$

is the local difference between the velocity of water and the velocity of flocs. Combining equations (2), (3) and (4) yields an expression for v_{d}, which can be simplified by a dimensional analysis (Bürger, 2000) into

$$v_{\mathrm{d}}=-\frac{1-\phi}{r\left(\phi\right)}\left(\frac{\partial\sigma_{\mathrm{e}}}{\partial z}-\Delta\rho g\phi\right). \tag{6}$$

The volume average velocity of the suspension q,

$$q=\phi v_{\mathrm{s}}+\left(1-\phi\right)v_{\mathrm{w}}, \tag{7}$$

is equal to 0 $\mathrm{m{\cdot}s^{-1}}$ in a closed system. Equations (5) and (7) thus lead to

$$v_{\mathrm{s}}=\left(1-\phi\right)v_{\mathrm{d}}. \tag{8}$$

Combining equations (1), (6) and (8) yields

$$\frac{\partial\phi}{\partial t}+\frac{\partial f_{\mathrm{bk}}\left(\phi\right)}{\partial z}=\frac{\partial}{\partial z}\left(\frac{f_{\mathrm{bk}}\left(\phi\right)\sigma_{\mathrm{e}}'\left(\phi\right)}{\Delta\rho g\phi}\frac{\partial\phi}{\partial z}\right), \tag{9}$$

where

$$f_{\mathrm{bk}}\left(\phi\right)=\frac{\Delta\rho g\phi^{2}\left(1-\phi\right)^{2}}{r\left(\phi\right)} \tag{10}$$

is the Kynch batch flux density function that accounts for hindered settling. Considering that $\phi = C/\rho_s$, equation (9) can be rewritten as

$$\frac{\partial C}{\partial t} + \frac{\partial f_{bk}(C)}{\partial z} = \frac{\partial}{\partial z}\left(d_{comp}(C)\frac{\partial C}{\partial z}\right), \tag{11}$$

with

$$d_{comp}(C) = \begin{cases} 0, & \text{if } 0 \leq C < C_c, \\ \dfrac{\rho_s}{\Delta\rho g C} f_{bk}(C)\,\sigma_e'(C), & \text{if } C \geq C_c. \end{cases} \tag{12}$$

In practice, functions f_{bk} and σ_e, of difficult evaluation, are approximated using phenomenological functions.

Phenomenological functions The Kynch batch flux density function (Kynch, 1952) is defined as

$$f_{bk}(C) = C v_{hs}(C). \tag{13}$$

Different hindered settling velocity expressions are available in the literature (Vesilind, 1968; Cole, 1968; Takács et al., 1991; Cho et al., 1993). In this work, the hindered settling velocity v_{hs} is defined by the formula of Vesilind (1968):

$$v_{hs}(C) = v_0 e^{-r_V C}, \tag{14}$$

where v_0 is the maximum theoretical settling velocity and $r_V > 0$ is a parameter. The modelling approaches presented in this work can be applied to other settling velocity functions, such as that of Cole (1968).

The effective solids stress σ_e is calculated using the formula proposed by De Clercq et al. (2008) :

$$\sigma_e = \begin{cases} 0, & \text{if } 0 \leq C < C_c, \\ \alpha \ln\left(1 + \dfrac{C - C_c}{\beta}\right), & \text{if } C \geq C_c. \end{cases} \tag{15}$$

The effective solids stress accounts for the ability of a thickened sludge blanket, in which the flocs are in permanent contact with each other, to resist to deformation (Buscall and White, 1987; Aziz et al., 2000; Bürger et al., 2000a).

As suggested by Kinnear (2002) and De Clercq (2006), we consider that the critical concentration C_c is (i) time-dependent (Kinnear, 2002) and (ii) equal to the concentration in the layer of sludge adjacent to the sludge blanket interface (De Clercq, 2006). We obtain this concentration experimentally (Locatelli et al., 2015b). Figure 2 shows the evolution of the critical concentration during the sedimentation. In compression, the deformed sludge blanket exhibits a behaviour similar to creep. The experimental results indicate

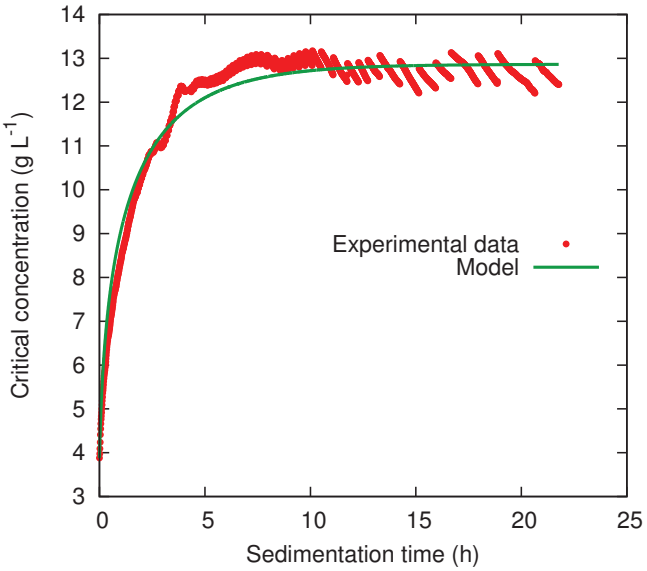

Figure 2 – Measurements and model of the critical concentration evolution during the sedimentation. Initial concentration of the sludge: 3.9 g·L^{-1}; temperature: 18.0 ℃.

that the variation of the critical concentration (figure 2) can be approximated by the following equation:

$$\frac{dC_\mathrm{c}}{dt} = a\left(\frac{1}{C_\mathrm{c}^2} - \frac{1}{C_\mathrm{m}^2}\right), \tag{16}$$

where C_m is the maximum critical concentration and a is a parameter. By discretising equation (16) using a finite difference scheme, it is possible to calculate the critical concentration values knowing the initial sludge concentration. Parameters a and C_m can then be evaluated by fitting the values thus calculated to the experimental critical concentration values using a spreadsheet to minimise the sum of the squared differences between calculated and experimental values. Using the measured data, we obtain $C_\mathrm{m} = 12.86$ g·L^{-1} and a $= 0.66$ g^3·L^{-3}·s^{-1}.

Finally, the settling equations hold four unknown parameters: α, β, v_0 and r_V, present in phenomenological equations (14) and (15). These parameters cannot be measured experimentally and introduce uncertainty in the model. It is therefore crucial to evaluate their influence on the model solution.

2.2 Numerical method

Equation (11) can be seen as a mixed hyperbolic–parabolic equation. The operator splitting strategy is adopted. The initial evolution problem is split

into a convection problem,

$$\frac{\partial C}{\partial t} + \frac{\partial f_{\mathrm{bk}}(C)}{\partial z} = 0, \tag{17}$$

and a diffusion problem,

$$\frac{\partial C}{\partial t} = \frac{\partial}{\partial z}\left(d_{\mathrm{comp}}(C)\frac{\partial C}{\partial z}\right), \tag{18}$$

the solution of which can be carried out independently using specific and highly efficient discretisation schemes (Karlsen and Risebro, 1997). For the space discretisation we consider a uniform mesh size $\Delta z > 0$.

Since the conservation laws may be discontinuous, we use the cell average approach. The hyperbolic problem (17) is solved using a so-called finite volume method based on the calculation of the state variable on the control volume $[z_{\mathrm{j\text{-}1/2}}, z_{\mathrm{j+1/2}}]$ where $z_{\mathrm{j+1/2}}{=}z_{\mathrm{j}} + \Delta z/2$. We use in this study the following standard form of a finite volume scheme for conservation laws proposed by Godunov (1959) :

$$C_j^{n+1} = C_j^n - \frac{\Delta t}{\Delta z}\left(F_{j+1/2}^n - F_{j-1/2}^n\right), \tag{19}$$

where $F_{j+1/2}^n$ is the flux of the Riemann problem at the interface $z_{\mathrm{j}} + \Delta z/2$. We moreover adopt the Godunov flux (Godunov, 1959), which is identical to the standard upwind scheme in the context of the linear transport equation. In the present case, the flux function has a single maximum and no minima (figure 3), hence the Godunov flux may be written as

$$F_{j+1/2}^n = F(C_j^n, C_{j+1}^n) = \min\Big[f_{\mathrm{bk}}\left(\min(C_j^n, 1/r_{\mathrm{V}})\right), f_{\mathrm{bk}}\left(\max(C_{j+1}^n, 1/r_{\mathrm{V}})\right)\Big]. \tag{20}$$

This explicit scheme is stable under the classical Courant condition

$$f'_{\mathrm{bk}}\Delta t/\Delta z \leq 1. \tag{21}$$

In equation (18), the compression function is evaluated by approximating its primitive with respect to C. This yields

$$D(C) = \int_{C_{\mathrm{c}}}^{C} d_{\mathrm{comp}}(s)\,\mathrm{d}s. \tag{22}$$

Following the Leibniz rule, equation (18) becomes:

$$\frac{\partial C}{\partial t} = \frac{\partial^2 D(C)}{\partial z^2}. \tag{23}$$

The diffusive equation is solved using the classical finite difference scheme as presented in Bürger et al. (2000b). This explicit scheme is stable under the classical stability condition

$$d_{\mathrm{comp}}(C)\Delta t/\Delta z^2 \leq 1/2. \tag{24}$$

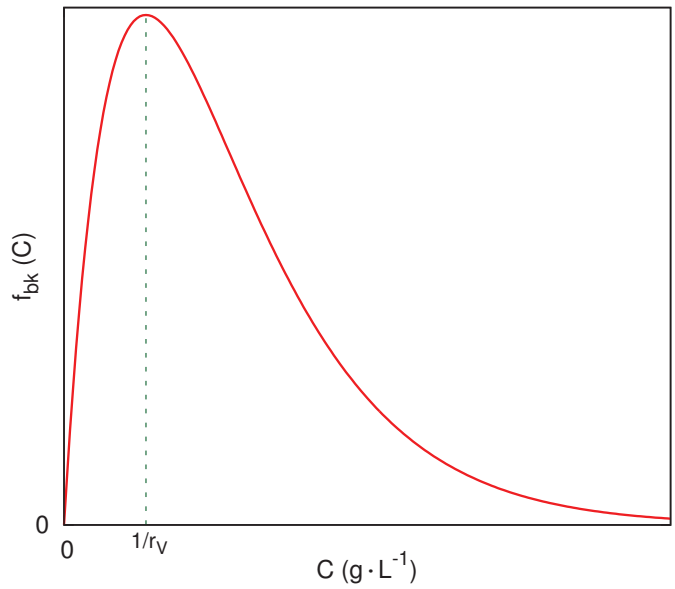

Figure 3 – Representation of the Kynch batch flux density function f_{bk}

3 Sensitivity of the settling model

Analysis of the sensitivity to some behaviour law parametrisation, some initial and/or boundary conditions is a classical issue in the study of physical and biochemical processes. In general terms, this measures the response of a model $\mathcal{M}$ under study, namely the outputs, to a change in the its parameters P, namely the inputs. The interest is threefold. First, a sensitivity analysis gives an insight into and knowledge on the physical behaviour of the model and how it is impacted by change on one of the inputs. Second, it allows to assess the uncertainties in the modelling parameters and how the outputs may be altered by some parameter misfit (under- or overestimation, for instance). In a first attempt, such qualitative information may deduced from repeated evaluations of the model. Third, much more valuable qualitative and quantitative information on the model may be obtained from the derivatives of the model as sensitivity computations provide gradients necessary to some of the parameter identification methods.

Assuming the model $\mathcal{M}$ is differentiable with respect to the parameters P, the sensitivity $s^P_{\mathcal{M}}(P_0)$ at point P_0 may be either approximated using a first order finite difference scheme

$$s^P_{\mathcal{M}} \simeq \frac{\mathcal{M}(P0 + \delta P) - \mathcal{M}(P_0)}{\delta P}, \tag{25}$$

or computed as

$$s^P_{\mathcal{M}}(P_0, \delta P) = \frac{\partial \mathcal{M}}{\partial P}(P_0).\delta P, \tag{26}$$

where δP is a direction of perturbation related to P.

Within simulation codes, sensitivities may notably be approximated by the perturbation method (25), or computed through the implementation of the differentiated continuous model, the differentiation of the discrete model or the differentiation of the code implementing the model. As presented in the paper, the most general, accurate and simple option is offered by Automatic Differentiation (AD) (Griewank and Walther, 2008a). Some of the principles and benefits of AD are hereafter discussed on the code implementing the settling model.

3.1 Settling code

The numerical methods and the phenomenological laws (13)–(16) are implemented as Fortran 90 subroutines and functions, the names of which are listed in the call graph of the original code, see table 2. The top routine, `SETTLING_MODEL`, first calls the subroutine `INITIALIZE_CZ` to set the initial concentration C_0 and to mesh the settling column. The subroutine `COMPRESSION_FCT` uses the function `DCOMP` to calculate the values of the compression function defined by equation (12) prior to the simulation of the sedimentation. This concludes the initialisation phase of the program. The actual simulation of the sedimentation begins by the calculation of the time step size in the subroutine `DT_STABILITY_CRITERION`. This uses the values of the function d_{comp} (12) and of the derivative of function f_{bk} (13) in order to meet the stability conditions (21) and (24) at each time step. As explained in section 2.2, the subroutine `GODUNOV_FLUX` calculates the value of the convective flux using the function f_{bk} (calculated by the function `KYNCH_FCT`) according to equation (17). The subroutine `DIFFUSIVE_FLUX` calculates the value of the diffusive flux (18) using function d_{comp} (calculated by the function `DISP`). Concentration values are then updated in subroutine `UPDATE_C`. The settling velocity is calculated by the subroutine `SEDIMENTATION_VELOCITY` from the concentration values. Finally, the subroutine `UPDATE_CriticalC` updates the critical concentration C_{c} according to equation (16). The resulting code contains about 700 lines. Although not discussed in the present paper, this code already includes statements for Cole's formula (Cole, 1968).

From a computer point of view, given inputs, the execution flow of the program includes information about how it starts, the actual order of execution of the statements and how it terminates. Conditional statements are particular statements since they determine the flow of the execution of the code.

```
subroutine SETTLING_MODEL
    Calls subroutine INITIALIZE_CZ
    Calls subroutine COMPRESSION_FCT
        Calls function DCOMP
    Calls subroutine DT_STABILITY_CRITERION
        Calls function DFDC
        Calls function DCOMP
    Calls subroutine GODUNOV_FLUX
        Calls function KYNCH_FCT
    Calls subroutine DIFFUSIVE_FLUX
        Calls function DISP
    Calls subroutine UPDATE_C
    Calls subroutine SEDIMENTATION_VELOCITY
        Calls function KYNCH_FCT
    Calls subroutine UPDATE_CriticalC
```

Table 2 – Original call graph

3.2 Automatic differentiation

Automatic Differentiation (AD) is a set of techniques to augment computer codes with derivative computation. Within AD, any execution flow is viewed as a composition of arithmetic operation and intrinsic functions. This sequence of operations may be differentiated applying the chain rule and classical rules such as "the derivative of a sum is the sum of the derivatives", and so forth. This differentiation mode is called tangent linear mode (or forward mode). It is generally used for sensitivity analyses. Note that the so-called adjoint mode (reverse mode), often intended to be used parameter identification (of a large number of inputs), is out of scope for this work.

AD gives rise to two kind of software. On the one hand, source transformation tools like Tapenade (Hascoët and Pascual, 2004) or Adifor (Bischof et al., 1995) are able to generate the source codes containing derivative statements. On the other hand, operator overloading tools such as Adol-C (Griewank et al., 1996) or Rapsodia (Charpentier and Utke, 2009) may be used at compile time to propagate derivatives at runtime. Among the available software, we choose Tapenade (Hascoët and Pascual, 2004) since it may be applied to general Fortran codes. This AD tool may be invoked in three different manners. For small codes (less than 3000 lines), the free web interface[1] gives access to the "Tapenade On-line Automatic Differentiation Engine". The resulting code may be downloaded from the website. Larger codes require to download the Tapenade software for a local installation. Differentiation is then performed using the graphical user interface.

[1] http://tapenade.inria.fr:8080/tapenade/index.jsp

A Tapenade command may also be used. In any case, the user provides the source of its code, the name of the top routine and the “independent” input variables. The differentiation is performed with respect to these independent variables. Any variable that depends on a independent variables is recognised as a “dependent variable" by Tapenade.

Given a code and differentiation options, Tapenade first proceeds to a syntactic analysis of the code structure and statements. If there exist, Tapenade indicates parser errors and warnings. Syntactic errors have to be cured (or at least understood) before the actual differentiation phase. When the information provided to Tapenade is coherent, the tangent mode option generate a tangent linear code differentiated with respect to the independent variables (the parameters of interest, for instance) and the dependent variables thanks to the chain rule. At runtime, this linear code allows for the propagation of one direction of perturbation to compute the sensitivity of the dependent variables to this perturbation. The tangent multi-directional mode allows for the propagation of several directions of perturbation.

3.3 Differentiation of the settling code

The settling code, tab 2 is differentiated with respect to v_0, r_V, α and β using Tapenade on the top routine `SETTLING_MODEL`. The differentiation of the 700 lines of settling code is carried out in about 0.2s. The generated tangent linear code contains 1007 lines. The call graph of the tangent linear code is displayed in table 3. The Tapenade's naming convention for the tangent linear routine and variable names is to suffix routine names with a `_D` and variable names with a `D`. Note that Fortran is not case sensitive. Note that the initialisation routine `INITIALIZE_CZ` and the `DISP` function are independent from the former four parameters.

The interested reader may observe some part of the differentiation process on a Kynch batch flux density function (Listing 1) that accounts for Vesilind's formula for $n = 1$ and Cole's formula for $n = 2$.

Listing 1 – Kynch batch flux density function

```
DOUBLE PRECISION FUNCTION kynch_fct(C,v0,rv,vmax,n)
INTEGER, INTENT(IN)::n !n=1:Vesilind; n=2:Cole
DOUBLE PRECISION, INTENT(IN)::C,v0,rv,vmax
DOUBLE PRECISION::Cmin !used for Cole
IF (n==1) THEN          !Vesilind's formula
  kynch_fct=C*v0*EXP(-rv*C)
ELSE IF (n==2) THEN  !Cole's formula
  Cmin=(v0/vmax)**(1/(rv+1)) !min. concentration
  IF (C.LT.Cmin) THEN
    kynch_fct=C*vmax
  ELSE
    kynch_fct=v0*rv**(-rv)
  ENDIF
ENDIF
END FUNCTION kynch_fct
```

```
 subroutine SETTLING_MODEL_D
     Calls subroutine COMPRESSION_FCT_D
         Calls function DCOMP_D
     Calls subroutine DT_STABILITY_CRITERION_D
         Calls function DCOMP_D
         Calls function DFDC_D
     Calls subroutine GODUNOV_FLUX_D
         Calls function KYNCH_FCT_D
     Calls subroutine DIFFUSIVE_FLUX_D
     Calls subroutine UPDATE_C_D
     Calls subroutine SEDIMENTATION_VELOCITY_D
         Calls function KYNCH_FCT_D
     Calls subroutine UPDATE_CriticalC_D
```

Table 3 – Differentiated call graph

Following the chain rule, Tapenade differentiates the routine `kynch_fct` with respect to v_0, r_V and C. The resulting tangent linear routine is displayed in Listing 2.

Listing 2 – Differentiated Kynch function

```
!   Generated by TAPENADE  (INRIA, Tropics team)
! Tapenade 3.6 (r4512) -  3 Aug 2012 15:11
!
! Differentiation of kynch_fct in
! forward (tangent) mode (with options i4 dr8 r4):
!  variations   of useful results: kynch_fct
!  with respect to varying inputs: v0 rv c
DOUBLE PRECISION FUNCTION KYNCH_FCT_D(c, cd, &
&  v0, v0d, rv, rvd, vmax, n, kynch_fct)
  IMPLICIT NONE
!n=1:Vesilind; n=2:Cole
  INTEGER, INTENT(IN) :: n
  DOUBLE PRECISION, INTENT(IN) :: c, v0, rv, vmax
  DOUBLE PRECISION, INTENT(IN) :: cd, v0d, rvd
!used for Cole
  DOUBLE PRECISION :: cmin
  DOUBLE PRECISION :: pwx1
  DOUBLE PRECISION :: pwy1
  DOUBLE PRECISION :: pwy1d
  DOUBLE PRECISION :: pwr1
  DOUBLE PRECISION :: pwr1d
  DOUBLE PRECISION :: kynch_fct
  INTRINSIC EXP
  IF (n .EQ. 1) THEN
!Vesilind's formula
    kynch_fct_d = (cd*v0+c*v0d)*EXP(-(rv*c)) &
&      - c*v0*(rvd*c+rv*cd)*EXP(-(rv*c))
    kynch_fct = c*v0*EXP(-(rv*c))
```

δ	$r_\delta(C)$
1.E-2	1.0259866417644863
1.E-3	1.0024474525039548
1.E-4	1.0001946229756491
1.E-5	1.0000132254158343
1.E-6	1.0000013360132738
1.E-7	1.0000003016678352
1.E-8	1.0000003796475669
1.E-9	0.9999931386725000
1.E-10	1.0000844863579579
1.E-11	0.9995887580649243

Table 4 – Taylor test on the sensitivity of the concentration $C(0.3)$ with respect to a perturbation of v_0 .

```
  ELSE IF (n .EQ. 2) THEN
!Cole's formula
      ! * removed since not used in the paper
      ! * may be generated using Tapenade
      !   on kynch_fct
    END IF
  ELSE
    kynch_fct_d = 0.D0
  END IF
END FUNCTION KYNCH_FCT_D
```

The correctness of the sensitivity process is checked with a classical Taylor test. Following Tapenade's naming conventions, the tangent linear concentration is denoted by C_d. This compares the sensitivity result C_d computed with the tangent linear code at point $(v_0, r_\mathrm{V}, \alpha, \beta) = x$ in the direction $(v_{0,d}, r_{\mathrm{V,d}}, \alpha_\mathrm{d}, \beta_\mathrm{d}) = x_\mathrm{d}$ to first order finite difference approximations computed with the settling model as follows

$$r_\delta(C) = \frac{|C(x + \delta x^d) - C(x)|}{\delta} \frac{1}{|C^d(x, x^d)|}, \tag{27}$$

where δ is a small parameter. Ratios computed at $z = 0.3m$ and $t = 0.25h$ using parameter values x displayed in table 5 and the direction of perturbation $x_\mathrm{d} = (1, 0, 0, 0)$ are reported in Table 4. Theoretically, these ratio should tend linearly toward 1 as δ tends to 0 since small δ are necessary to minimise the numerical errors coming from the finite difference approximation. However, the subtraction of too close floating-point numbers yields a cancellation error that dominates the truncation error coming from the finite difference computation. A Taylor test presenting such a behaviour indicate that the implemented sensitivity computation is correct. This is the case in

table 4. Such Taylor tests were carried out with in a systematic manner to check the correctness of the derivative computations.

4 Simulation results and sensitivity analysis

4.1 Model output

The model produces 1D concentration and velocity profiles. Figure 4 shows results obtained with the parameter values given in table 5. In all the simulations presented in this paper, the initial concentration used was $C_0 = 3.9$ g·L^{-1} (experimental value).

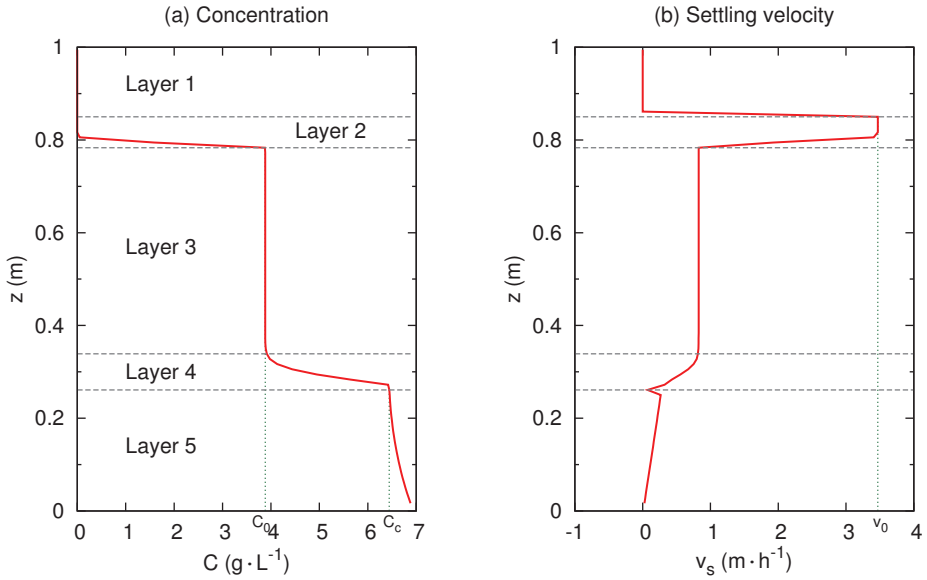

Figure 4 – Calculated profiles of (a) concentration and (b) velocity after 15 min of sedimentation.

Table 5 – Sets of parameters used in the simulations

First set of parameters (S1)			
v_0 (m·h^{-1})	r_V (L·g^{-1})	α (Pa)	β (g·L^{-1})
3.47	0.37	4	4
Second set of parameters (S2)			
v_0 (m·h^{-1})	r_V (L·g^{-1})	α (Pa)	β (g·L^{-1})
20.08	0.48	23.45	11.62

In figure 4, the height z is shown in ordinate, meanwhile the concentration C and settling velocity v_s are shown in abscissa to make their variation clear. Five horizontal layers with specific behaviours can be distinguished.

- **Layer 1** This is the clear supernatant. No sludge remains in this zone.
- **layer 2** This layer contains the residual sludge particles between the clear supernatant and the sludge blanket. At the top of layer 2, the concentration is very low, hence the settling velocity is close to the maximum theoretical value v_0 (equation (14)). Below, the concentration increases up to the initial concentration C_0 at the level of the sludge blanket interface.
- **Layer 3** This layer contains the sludge that still settles with the initial concentration and settling velocity; there is no concentration nor velocity gradient. This sedimentation mode is usually referred to as "zone settling".
- **Layer 4** A first thickening zone appears. The concentration increases from the initial concentration up to the critical concentration at the bottom of zone 4. Since the concentration is still lower than the critical concentration, the flocs are not in permanent contact with each other, which allows a sharp concentration gradient.
- **Layer 5** The concentration reaches the critical concentration C_c at the top of layer 5, this layer is therefore in compression. The flocs are in permanent contact with each other and form a matrix able to withstand a certain amount of stress quantified by the effective solids stress σ_e (equation (15)). The development of a concentration gradient is hampered by the increased resistance of the sludge blanket to deformation.

The four parameters (v_0, r_V, α, β) are expected to have an influence on the value of the concentration, but also on the height of the interfaces between the different regions described above. The next section studies this influence in detail by means of sensitivity analysis.

4.2 Sensitivity analysis with the parameter set S1

We begin by using classical values for the settling parameters (Bürger et al., 2013) (table 5). Figure 5 shows concentration and settling velocity profiles obtained with the parameter set S1 at different times of the simulation. The five regions described earlier are still visible on the profile after 30 min of sedimentation. After 45 min, the zone settling region has almost disappeared. At 1 h, the sludge blanket is entirely in compression. The parameters are

submitted to a perturbation of + 10 % of their initial value. Figure 6 shows results and sensitivity profiles obtained after 15 min of sedimentation.

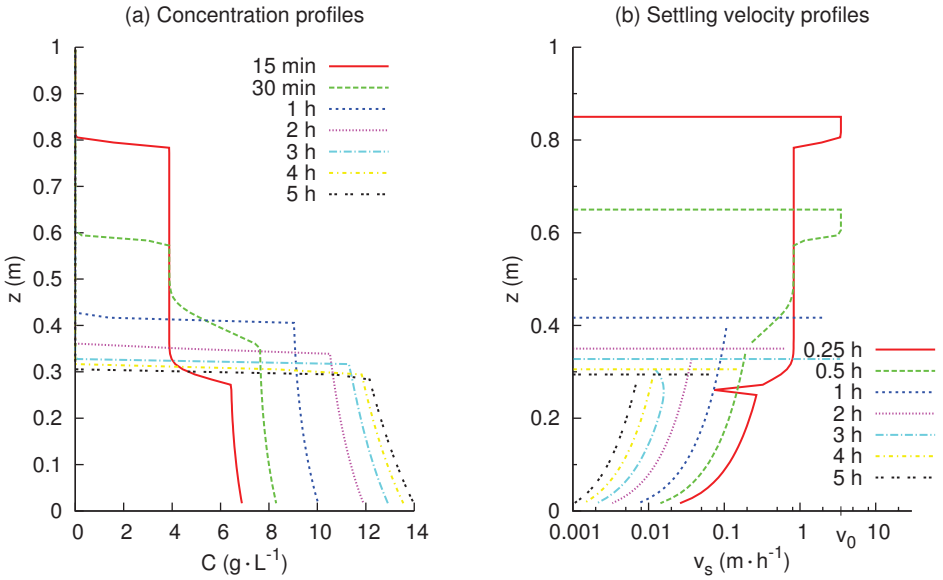

Figure 5 – Sedimentation profiles calculated at different times with the parameter set S1: (a) concentration, (b) velocity.

On the one hand, the sensitivity profiles obtained for the concentration indicate different behaviours.

- The concentration profile is mainly sensitive to the Vesilind parameters v_0 and r_V. These have, as expected, opposed influences.
- At a given time, an increase in v_0 tends to lower the sludge blanket and raise the top of the compression region. Indeed, the formula of Vesilind (equation (14)) produces higher settling velocities as v_0 increases, which accelerates the rate of fall of the sludge blanket interface as well as the thickening rate of the bottom part of the suspension. On the contrary, an increase in r_V slows the settling velocity down, producing an opposite effect.
- The influence of the four parameters on the concentration profile is mainly local. Nevertheless, a slight influence can be seen in the compression region and will be focused on thereafter.

On the other hand, the sensitivity profiles obtained for the velocity reveal sharp local, as well as noticeable distributed influences.

- Between 0.77 m and 0.85 m, the sensitivity profile for v_0 shows the important influence of this parameter on the maximum settling velocity. It also has a sizeable impact on v_s in the entire zone settling region.
- As opposed to v_0, the parameter r_V has little influence on the maximum settling velocity. However, as for the concentration, it has an influence opposite to that of v_0 near the top of the sludge blanket and in the zone settling region.

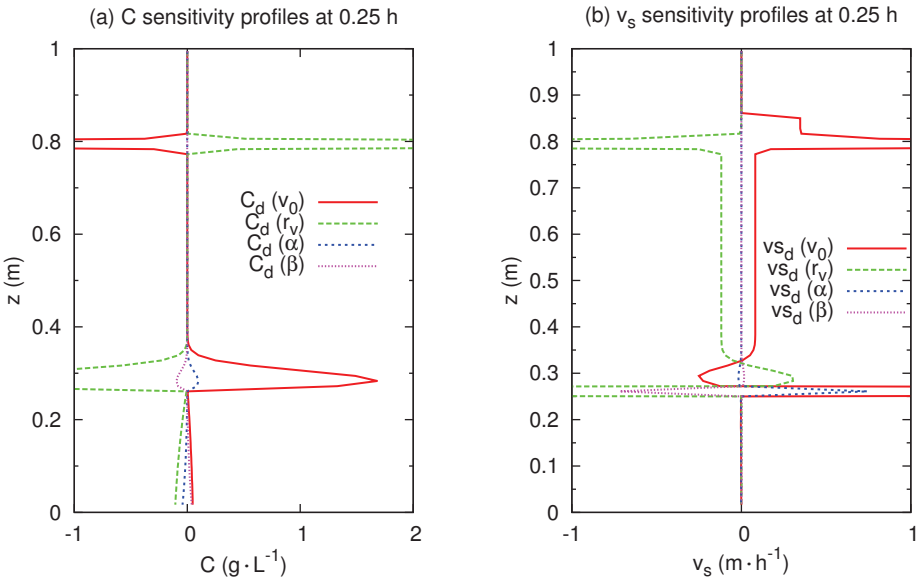

Figure 6 – Sensitivity profiles after 15 min of sedimentation: (a) concentration, (b) settling velocity.

A zoom on the sensitivity profiles in the compression region is shown in figure 7. This figure highlights the specific influences of each of the four parameters.

- The sensitivity profile for v_0 indicates that an increase of this parameter tends to globally augment the concentration in the compression layer. A higher v_0 leads to higher initial settling velocities, thus increasing the rate of sludge accumulation at the bottom of the settling column.
- On the contrary, the Vesilind parameter r_V globally reduces the concentration inside of the compression layer when increased. The higher this parameter, the lower the initial settling velocity. Therefore, it lowers the rate of sludge accumulation, thus the concentration at the bottom of the settling column.

- The sensitivity profile for α is convex, which shows that a perturbation of this parameter reduces the concentration mostly in the lower part of the compression layer. Thus, it also reduces the concentration gradient in this layer as compared to the initial concentration profile (figure 6). In the compression function (15), the parameter α accounts for the ability of the sludge blanket to resist to deformation. As such, it tends to entail more homogeneous concentration profiles in the compression layer.

- As opposed to α, the parameter β tends to increase the concentration mostly in the lower part of the compression layer. In the compression function (15), beta quantifies the propensity of the sludge blanket to deform under shear, thus to thicken under its own weight, yielding higher concentration gradients in the compression layer.

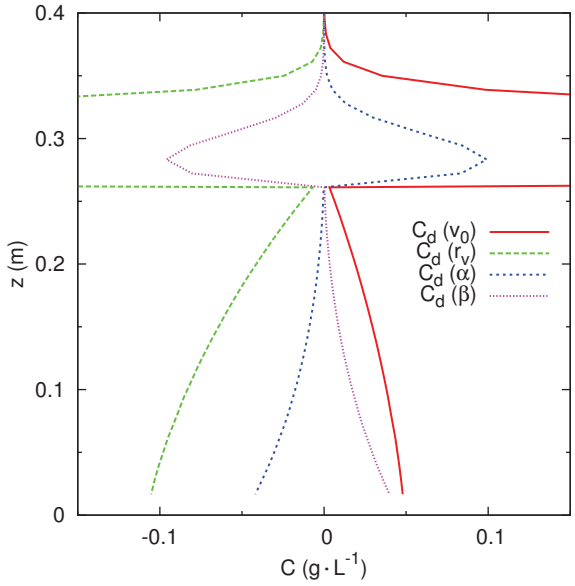

Figure 7 – Zoom on the sensitivity profiles in the compression region after 15 min of sedimentation simulated with the parameter set S1.

Figure 8 shows the sensitivity results after 5 h of sedimentation. A this time, the sludge blanket is entirely in compression.

- The parameter of Vesilind v_0 tends to lower the position of the sludge blanket interface, as it did after 15 min (figure 6). However, as shown in figure 6, it has the effects of lowering the sludge blanket interface and increasing the thickness of the compression layer. These effects tend to compensate each other when the sludge blanket is entirely in

compression. When this is the case, the impact of v_0 is thus strongly weakened, as it can be observed in figure 8.

- The parameter r_V tends to raise the position of the sludge blanket interface as it did earlier. Its influence is noticeably stronger than that of v_0. This means that the parameters of the Vesilind function used to describe the hindered settling phase display a significant influence during the compression phase, which suggests that the influence of the Vesilind function overlaps part of the compression behaviour. This agrees with the conclusions of Torfs et al. (2015).

- This figure confirms that the influence of v_0 becomes small as compared to that of the other parameters. This parameter mainly affects the beginning of the sedimentation.

- On the contrary, the second Vesilind parameter r_V has a significant influence on the concentration. The perturbation profile associated to this parameter is convex. Therefore, it tends to oppose the thickening of the sludge blanket in a manner similar to that of α.

- The influences of α and β after 5 h, similar to the ones observed after 15 min, have increased.

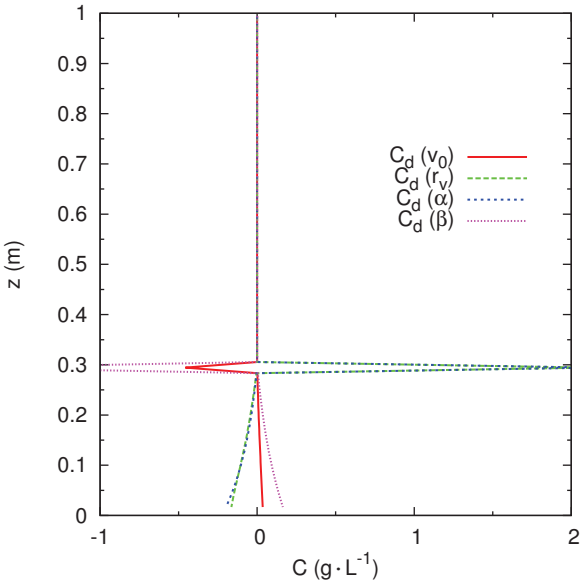

Figure 8 – Concentration sensitivity profiles after 5 h of sedimentation with the parameter set S1.

4.3 Sensitivity analysis with the parameter set S2

A second simulation is run using the set of parameter values S2 in order to compare the sensitivity of a solution obtained with a sludge of different properties to the previous results. The values of the parameters used are presented in table 5. These parameter values are consistent with well flocculated sludge particles with high initial settling velocity and a sludge blanket with a good resistance to deformation. Figure 9 shows concentration and settling velocity profiles obtained with the parameter set S2 at different times of the simulation.

- The chosen Vesilind parameters v_0 and r_V yield higher initial settling velocities than the values of the previous simulation. The sludge blanket is thus already entirely in compression after 15 min of sedimentation.

- Figure 9 shows that, after 5 h of sedimentation, the sludge blanket interface is slightly higher than with the previous simulation at the same time. This is a consequence of the higher values of α and r_V.

- The maximum concentration, at the bottom of the sludge blanket, is equal to 12.9 g·L^{-1} at 5 h. This value is lower than the maximum concentration obtained with the previous parameters at the same time (14 g·L^{-1}). In addition, the concentration gradient between the sludge blanket interface and the bottom of the settling column is smaller than in the previous simulation. This observation is consistent with the higher value of α.

Figure 10 shows the concentration sensitivity profiles after 15 min of sedimentation.

- The sensitivity profiles display the same tendencies as those observed at the same time in the compression region with the parameter set S1 (figure 7). This is consistent with the fact that the sludge blanket is already entirely in compression with the current set of parameters.

- the values of perturbations associated to v_0 and β are now comparable, as opposed to the sensitivity profiles obtained with the previous parameter set at the same time, in which case the perturbation due to β was weaker.

Figure 11 shows the sensitivity profiles after 5 h of sedimentation.

- The perturbations associated with v_0, α and β, though similar, are smaller than the ones obtained with the previous simulation at the same time.

Figure 9 – Sedimentation profiles calculated at different times with the parameter set S2: (a) concentration, (b) velocity.

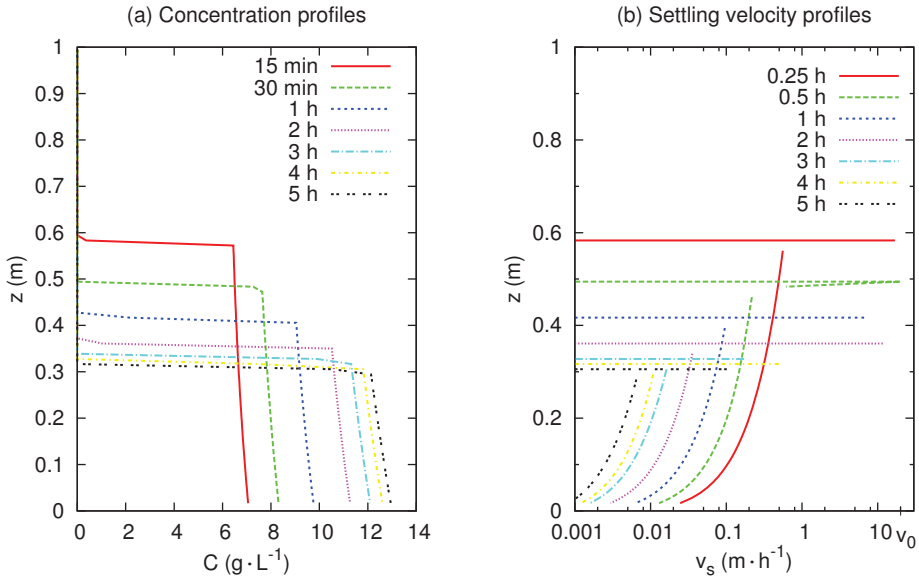

- The perturbation associated to r_V is noticeably different than with the previous simulation. In the current case, the perturbation profile associated to this parameter is concave. Thus, the perturbation is more distributed along the concentration profile than with the parameter set S1.

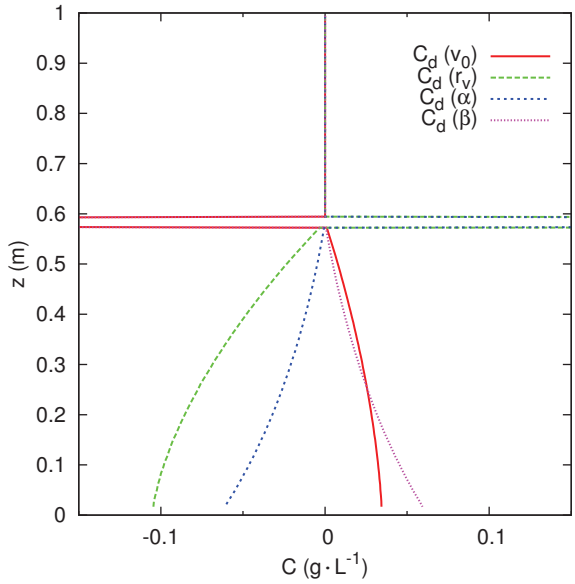

Figure 10 – Concentration sensitivity profiles obtained with the parameter set S2 after 15 min of sedimentation.

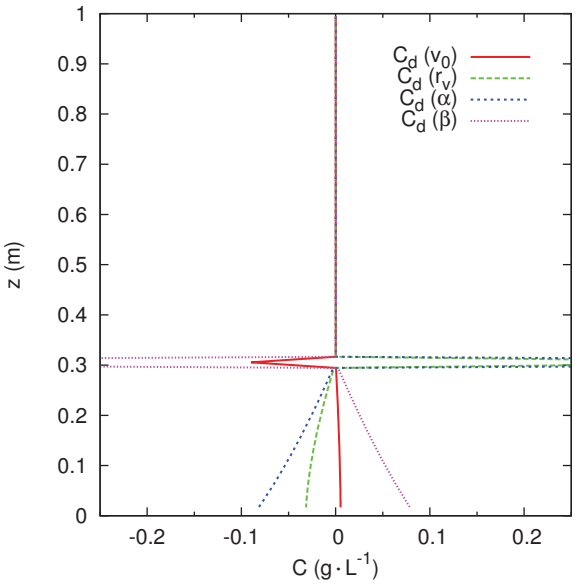

Figure 11 – Sensitivity profiles obtained with the parameter set S2 after 5 h of sedimentation.

The sensitivity profiles show that the model solution is less sensitive to variations of the initial parameter values with the second set of parameters than with the first one. This shows that the sludge properties have a signif-

icant impact on the sensitivity of the model solution, which can impact the identification process.

5 Conclusions

A 1D model of activated sludge settling and compression is designed. This model simulates the settling and compressive fluxes using well-known phenomenological functions, and introduces a new equation to compute the evolution of the critical concentration with to time. This equation is developed on the basis of a detailed experimental investigation of the settling process by the mean of a settling column equipped with an ultrasonic transducer.

The settling and compression functions involve four parameters that require identification. In order to provide a detailed description and understanding of the influence of these parameters on the model solution, a sensitivity analysis is performed. The use of automatic differentiation by the mean of Tapenade (Hascoët and Pascual, 2004) allows for the calculation of precise sensitivity profiles for the model parameters. The results indicate that the sensitivity of the model solution varies with the height in the sludge blanket as well as the time of sedimentation. The four parameters have different and, sometimes, competing influences. Therefore, they allow for the modelling of a wide variety of sludge properties. Two simulations are performed using different sets of parameter values. The results show that the shape of the sensitivity profile associated to a parameter may change according to the value of this parameter.

The use of automatic differentiation is a mean of getting codes for the calculation of the model sensitivity to a change in the parameter values. The sensitivity analysis is made straightforward by the possibility of calculating the perturbations for all parameters in a single run. This method therefore accelerates the analysis process while reducing the risk of error associated with manual code differentiation. Furthermore, the automatic differentiation of the code is a powerful tool for parameter identification. Further work will be undertaken to calibrate the model parameters using the experimental data obtained during the study presented in this paper.

Adjoint automatic differentiation and parameter identification for an activated sludge settling model

For submission in Computers & Chemical Engineering

Florent Locatelli[a], Isabelle Charpentier[a], Pierre François[a], Julien Laurent[a], Robert Mose[a]

Icube UMR 7357, Université de Strasbourg, CNRS, ENGEES, 2 rue Boussingault, 67000, Strasbourg, France

Abstract

This paper discusses the implementation of a gradient-based data assimilation process designed for the Bürger–Diehl model (Bürger et al., 2013) with a particular attention to the adjoint implementation issue by means of automatic differentiation. Eight experiments are carried out to identify phenomenological laws – Kynch batch flux density function and compression function – with sludge blanket interface and concentration data up to 0.5 h in order to capture the early behaviour of the mixture and notably the height of the sludge blanket interface. Using identified parameters, numerical results show a good agreement between the model and data up to 2 h of sedimentation.

1 Introduction

Secondary settling tanks are often oversized to account for a lack of hydraulic engineering analysis, or poorly designed due to a lack of understanding of the influences of the tank geometry on operation. Accurate prediction tools are therefore required to optimise settling tank design. The very first steps of prediction rely on both quantitative measurements of the phenomenon under study (a water treatment process, for instance) and the design of a parametrised model capable of delivering a good qualitative approximation. Data assimilation is a set of techniques for the comparison of data with the model solutions. Its applications are concerned with model validation, model tuning, reconstruction of events, prediction and so forth. A minimisation problem is set up with an objective function, the so-called cost function, that measures some discrepancies between data and the model solutions. Among the methods, the variational data assimilation technique introduced

by Le Dimet and Talagrand (1986) in the context of weather forecast has proven its efficiency in various cases.

Activated sludge is a widespread technique in sewage treatment plants. The wastewater is mixed with a bacterial suspension that consumes and degrades organic matter and pollutants in a biological reactor. Particle aggregates called flocs are a by-product of the process. These are composed of bacteria, mineral and residual organic matter, and water. The resulting suspension is sent to a secondary settling tank (or *clarifier*) where the flocs can settle in quiescent conditions while the supernatant overflows at the top. In recent years, a few studies led to the development of non-invasive experimental techniques, which allow gathering comprehensive data without disturbing activated sludge settling, yielding precise results De Clercq et al. (2002, 2005); Locatelli et al. (2015b). Such data offer opportunities for the development and calibration De Clercq et al. (2008) of secondary clarifier models Bürger (2000); Diehl (2015). As reviewed in Diehl (2015), several authors (see James and Sepulveda (1994); Castro and Zuazua (2011); Betancourt et al. (2014) for instance), discuss gradient methods for identification purposes within nonlinear convection-diffusion models, the underlying principles of which are issued from very early work on optimal controls Lions (1971) as for Le Dimet and Talagrand (1986). Most of them describe adjoint models, but do not fully discuss the implementation from software point of view.

This paper discusses the implementation a gradient-based data assimilation process designed for the Bürger–Diehl model Bürger et al. (2013) with a particular attention to the adjoint implementation issue. Even the tangent linear differentiation task is not a difficult one, handcoding often reveals to be an error-prone process. This is even more true for the adjoint differentiation. Automatic Differentiation (AD) Griewank and Walther (2008b), also known as computational differentiation, is a set of techniques and tools that allow to augment computer codes with derivative computations. It may be applied with confidence, even on very large codes Charpentier (2000). A brief general description of AD is provided to discuss the use of the Tapenade AD tool Hascoët and Pascual (2013) on the settling model. Identification experiments are carried out using sludge concentration data Locatelli et al. (2015b,a) to capture the early behaviour of the mixture. Prediction experiments using estimated parameters are then discussed from a mechanical point of view.

The layout of the paper is as follows. Section 2 briefly presents data, the settling model, and the underlying numerical methods and the objective functions. The data assimilation process is described in Section 3 with a particular attention to automatic differentiation aspects. Calibration results are discussed in Section 4. Section 5 provides conclusions and an outlook.

2 Data and modelling of the batch settling process

The sedimentation of suspensions in a closed system, also called batch settling process, is studied from the experimental and theoretical points of view by means of a settling column. A schematic diagram is displayed in figure 1. On the one hand, the proposed experimental setup has a volume of approximately 113 L for an overall height of 1 m. Batch settling experiments, see Locatelli et al. (2015b) for more detail, are carried out using activated sludge samples taken in a wastewater treatment plant and stirred to a homogeneous concentration. On the other hand, under the former assumption, a one-dimensional model is developed for numerical settling experiments following Bürger et al. (2013). Considered individually, each of these approaches raise important issues such the design of non-invasive device to measure actual velocity and concentration profiles, or the use of phenomenological laws in the modelling.

Data assimilation is a powerful computational methodology to tune a model with data as long as data and the model are actually comparable. As a preamble, this section discusses experimental data and Modelling, as well as the objective function that enables to compare them. A particular attention is brought to the resulting computer code.

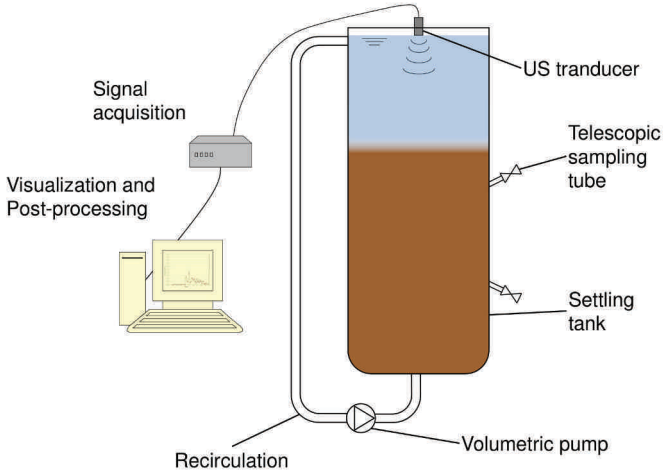

Figure 1 – Diagram of the experimental setup

2.1 Experimental data

A former work Locatelli et al. (2015b) discusses the use of a non-invasive method based on an ultrasonic transducer located above the settling column. The analysis of the measured signals according to the ultrasonic velocity profile method Takeda (1995) provides the complete settling velocity profiles

of activated sludge suspensions. The Doppler frequency shift values $f_D(z)$ are calculated along the column by a Fast Fourier Transform of the backscattered signal. The settling velocity v_s ($m \cdot s^{-1}$) can be deduced from the Doppler frequency shift f_D (Hz) following:

$$v_s = \frac{c f_D}{2 f_c}, \tag{1}$$

where c is the sound velocity ($m \cdot s^{-1}$) and f_c is the carrier wave frequency (Hz).

The sensitivity analysis described in a companion paper Locatelli et al. (2015a) shows that the concentration is the most sensitive variable to perturbations in the Modelling parameters. The concentration profiles are deduced from the experimental velocity data by means of numerical tracers (Locatelli et al., 2015b). The column is discretised in n_l layers, and N tracers are defined at regular interval along its axis, with $N > n_l$. At the beginning of an experiment, the number of tracers in a layer i is:

$$n_t(i, t = 0) = n_{t,0} = \frac{N}{n_l}. \tag{2}$$

Each tracer carries the value of the initial concentration and has a vertical position z. The vertical move of a tracer is calculated using the measured settling velocity at height z. At time t, the concentration in a layer i, $C(i,t)$, can be calculated from the number of tracers $n(i,t)$ it contains as:

$$C(i,t) = \frac{n(i,t)}{n_{t,0}} C_0. \tag{3}$$

Experimental concentration profiles are plotted in figure 2.a. Irregularities are the result of small fluctuations in the velocity data. In the upper part of the column, a sharp increase of concentration materialises the interface between the sludge blanket and the sludge-free supernatant. During the first hours of sedimentation, the sludge thickens with a comparatively low concentration gradient. During the batch settling process, the activated sludge exhibits two main behaviours:

- hindered settling: also called "zone settling" because the whole upper region of the sludge suspension settles at constant, homogeneous velocity and concentration,
- compression settling: at the bottom of the sludge blanket, below the zone settling region, the suspension thickens so that the particles are eventually in permanent contact with each other. The limit between the thickening and zone settling regions moves progressively upward until all the interstitial water is expelled toward the top of the settling column and the whole sludge blanket is in compression.

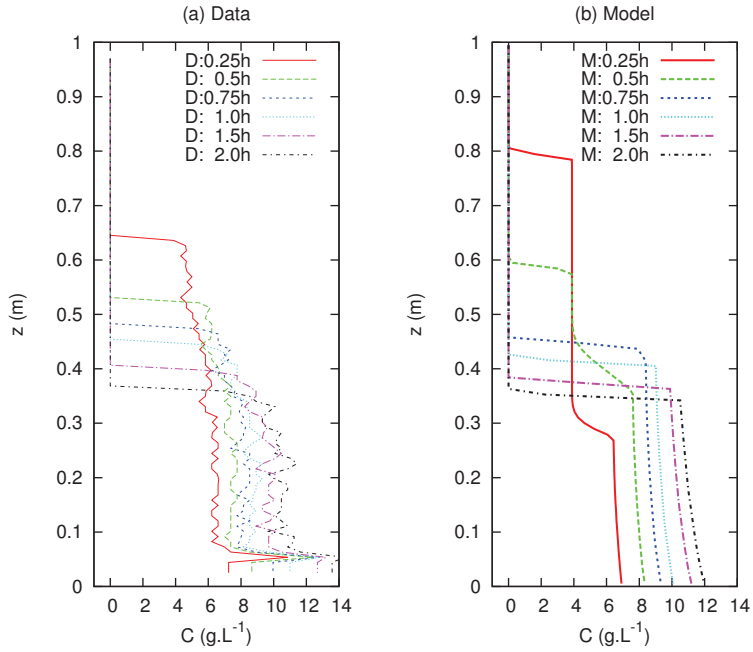

Figure 2 – Concentrations along the column axis. (a): Data; (b): uncalibrated model.

2.2 Settling column model

In spite of their relative simplicity, single-phase, one-dimensional approaches are key tools for the Modelling of secondary settling tanks. This type of model provides the main outputs of interest regarding secondary settling tank monitoring, i.e. underflow and effluent concentrations. In addition, such models can be incorporated in integrated wastewater treatment plant models (Vanhooren et al., 2003; Gernaey et al., 2004; Brdys et al., 2008).

Mechanistic one-dimensional settling models basically consist in the application of the equations of conservation of mass and momentum to the relative motions of particles and water. This yields equations based on the fundamental physical parameters of activated sludge suspensions (Bürger, 2000). Practically, several parameters, e.g. the drag coefficient of flocs, the pore pressure or the effective solids stress, are difficult or impossible to measure directly. Therefore, mechanistic equations are combined with phenomenological functions to design simpler and faster models that nevertheless require calibration with respect to experimental data.

Following Bürger (2000) and Bürger et al. (2013), the main equation of the model is

$$\frac{\partial C}{\partial t} + \frac{\partial f_{\mathrm{bk}}(C)}{\partial z} = \frac{\partial^2 D(C)}{\partial z^2}, \tag{4}$$

where C is the concentration ($\mathrm{g{\cdot}L^{-1}}$), and the Kynch batch flux density function f_{bk}, which accounts for hindered settling, as well as the primitive D of the compression function d_{comp} are physical parametrisations. For the sake of conciseness, the dependence of C in the time variable t and the space variable z is omitted hereafter.

The numerical method used is derived from (Bürger et al., 2013). The left-hand side convective part is computed first. It models hindered settling using function f_{bk}:

$$f_{\mathrm{bk}}\left(C\right) = Cv_{\mathrm{s}}\left(C\right), \text{ with } v_{\mathrm{s}}\left(C\right) = v_0 e^{-r_{\mathrm{V}}C}, \tag{5}$$

where the parameters v_0 and r_{V} define the sedimentation velocity parametrisation v_{s} proposed by Vesilind (1968). The Kynch batch flux is calculated using a Godunov method Godunov (1959). The compression of the sludge, right-hand side of equation (5), is modelled using the parameterised function D,

$$D\left(C\right) = \int_{C_{\mathrm{c}}}^{C} d_{\mathrm{comp}}\left(C\right) \mathrm{d}s, \tag{6}$$

where the compression function d_{comp},

$$d_{\mathrm{comp}}(C) = \begin{cases} 0, & \text{if } 0 \leq C < C_{\mathrm{c}}, \\ \dfrac{\rho_{\mathrm{s}}}{\Delta\rho g C} f_{\mathrm{bk}}\left(C\right) \dfrac{\partial \sigma_{\mathrm{e}}}{\partial C}(C), & \text{if } C \geq C_{\mathrm{c}}. \end{cases} \tag{7}$$

depends on the solids density ρ_{s} ($\mathrm{kg{\cdot}m^{-3}}$), the difference $\Delta\rho$ ($\mathrm{kg{\cdot}m^{-3}}$) between the densities of the solids and water, the gravitational constant g ($\mathrm{m{\cdot}s^{-2}}$) and the derivative of the effective solids stress function σ_{e} (Pa). The phenomenological function

$$\sigma_{\mathrm{e}} = \begin{cases} 0, & \text{if } 0 \leq C < C_{\mathrm{c}}, \\ \alpha \ln\left(1 + \dfrac{C - C_{\mathrm{c}}}{\beta}\right), & \text{if } C \geq C_{\mathrm{c}}, \end{cases} \tag{8}$$

depends on the unknown parameters α and β and the critical concentration C_{c} above which the sludge is in compression. A schematic view of the computer code is provided in table 1. The interested reader is referred to Locatelli et al. (2015a) for further information about the different subroutines.

From a numerical point of view, stability criterions determine the value of the time step. The column is discretised using 90 equispaced points along the column. The spatial step size (approximately 0.01 m) is computed with respect to the water height in the experimental settling column to consider the same sludge quantity in both the experiments and the simulations. For reproducibility purposes, concentration profiles computed with classical parameter values Bürger et al. (2011) are plotted in figure 2.b. Although data and simulated profiles present similar behaviours, figure 2 highlights the need for model tuning to reproduce the observed settling process and calibrate the simulation tool.

```
subroutine SETTLING_MODEL
    Calls subroutine INITIALIZE_CZ
    Calls subroutine COMPRESSION_FCT
        Calls function DCOMP
    Calls subroutine DT_STABILITY_CRITERION
        Calls function DFDC
        Calls function DCOMP
    Calls subroutine GODUNOV_FLUX
        Calls function KYNCH_FCT
    Calls subroutine DIFFUSIVE_FLUX
        Calls function DISP
    Calls subroutine UPDATE_C
    Calls subroutine SEDIMENTATION_VELOCITY
        Calls function KYNCH_FCT
    Calls subroutine UPDATE_CRITICALC
    Calls subroutine COST_FUNCTION
```

Table 1 – Original call graph

Parameter	Value	Signification
v_0	3.47 $\mathrm{m{\cdot}h^{-1}}$	Vesilind function parameter
r_V	0.37 $\mathrm{kg^{-1}{\cdot}m^3}$	Vesilind function parameter
α	4.0 Pa	Compression function parameter
β	4.0 $\mathrm{kg{\cdot}m^{-3}}$	Compression function parameter
C_0	3.88 $\mathrm{kg{\cdot}m^{-3}}$	Initial sludge concentration
g	9.81 $\mathrm{m{\cdot}s^{-2}}$	Gravitational acceleration
N_z	90	Space discretisation
ρ_s	1050 $\mathrm{kg{\cdot}m^{-3}}$	Solids density
ρ_w	998 $\mathrm{kg{\cdot}m^{-3}}$	Water density
z_max	0.975 m	Experimental column height

Table 2 – Modelling parameters.

2.3 Objective function

The phenomenological laws (5) and (8) host four undetermined parameters, the values of which govern the behaviour of the computed concentration profiles. In a former work Locatelli et al. (2015a), sensitivity analysis performed with respect to these parameter notably reveals a larger sensitivity of the concentration to perturbation of the Vesilind parameters v_0 and r_{V}. As a consequence, discrepancies between data and simulation results are evaluated comparing concentration profiles by means of the least square objective function:

$$\mathcal{J}(C(p)) = \int_0^T \int_0^{z_{\max}} |\mathcal{H}C(p) - C^o|^2 dz dt, \tag{9}$$

where T is the simulation time (h), $p = (v_0, r_{\mathrm{V}}, \alpha, \beta)$ is the set of parameters to identify, C^o represents the experimental data concentration profiles (see subsection 2.1) interpolated using the model discretisation, and $C(p)$ represents the concentration profiles simulated along the time integration of the model. The observation operator $\mathcal{H}$ is introduced to measure quadratic errors at data times and heights.

The experimental set up and further data processing provide a plenty of concentration data profiles. Note that observations profiles C^o have to be significantly undersampled since a few data are theoretically and practically sufficient to ensure the identification of four parameters. Besides, the other concentration data may be used to validate the identification process. For identification/validation purposes, we arbitrarily choose the concentration profiles presented in figure 2.a.

3 Data assimilation and differentiation

Calibration of a model is an important aspect of geophysical and chemical sciences. Data assimilation allows for parameter estimation and model tuning through the solution of a minimisation problem. This compares acquired data containing partial noisy information about the phenomenon under study and model solutions obtained for a prescribed set of parameters. The paper is concerned with the efficient variational data assimilation technique (Le Dimet and Talagrand, 1986) that solves the minimisation problem by means of a gradient method. The guidelines of this classical method are hereafter recalled for a one-dimensional column model with a particular attention to implementation of the adjoint code by means of automatic differentiation.

3.1 Inverse problem

For the sake of conciseness and generality Charpentier (2007), the data assimilation process is first described in general term.

General model Let $C(p)$ be the state variable belonging to the set $\mathbf{C}$ of the admissible concentration states along the settling column. Let p be a set of parameters belonging to the admissible sets of parameters $\mathbf{P}$. For the sake of conciseness, the governing equations of the column (4)–(8) are written as the simplified model $\mathcal{M}: \ \mathbf{C} \times \mathbf{P} \mapsto \mathbf{C}$ following

$$\mathcal{M}(p) = \begin{cases} \dfrac{dC(p)}{dt} = M(C(p)) \quad \text{in} \quad (0,T), \\ C(0) = C_0, \end{cases} \tag{10}$$

where M is the nonlinear operator from $\mathbf{C}$ to $\mathbf{C}$ that describes the dynamic behaviour of the model and C_0 is the initial homogeneous sludge concentration. The solution of $\mathcal{M}(p)$ is the state concentration $C(p)$.

General objective function Data are injected into the modelling process by means of the objective function

$$\begin{gathered} \mathcal{J}: \mathbf{C} \to I\!R \\ \mathcal{J}(\mathcal{M}(C_0,p)) = \frac{1}{2}\int_0^T |\mathcal{H}C(p) - C^o|^2 dt, \end{gathered} \tag{11}$$

where $\mathcal{H}$ is a linear observation operator that maps $\mathbf{C}$ to the discrete observation space $\mathbf{C}^o$. Let p_m be the set of parameters such that the solution $C = \mathcal{M}(p)$ of (10) fits at best observed data C^o along the column. Under differentiability assumption, the solution p_m of the minimisation problem

$$\begin{gathered} \textit{Find } p \in \times\mathbf{P} \textit{ such that} \\ \min_{p\in\mathbf{P}} \mathcal{J}(\mathcal{M}(p)) = \min_{p\in\mathbf{P}} (\mathcal{J}\circ\mathcal{M})(p) = p_m \end{gathered} \tag{12}$$

may be computed solving

$$\textit{Find } p \in \mathbf{P} \textit{ such that } \nabla(\mathcal{J}\circ\mathcal{M})(p) = 0, \tag{13}$$

where $\nabla(\mathcal{J}\circ\mathcal{M})$ is the gradient of $(\mathcal{J}\circ\mathcal{M})$ calculated with respect to p. The solution for (13) may be computed by means of an iterative gradient method.

Gradient computation is an key tool in scientific computing. Nowadays, automatic differentiation (Griewank and Walther, 2008b) may be applied to general codes representing mathematical functions to obtain codes that allow for accurate and efficient derivative computations in a simple manner.

3.2 Automatic differentiation

The differentiation of $(\mathcal{J}\circ\mathcal{M})$ with respect to p requires the differentiation of the original model (10). The following two subsections describe the tangent linear mode and adjoint modes of differentiation of the computer

code related to the settling model. The proposed description is intended to be general following AD principles. In other words, tangent linear and adjoint equations related to (4)–(8) are useless and thus not discussed since the actual differentiation is carried out on the code using an AD tool.

3.3 Tangent linear mode of differentiation

The tangent linear mode of differentiation, also called forward mode, mimics the classical manual differentiation following rules such as "the derivative of the sum is the sum of the derivatives". It thus constitutes an affordable preamble to the more tricky adjoint mode of differentiation.

Applying the chain rule, the differentiation of $(\mathcal{J} \circ \mathcal{M})$ with respect to the parameters p in the direction of perturbation δp yields

$$\delta_j = \nabla(\mathcal{J} \circ \mathcal{M})(p).\delta_p = \nabla\mathcal{J}(\mathcal{M}(p)).\nabla\mathcal{M}(p).\delta p, \tag{14}$$

where $\nabla\mathcal{M}$ is the Jacobian of $\mathcal{M}$ computed with respect to p and $\nabla\mathcal{J}$ is the gradient of $\mathcal{J}$ computed with respect to C. The real-valued output perturbation δ_j is the sensitivity of $\mathcal{J} \circ \mathcal{M}$ computed at point p in the direction δ_p.

On the one hand, tangent linear models are well-adapted to the sensitivity analyses of large state variables with respect to a few directions of perturbation. A recent example Locatelli et al. (2015a) is the sensitivity study of concentration profiles $C = \mathcal{M}(p)$ to parameters v_0, r_V, α and β. On the other hand, the computation of the gradient $\nabla\mathcal{J}$ may require as many evaluations of (14) as the dimension of the set of parameters p, four in the present case. According to the theoretical bounds computed by Morgensten (1985), the operation count for the computation of one component of the gradient is at most 4 times larger than those of the original code integration. This ratio thus raises 4×4 times for the gradient computation with respect to v_0, r_V, α and β.

Although the tangent linear differentiation task is not a difficult one, handcoding often reveals to be an error-prone process. Any automatic differentiation tool allows for the differentiation of computer codes in tangent linear mode. The interested reader is referred to autodiff.com, the website of the automatic differentiation community, for complementary detail. Among the available software, we choose Tapenade Hascoët and Pascual (2013), developed at INRIA Sophia-Antipolis by the TROPICS team, since it is freely available for research purposes and may be applied to general fortran codes. This AD tool may be invoked in three different manner. For small codes (less than 3000 lines), the web interface gives access to the "Tapenade On-line Automatic Differentiation Engine"[1]. The resulting code may be downloaded from the website. Larger codes require to download the Tapenade software

[1] http://tapenade.inria.fr:8080/tapenade/index.jsp

for a local installation. Differentiation is then performed using the graphical user interface. A Tapenade command may also be used.

The original code, table 1, is differentiated providing the source files, the name `SETTLING_MODEL` of the top routine to be differentiated, the "independent" input variables, here variables `v0 rv alpha beta`. The differentiation of the settling code takes about 3.9s in tangent linear mode. The Call graph of the tangent linear code produced by Tapenade is very similar to the call graph of the original code, the routines of which are suffixed with a `_D` when differentiated. This tangent linear code gives access to the calculation of the discrepancy $\mathcal{J} \circ \mathcal{M}(p)$ and a directional derivative $\delta_j = \nabla(\mathcal{J} \circ \mathcal{M})(p).\delta p$.

3.4 Adjoint mode of differentiation

The so-called "adjoint" mode enables to overcome the deadlock of the possibly large dimension of the parameter set p. For theoretical purposes, the nonlinear model $\mathcal{M}$ and the nonlinear $\mathcal{J}$ are extended so that their domain and codomain are identical. From a theoretical point of view, the Jacobians of $\mathcal{M}$ and $\mathcal{J}$ are then square real matrices of the same dimension and one may prove that

$$\begin{aligned}(\nabla\mathcal{J}(\mathcal{M}(p)).\nabla\mathcal{M}(p).\delta p, \delta j) &= (\delta p, [\nabla\mathcal{J}(\mathcal{M}(p)).\nabla\mathcal{M}(p)]^*.\delta j) \\ &= (\delta p, [\nabla\mathcal{M}(p)]^*.[\nabla\mathcal{J}(\mathcal{M}(p))]^*.\delta j),\end{aligned} \tag{15}$$

where the terms $[\nabla\mathcal{M}(p)]^*$ and $[\nabla\mathcal{J}(\mathcal{M}(p))]^*$ are the transpose of $\nabla\mathcal{M}(p)$ and $\nabla\mathcal{J}(\mathcal{M}(p))$, respectively. From a computer point of view, the former domain extension signifies that the arguments of functions $\mathcal{M}$ and $\mathcal{J}$ are assumed to comprise all the variables involved in the computations. This is not a requirement in practical use. The adjoint operator to the related nonlinear operator $\mathcal{J} \circ \mathcal{M}$ is the linear operator $[\nabla\mathcal{M}(p)]^*.[\nabla\mathcal{J}(\mathcal{M}(p))]^*$. Given a perturbation δj, the adjoint operator is evaluated from the right to the left. More precisely, the transposition of the operators signifies that the adjoint of the objective function $\mathcal{J}$ is computed first. Then, the adjoint operator of $\mathcal{M}$ is evaluated.

The effect of the transposition may be observed in the call graph of the adjoint routine `SETTLING_MODEL_B` generated by Tapenade from the `SETTLING_MODEL` routine, see table 3. Using Tapenade naming convention, adjoint routines are suffixed with a `_B` and contain the necessary information for the evaluation of the adjoint statements. The differentiation of the settling code takes about 6.7s in adjoint mode. As expected from (15), adjoint routines are called in the reverse order.

The extension of the domain and codomain is a theoretical argument only. Keeping in mind that the result of the objective function $\mathcal{J}$ is a real number, this signifies that the computation of $\nabla(\mathcal{J} \circ \mathcal{M})$ requires a unique evaluation of the adjoint operator $[\nabla(\mathcal{J} \circ \mathcal{M})]^*$. Theoretical results (Morgensten (1985)) indicate that the ratio between the number of operations of the adjoint code

```
subroutine SETTLING_MODEL_B
    Calls subroutine COST_FUNCTION_B
    Calls subroutine UPDATE_CRITICALC_B
    Calls subroutine SEDIMENTATION_VELOCITY_B
        Calls subroutine KYNCH_FCT_B
    Calls subroutine UPDATE_C_B
    Calls subroutine DIFFUSIVE_FLUX_B
    Calls subroutine GODUNOV_FLUX_B
        Calls subroutine KYNCH_FCT_B
    Calls subroutine DT_STABOBS_CRITERIONS_B
        Calls subroutine DCOMP_B
        Calls subroutine DFDC_B
    Calls subroutine COMPRESSION_FCT_B
        Calls subroutine DCOMP_B
```

Table 3 – Adjoint call graph

and the number of operations of the original code may be lower than 5, whatever the dimension of the input space.

3.5 Validation tests

AD codes compute derivatives up to the machine precision and this is of prime interest for the solution of inverse problems requiring accurate gradient evaluations. The correctness of the differentiated codes generated using the Tapenade AD tool is verified through a so-called Taylor test, then a comparison of gradient components computed using the tangent linear and the adjoint code.

Taylor test for the adjoint code The differentiated codes generated using the software Tapenade (Hascoët and Pascual (2013)) are verified through a Taylor test (16). This compares the AD computed derivative with first order finite differences

$$r_\omega = \frac{|(\mathcal{J}o\mathcal{M})(p+\omega e^i) - (\mathcal{J}o\mathcal{M})(p))|}{\omega|\nabla(\mathcal{J}o\mathcal{M})^*(p).e^i|}, \tag{16}$$

where $\omega \in I\!R$ tends to 0 and $e^i = \delta p$ is a vector of the canonical basis of $I\!R^4$.

Table 4 presents the Taylor test carried out with respect to v_0 using $p = (v_0, r_V, \alpha, \beta) = (3.47, 0.37, 4.0, 4.0)$, $e_i = (1, 0, 0, 0)$ and $t = 0.5$ h. One observes that the ratio r_ω tends linearly towards 1 until some ω of the order of 10^{-8} (which is the optimal value for the finite difference computation). For $\omega \leq 10^{-8}$, the subtraction of too close floating-point numbers carried out in the finite difference approximation results in a cancellation error that

Table 4 – Result of the Taylor test for a derivation of the code with respect to v_0.

ω	$\frac{\lvert(\mathcal{J}o\mathcal{M})(p+\omega e^i)-(\mathcal{J}o\mathcal{M})(p))\rvert}{\omega\lvert\nabla(\mathcal{J}o\mathcal{M})^*(p).e^i\rvert}$
1.E-01	3.2286904326109673
1.E-02	0.93942255406212860
1.E-03	0.99200631259904126
1.E-04	0.99932700072451730
1.E-05	0.99992695585847757
1.E-06	0.99999266402412201
1.E-07	0.99999885512424425
1.E-08	0.99999919479988553
1.E-09	0.99997275739455116
1.E-10	0.99993142337073115
1.E-11	0.99921933226729687
1.E-12	0.97523741349646476
1.E-13	0.94945480457901732

dominates the truncation error. This is an expected behaviour: the derivatives computed with respect to a perturbation of v_0 are correct. Taylor tests performed with to the other three parameters present a similar behaviour.

Tangent linear derivatives vs. adjoint derivatives AD provides tangent linear and adjoint codes for the computation of the first order derivatives of the settling code. Gradient components of $(\mathcal{J}\circ\mathcal{M})$ computed at time $T = 0.5$ h with the different methods are reported in Table 5. One observes that gradient components obtained with the tangent linear code and the adjoint code are identical identical down to the 12^{th} digit. As expected from the Taylor test, the finite difference (FD) approximations carried out with the optimal parameter $\omega = 10^{-8}$ disagree with AD computed derivatives at the level of the 7^{th} digit.

These two tests indicate that the adjoint subroutine `SETTLING_MODEL_B` is correct and may be used with confidence in an optimisation process.

4 Identification results

The method detailed previously allows calculating parameter values using the experimental data and different objective functions. This process is discussed hereafter.

Table 5 – Comparison of computed gradient components, parameter set $T = 0.5$.

Code	$\nabla(\mathcal{J} \circ \mathcal{M})$ computed with respect to			
	v_0	r_V	α	β
Tangent linear	-34.724331	311.007212	-1.484024	1.409808
Adjoint	-34.724331	311.007212	-1.484024	1.409808
FD approximation	-34.724303	311.007654	-1.484029	1.409925

Parameter	Initial guess	Lower bound	Upper bound
v_0 ($\mathrm{m{\cdot}s^{-1}}$)	3.47	0.50	12.0
r_V ($\mathrm{L{\cdot}g^{-1}}$)	0.37	0.50	2.00
α (Pa)	4.00	1.00	6.00
β ($\mathrm{g{\cdot}L^{-1}}$)	4.00	1.90	7.00

Table 6 – Initial guess and ranges for the parameters.

4.1 Numerical setting

Unknown parameters are searched within typical ranges for sludge columns to avoid too small time steps during the iterative process. Parameters of the Vesilind function v_0 and r_V are correlated and there does not exist a unique solution to the identification problem. The initial guess, lower and upper bounds for the 4 parameters are reported in Table 6. One notices that the lower bound for r_V is set to 0.50 to enable calculation with values of v_0 up to 12.0. Other Modelling parameters are set constant, see table 2.

The applied optimisation process is driven by the bound-constrained quasi-Newton algorithm proposed by Byrd et al. (1995). Note that a successful data assimilation process assumes a Gaussian noise on the data. Consequently, the identification may occur even the standard deviations of the samples are large. However, smaller the standard deviations, smaller the errors.

4.2 Identification experiments

The parameter identification is carried out with data at times 0.25 h and 0.5 h in order to capture the early behaviour of the mixture and notably the height of the sludge blanket interface. Eight numerical experiments have been designed. These use objective functions related to the sludge blanket interface or concentration profiles. These experiments are labelled as follows:

Table 7 – Objective functions used in the experiments

Data	Label	Discrete cost function
SB Interface at 0.25 h	I1	$\mathcal{J}_1^{\mathrm{I}} = \sum_{i=30,40,3} \lvert C(i) - C^o(i)\rvert^2$
SB Interface at 0.5 h	I2	$\mathcal{J}_2^{\mathrm{I}} = \sum_{i=42,52,3} \lvert C(i) - C^o(i)\rvert^2$
Concentration Profile	P	$\mathcal{J}^{\mathrm{P}} = \sum_{i=3,90,2} \lvert C(i) - C^o(i)\rvert^2$

Table 8 – Identified parameters for the different experiments.

Label	v_0	r_{V}	α	β
I1P2	12.000000	0.594969	4.640981	3.390977
P1P2	12.000000	0.585853	4.987951	3.061325
P1	12.000000	0.567303	5.806623	1.900000
P1I2	12.000000	0.568274	4.348004	3.669689
P2	9.723967	0.562752	5.827704	1.899999
I1I2	10.580728	0.582007	4.113836	3.891088
I2	9.163166	0.557054	4.090902	3.913035
I1	–	–	–	–

- the letter I means that the position of the sludge blanket interface is used,
- the letter P means that the concentration profile is used.

The number following the letter, 1 or 2, indicates the observation time, 0.25 h or 0.5 h respectively. As an example, the label I1P2 signifies that the sludge blanket interface at time 0.25 h and the concentration profile at time 0.5 h serve as data in this identification experiment. The objective functions are provided in Table 7.

Table 8 summarises the list of the experiments and provides the corresponding identified parameter values. Experiments resulting in very similar settling curves are grouped together.

4.3 Discussion

Early behaviour A settling curve plots the position of the sludge blanket interface. The sensitivity analysis (Locatelli et al., 2015a) showed that the model parameters have a very important influence on the position of the sludge blanket interface, particularly during the hindered settling phase. Four of the optimised settling curves are plotted, along with the curves related to the initial guess and the data. Figure 5.a shows that the best fit is obtained with experiment I1P2 using interface data at time 0.25 h and profile data at time 0.5 h. Experiments P2 and I2 overestimate the height of the sludge blanket during the first 0.4h of sedimentation since lower values of v_0 were identified for these two experiments. This is consistent with the sensitivity analysis Locatelli et al. (2015a) that proves the significant influence of this parameter on the position of the sludge blanket during the zone settling phase. After 0.4 h, settling curves related to experiments P2, I2 and I1P2 exhibit the same behaviour. This signifies that considering only data at 0.5 h suffices to provide a good fit with the data up to 3 h of sedimentation, although this does not allow reliably modelling the earlier stages of sedimentation Experiment P2 also tends to underestimate the sludge blanket height up to 2 h. Though this experiment led to the same value of v_0 as experiment I1P2, it yielded a lower value of r_V. This is consistent with the role of r_V in the formula of Vesilind (5), where it controls the rate of decrease of the zone settling velocity with respect to the concentration C.

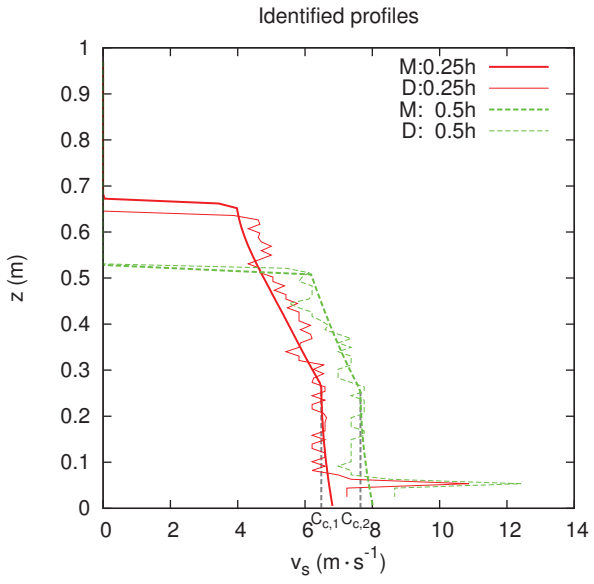

Figure 3 – Optimised concentration profiles obtained with the parameter set I1P2 versus concentration data at 0.25 h and 0.5 h.

Figure 3 shows that the experimental concentration profile is well reproduced by the model with the parameter set I1P2, particularly the evolution of the critical concentration and the position of the limit between the hindered settling layer and the compression layer. The position of the interface between the sludge blanket and the supernatant is slighty off at 0.25 h, but almost superimposed on the experimental data at 0.5 h. In order to test the predictivity of the model, simulation results obtained with the parameters of experiment I1P2 are compared to experimental data at later times (figure 4). It appears that, despite concentration fluctuations, the model is able to simulate the behaviour of the concentration profile accurately. During the first 2h of sedimentation, the discrepancy between the simulated interface and the data remains marginal. This time is consistent with the duration of industrial processes and batch settling experiments.

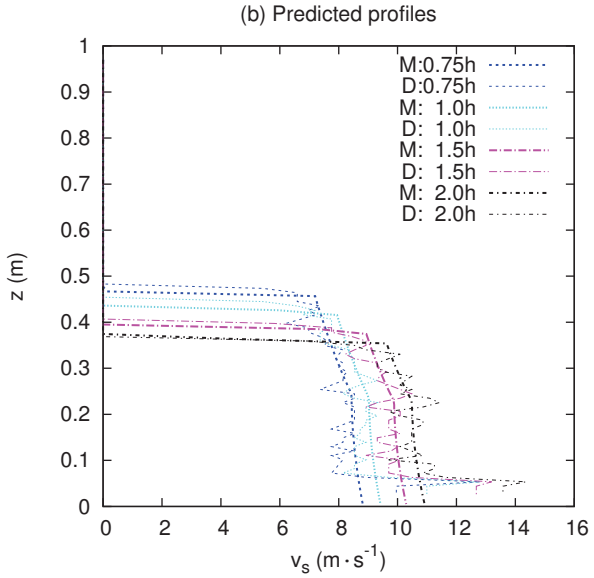

Figure 4 – Predicted concentration profiles obtained with the parameter set I1P2.

Long time behaviour and log-log plot As discussed before, the parameter set obtained with experiment I1P2 is the most satisfactory along the first 3 hours. However, figure 5.b shows that, after 3 h of sedimentation, the model results diverge from the experimental data and overestimate the sludge blanket height. The log-log scale we use emphasises the discrepancy between the model solutions and experimental results. The experimental settling curve presented in figure 5, as well as results of similar tests performed with different sludge concentrations Locatelli (2015), show a linear behaviour in log-log

plot, which reveals that the sludge blanket interface moves according to a power law. This observation highlights the model shortcomings and shows ways to improve it by demonstrating that it reaches a state of equilibrium too quickly. The observed discrepancies can also be explained by the fact that the exponential Vesilind function simulates some effects of the compression, and thus impinges on the influence of the compression function (Torfs et al., 2015). Additionally, the other model parameters, particularly those of the compression function, may vary with time, as the critical concentration.

5 Conclusions

The automatic differentiation and variational data assimilation methodologies have proven their efficiency for the identification of various inputs of the model and may be used to identify other parametrisations, including phenomenological laws such as the Cole function or spline–based parametrisations, for instance.

The early behaviour is well reproduced using a few interface data and concentration profiles up to 3 h of sedimentation. This time is consistent with the durations of industrial processes and batch settling experiments. The log-log scale we use emphasises the discrepancy between the model solutions and experimental results for longer experiments. The experimental settling curve shows a linear behaviour in log-log plot, which reveals that the sludge blanket interface moves according to a power law. The model we use is unable to reproduce this behaviour. This observation highlights the model shortcomings and suggests that the phenomenological laws have to be improved, notably by including parameters varying with time.

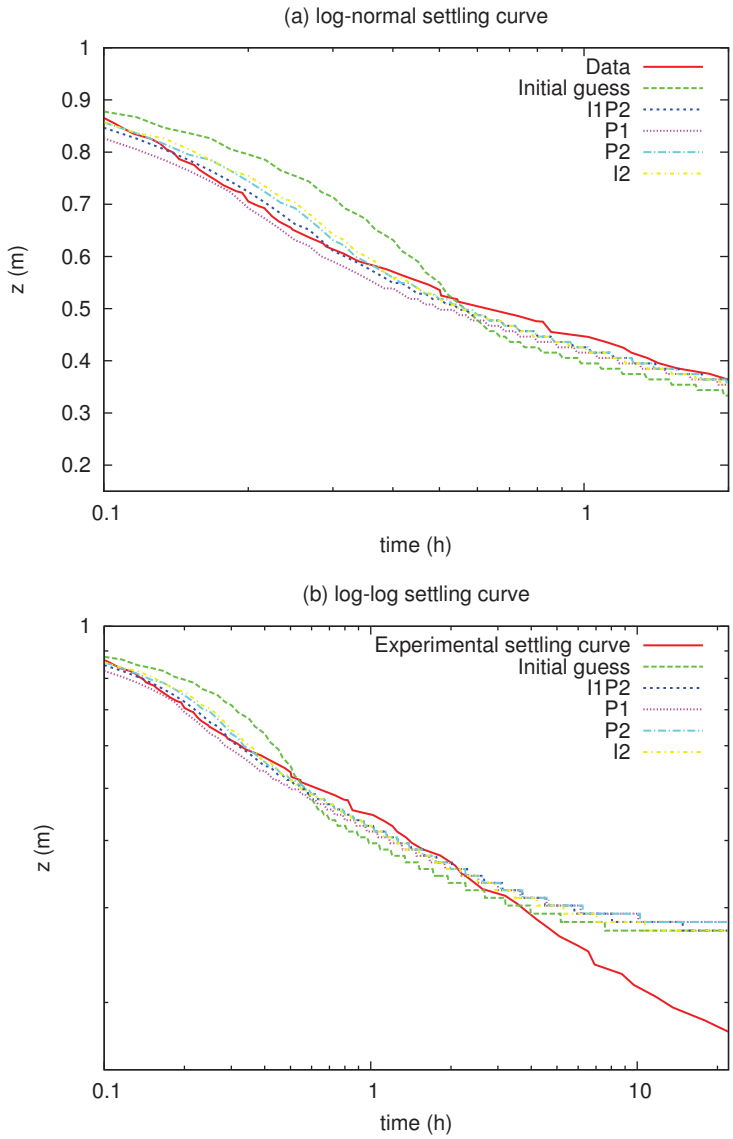

Figure 5 – (a) Settling curves during 2 h with the time in log-scale and (b) settling curves during 22 h in log-log scale

Conclusions and perspectives

Conclusions

The work carried out during the course of this Ph.D. thesis led to the development of a consistent methodology combining an experimental process and a modelling approach aimed at a better understanding of activated sludge batch settling. An experimental setup was designed for this purpose. It is based on a settling column and the application of the Ultrasonic Velocity Profile measuring method (Takeda, 1995). This method has several advantages. First, it is non-invasive, and therefore does not disturb the sedimentation process. Second, the acquisition frequency is adjustable, allowing for long term experiments. Third, it can be implemented in actual wastewater treatment plants. This method allows detecting the sludge blanket interface and measuring the complete settling velocity profile with great precision. The experimental setup thus made studying the internal behaviour of settling activated sludge possible.

Numerous tests were performed, yielding results of different natures. Irregularities in the behaviour of the sludge samples studied were detected early in the experimental phase on the basis of the settling curves. In order to explain these irregularities, the influences of the non-volatile fraction of the sludge and temperature of the suspension were investigated. Loess was used as an additive to artificially modify the non-volatile fraction of the sludge. The impact of this fraction on the hindered settling velocity was quantified and a relationship was deduced from the experimental results. Pycnometry measurements were carried out; the results obtained were used to express the modification of the sludge density as a function of the additional amount of loess. Although the non-volatile fraction was noted to have an important impact on the hindered settling velocity, only a marginal change of the settling velocity during the compression phase was observed. In order to isolate the influence of temperature of the suspension, experiments were performed in a small settling column. The obtained results showed that increasing the temperature tends to increase the settling velocity.

The long term behaviour of activated sludge was studied during extended batch settling experiments. A relationship was deduced from the results to

express the settling velocity as a function of time and the height in the settling column. This relationship showed a good agreement with the experimental results during approximately 2 hours of sedimentation. Despite significant variations of the initial concentration and sludge blanket height from a sludge sample to another, the settling velocity appeared to follow a common trend. The velocity profiles showed that, after a few hours of sedimentation, the settling velocity gradient tends to disappear near the top of the sludge blanket, where the effects of gravity are counterbalanced by the resistance of the sludge to deformation. The obtained velocity data were used to evaluate the evolution of the concentration inside of the sludge blanket. It appeared that the concentration remains fairly homogeneous up to 2 h of sedimentation. Afterwards, a concentration gradient develops. However, the concentration remains comparatively constant in the vicinity of the sludge blanket interface. A relationship was proposed to express the evolution of the critical concentration of the sludge with time. Additionally, a hypothesis was formulated on the basis of the behaviour of the concentration, and a relationship was deduced to express the sludge blanket height as a function of time. This relationship was compared with good results to the experimental settling curves.

A rheological study was performed so as to propose a model adapted to activated sludge. An experimental procedure was developed, and a method to correct the bias introduced by the measuring equipment in the data was implemented. The Cross model was satisfactorily fitted to the data, and the evolutions of its parameters and of the observed yield stress with the concentration were expressed.

The experimental data obtained provided an extensive base for model testing. A 1D settling model was developed on the basis of the method proposed by Bürger et al. (2013) and integrating the critical concentration equation deduced from the experimental results. This model involves phenomenological equations for the hindered settling velocity and the effective solids stress of the sludge. In order to study the sensitivity of the model results to the phenomenological parameters, the settling code was differentiated using the automatic differentiation software Tapenade (Hascoët and Pascual, 2004). The specific influences of each model parameter were described. Following this sensitivity analysis, a gradient-based data assimilation process was implemented in order to evaluate the model parameters using the experimental data. Several sets of parameters were identified using the data of sludge blanket height and concentration. Among the identified parameter sets, the one providing the best fit with the experimental data was designated. The model thus parametrised allowed satisfactorily simulating the settling curve of the sludge used for the identification up to approximately 3 h. Afterwards, the model overestimates the sludge blanket height independently of the parameter set used. These results indicate that the model tends toward a state of equilibrium too quickly. The applied equa-

tions may be improved, for instance by taking the influence of the time on the involved parameters into account. Another source of discrepancy is due to the fact that the exponential Vesilind function models some effects of the compression and thus impinges on the influence of the compression function.

The methodology applied in this study, by combining detailed experimental results, a sensitivity analysis method and an identification process, offers promising possibilities for further improvement of activated sludge settling modelling.

Perspectives

The numerical method developed in this work may be used to improve the settling model. This can be done by including the influence of new variables, such as time, temperature or the non-volatile fraction of the sludge, in the model parameters. The experimental results obtained provide a good base material to this end. Other equations can also be tested to describe the sludge behaviour. The sensitivity analysis process allows determining the influence of the model parameters quickly and precisely. This process is flexible and can be applied to a variety of equations and models.

Combined with the developed experimental methodology, the model results can be confronted to precise data in a perspective of calibration and validation. Furthermore, the influences of additional sludge characteristics may be studied and quantified empirically. For instance, the manifest influence of the temperature of the suspension was highlighted and may be better described. Biological factors can also be considered and integrated in the numerical approach by using elements of the Activated Sludge Model. Indeed, products of the biological activity, such as extracellular polymeric substances (Mori et al., 2008) have been shown to impact the mechanical properties of the sludge, which can modify its behaviour during the compression phase. The denitrification process may also impair the sedimentation, as the dinitrogen bubbles produced can adhere to the flocs and prevent them from settling properly. However, it must be noted that the presence of bubbles in the suspension greatly affects the range of the ultrasonic equipment, for they drastically attenuate the signal. The flocculation of the sludge, by influencing the size of the particles, also has an influence on the hindered settling velocity. The characteristics mentioned may vary from one wastewater treatment plant to another. Since the experimental setup was designed to be transportable, extensive tests can be performed on different sites in order to evaluate the influences of specific aspects of the wastewater treatment process (flocculation agents, temperature, sludge age, filamentous bacteria, acidity, nitrous content, etc.).

The rheological study provided equations to link the value of the rheological parameters to the sludge concentration. Further tests can be performed

in order to account for such parameters as the temperature or the concentration of extracellular polymeric substances. The process of improving the rheological model can be enhanced by using sensitivity analysis techniques.

In further developments of the modelling methodology, a Computational Fluid Dynamics approach may be considered. A CFD model of the experimental settling column can easily be built due to its simple geometry, allowing for direct comparison between model and data. A CFD approach allows taking the rheological model of the sludge into account. Additionally, phenomenological hindered settling and compression equations, calibrated using the 1D approach, can be implemented in a CFD model. The influence of the hydrodynamics of the system on the parameters of these functions can thus be studied. The development of a CFD approach based on the key parameters identified by sensitivity analysis can thus be transposed to the modelling of actual secondary settling tanks. Based on a CFD work on the settling column, a CFD approach of the secondary settling tank can then be considered in order to study the impact of the 3D hydrodynamics (with possible instability developments and heterogeneity considerations) on the underflow and effluent concentrations.

Bibliography

Abda, F., Azbaid, A., Ensminger, D., Fischer, S., François, P., Schmitt, P., Pallarès, A., 2009. Ultrasonic device for real time sewage velocity and suspended particles concentration measurements. Water Sci. Technol. 60 (1), 117–125.

ANSYS®, 2012. Fluent, Release 14.5, Theory Guide, ANSYS, Inc.

Armbuster, M., Krebs, P., Rodi, W., 2001. Numerical modelling of dynamic sludge blanket behaviour in secondary clarifiers. Water Sci. Technol. 43 (11), 173–180.

Aziz, A. A. A., De Kretser, R. G., Dixon, D. R., Scales, P. J., 2000. The characterisation of slurry dewatering. Water Sci. Technol. 41 (8), 9–16.

Baines, W. D., Chu, V. H., 1996. Environmental Hydraulics. Kluwer Academic Publishers, Ch. Jets and Plumes, pp. 7–62.

Benedetti, L., Langeveld, J., Comeau, A., Corominas, L., Daigger, G., Martin, C., Mikkelsen, P., Vezzaro, L., Weijers, S., Vanrolleghem, P., 2013. Modelling and monitoring of integrated urban wastewater systems: Review on status and perspectives. Water Sci. Technol. 68 (6), 1203–1215.

Betancourt, F., Bürger, R., Diehl, S., Mejì as, C., 2014. Advanced methods of flux identification for clarifier-thickener simulation models. Minerals Engineering 63, 2–15.

Bischof, C., Carle, A., Hovland, P., Khademi, P., Mauer, A., 1995. Adifor 2.0 user's guide. Tech. rep., MCS-TM-192, Argonne National Laboratory, Argonne, IL, 1995.

Bolster, C. H., Hornberger, G. M., 2007. On the use of linearized langmuir equations. Soil Sci. Soc. Am. J. 71 (6), 1796–1806.

Brdys, M. A., Grochowski, M., Gminski, T., Konarczak, K., Drewa, M., 2008. Hierarchical predictive control of integrated wastewater treatment systems. Control Eng. Pract. 16 (6), 751–767.

Brennan, D., 2001. The Numerical Simulation of Two-Phase Flows in Settling Tanks. Ph.D. thesis, Imperial College of Science, Technology and Medicine, Department of Mechanical Engineering, University of London.

Bürger, R., 2000. Phenomenological foundation and mathematical theory of sedimentation-consolidation processes. Chem. Eng. J. 80, 177–188.

Bürger, R., Concha, F., Tiller, F., 2000a. Applications of the phenomenological theory to several published experimental cases of sedimentation processes. Chem. Eng. J. 80 (1–3), 105–117.

Bürger, R., Diehl, S., Farås, S., Nopens, I., 2012. On reliable and unreliable numerical methods for the simulation of the secondary settling tanks in wastewater treatment. Comput. Chem. Eng. 41, 93–105.

Bürger, R., Diehl, S., Farås, S., Nopens, I., Torfs, E., 2013. A consistent modelling methodology for secondary settling tanks: A reliable numerical method. Water Sci. Technol. 68 (1), 192–208.

Bürger, R., Diehl, S., Nopens, I., 2011. A consistent modelling methodology for secondary settling tanks in wastewater treatment. Water Res. 45, 2247–2260.

Bürger, R., Evje, S., Karlsen, K. H., Lie, K.-A., 2000b. Numerical methods for the simulation of the settling of flocculated suspensions. Chem. Eng. J. 80 (1–3), 91–104.

Bürger, R., Wendland, W., Concha, F., 2000c. Model equations for gravitational sedimentation-consolidation processes. ZAMM-Z. Angew. Math. Me. 80 (2), 79–92.

Buscall, R., White, L. R., 1987. The consolidation of concentrated suspensions. part 1.–the theory of sedimentation. J. Chem. Soc. Farad. T. 1 83 (3), 873–891.

Bye, C., Dold, P., 1998. Sludge volume index settleability measures: effect of solids characteristics and test parameters. Water Environ. Res. 70 (1), 87–93.

Byrd, R. H., Lu, P., Nocedal, J., Zhu, C., 1995. A limited memory algorithm for bound constrained optimization. SIAM J. Sci. Comput. 16, 1190–1208.

Cacossa, K. F., Vaccari, D. A., 1994. Calibration of a compressive gravity thickening model from a single batch settling curve. Water Sci. Technol. 30 (8), 107–116.

Castro, C., Zuazua, E., 2011. Flux identification for 1-d scalar conservation laws in the presence of shocks. Math. Comput. 80, 2025–2070.

Charpentier, I., 2000. The mesodif package for gradients computations with the atmospheric model meso-nh. Environ. modell. Softw. 15, 533–538.

Charpentier, I., 2007. Adjoint modeling experiments on eruptive columns. Geophys. J. Int. 169, 1356–1365.

Charpentier, I., Utke, J., 2009. Fast higher-order derivative tensors with rapsodia. Optim. Method. Softw. 24 (1), 1–14.

Cho, S. H., Colin, F., Sardin, M., Prost, C., 1993. Settling velocity model of activated sludge. Water Res. 27 (7), 1237–1242.

Cole, R. F., 1968. Experimental evaluation of the Kynch theory. Ph.D. thesis, University of North Carolina, Chapel Hill.

Couarraze, G., Grossiord, J., 1991. Initiation à la Rhéologie. Lavoisier Tec & Doc.

Cross, M. M., 1965. Rheology of non-newtonian fluids: a new flow equation for pseudoplastic systems. J. Coll. Sci. Imp. U. Tok. 20 (5), 417–437.

Dabak, T., Yucel, O., 1987. Modeling of the concentration particle size distribution effects on the rheology of highly concentrated suspensions. Powder Technol. 52 (3), 193–206.

Daigger, G. T., Roper, Jr., R. E., 1985. The relationship between svi and activated sludge settling characteristics. J. Water Pollut. Con. F., 859–866.

De Clercq, B., 2003. Computational fluid dynamics of settling tanks: development of experiments and rheological, settling, and scraper submodels. Ph.D. thesis, Faculty of Agricultural and Applied Biological Sciences, Ghent University.

De Clercq, B., Kinnear, D., Vanrolleghem, P., 2002. Hydraulic characterization of a wastewater treatment clarifier by an acoustic doppler current profiler. Adv. Fluid Mech. Ser. 32, 451–462.

De Clercq, J., 2006. Batch and continuous settling of activated sludge: in-depth monitoring and 1 D compression modelling. Ph.D. thesis, Faculty of Engineering. Ghent University.

De Clercq, J., Jacobs, F., Kinnear, D. J., Nopens, I., Dierckx, R. A., Defrancq, J., Vanrolleghem, P. A., 2005. Detailed spatio-temporal solids concentration profiling during batch settling of activated sludge using a radiotracer. Water Res. 39, 2125–2135.

De Clercq, J., Nopens, I., Defrancq, J., Vanrolleghem, P., 2008. Extending and calibrating a mechanistic hindered and compression settling model

for activated sludge using in-depth batch experiments. Water Res. 42 (3), 781–791.

Deininger, A., Holthausen, E., Wilderer, P. A., 1998. Velocity and solids distribution in circular secondary clarifiers: full scale measurements and numerical modelling. Wat. Res. 32 (10), 2951–2958.

Di Prima, R. C., Swinney, H. L., 1985. Hydrodynamic Instabilities and the Transition to Turbulence. Springer Berlin Heidelberg, Ch. Instabilities and transition in flow between concentric rotating cylinders, pp. 139–180.

Dick, R., Ewing, B., 1967a. The rheology of activated sludge. J. Water Pollut. Con. F. 39 (4), 543–560.

Dick, R. I., Ewing, B. B., 1967b. Evaluation of activated sludge thickening theories. J. Sanit. Eng. Div.-ASCE 93 (4), 9–30.

Dick, R. I., Vesilind, P. A., 1969. The sludge volume index: What is it? J. Water Pollut. Con. F. 41 (7), 1285–1291.

Diehl, S., 2015. Numerical identification of constitutive functions in scalar nonlinear convection-diffusion equations with application to batch sedimentation. Appl. Numer. Math. 95, 154–172.

Dochain, D., Vanrolleghem, P. A., 2001. Dynamical Modelling and Estimation in Wastewater Treatment Processes. IWA Publishing, Alliance House, 12 Caxton Street, London, UK.

Donnelly, R. J., 1958. Experiments on the stability of viscous flow between rotating cylinders. I. torque measurements. P. Roy. Soc. Lond. A Mat. 246 (1246), 312–325.

Eagles, P. M., 1974. On the torque of wavy vortices. J. Fluid Mech. 62, 1–9.

Eckert, S., Gerbeth, G., 2002. Velocity measurements in liquid sodium by means of ultrasound doppler velocimetry. Exp. Fluids 32 (5), 542–546.

Einstein, A., 1906. Eine neue Bestimmung der Moleküldimensionen. Ann. Phys.–Leipzig 19, 289–306.

Einstein, A., 1911. Berichtigung zu meiner Arbeit: „Eine neue Bestimmung der Moleküldimensionen“. Ann. Phys.–Leipzig 34, 591–592.

Elghobashi, S., 1994. On predicting particle-laden turbulent flows. Appl. Sci. Res. 52, 309–329.

Ferguson, J., Kemblowski, Z., 1991. Applied Rheology. Springer Verlag.

Garakani, A., Mostoufi, N., Sadeghi, F., Hosseinzadeh, M., Fatourechi, H., Sarrafzadeh, M., Mehrnia, M., 2011. Comparison between different models for rheological characterization of activated sludge. Iran J. Environ. Health 8 (3), 255–264.

Gernaey, K. V., van Loosdrecht, M. C. M., Henze, M., Lind, M., Jørgensen, S. B., 2004. Activated sludge wastewater treatment plant modelling and simulation: state of the art. Environ. Modell. Softw. 19 (9), 763–783.

Giokas, D., Daigger, G., Sperling, M., Kim, Y., Paraskevas, P., 2003. Comparison and evaluation of empirical zone settling velocity parameters based on sludge volume index using a unified settling characteristics database. Water Res. 37 (16), 3821 – 3836.

Giokas, D., Kim, Y., Paraskevas, P., Paleologos, E., Lekkas, T., 2002. A simple empirical model for activated sludge thickening in secondary clarifiers. Water Res. 36 (13), 3245–3252.

Godunov, S. K., 1959. A difference method for numerical calculation of discontinuous solutions of the equations of hydrodynamics. Mat. Sb. 89 (3), 271–306.

Griborio, A. G., 2004. Secondary clarifier modeling: a multi-process approach. Ph.D. thesis, University of New Orleans.

Griewank, A., Juedes, D., Utke, J., 1996. Algorithm 755: Adol-c: a package for the automatic differentiation of algorithms written in c/c++. ACM Trans. Math. Softw. 22 (2), 131–167.

Griewank, A., Walther, A., 2008a. Evaluating derivatives: principles and techniques of algorithmic differentiation, 2nd Edition. SIAM, Philadelphia.

Griewank, A., Walther, A., 2008b. Evaluating Derivatives: Principles and Techniques of Algorithmic Differentiation. SIAM.

Guibaud, G., Dollet, P., Tixier, N., Dagot, C., Baudu, M., 2004. Characterisation of the evolution of activated sludges using rheological measurements. Process Biochem. 39 (11), 1803–1810.

Hammadi, L., Ponton, A., Belhadri, M., 2011. Rheological study and valorization of waste sludge from wastewater treatment plants in the dredging operation of hydraulic dams. Energy Procedia 6, 302–309.

Harker, A. H., Temple, J. A. G., 1988. Velocity and attenuation of ultrasound in suspensions of particles in fluids. J. Phys. D Appl. Phys. 21 (11), 1576–1588.

Hascoët, L., Pascual, V., 2004. Tapenade 2.1 user's guide.

Hascoët, L., Pascual, V., 2013. The Tapenade Automatic Differentiation tool: Principles, Model, and Specification. ACM Trans. Math. Softw. 39 (3).

Henze, M., Gujer, W., Mino, T., van Loosdrecht, M., 2000. Activated Sludge Models ASM1, ASM2, ASM2D and ASM3. IWA Scientific and Technical Report 9, IWA Publishing, London, UK.

Hosseini, S., Patel, D., Ein-Mozaffari, F., Mehrvar, M., 2010. Study of Solid-Liquid Mixing in Agitated Tanks through Computational Fluid Dynamics Modeling. Ind. Eng. Chem. 49, 4426–4435.

James, F., Sepulveda, M., 1994. Parameter identification for a model of chromatographic column. Inverse Probl. 10, 1299–1314.

Joyner Jr., C., Reid, J., 1963. Applications of ultrasound in cardiology and cardiovascular physiology. Prog. Cardiovasc. Dis. 5 (5), 482–497.

Karl, J. R., Wells, S., 1999. Numerical model of sedimentation/thickening with inertial effects. J. Environ. Eng.-ASCE 125 (9), 792–806.

Karlsen, K. H., Risebro, N. H., 1997. An operator splitting method for non-linear convection-diffusion equations. Numer. Math. 77 (3), 365–382.

Kinnear, D. J., 2002. Biological solids sedimentation: a model incorporating fundamental settling parameters. Ph.D. thesis, Department of Civil and Environmental Engineering, University of Utah.

Kynch, G. J., 1952. A theory of sedimentation. T. Faraday Soc. 48, 166–176.

Laera, G., Giordano, C., Pollice, A., Saturno, D., Mininni, G., 2007. Membrane bioreactor sludge rheology at different solid retention times. Water Res. 41 (18), 4197–4203.

Lakehal, D., Krebs, P., Krijgsman, J., Rodi, W., 1999. Computing shear flow and sludge blanket in secondary clarifiers. J. Hydraul. Eng.–ASCE 125 (3), 253–262.

Laurent, J., Samstag, R. W., Ducoste, J. M., Griborio, A., Nopens, I., Batstone, D. J., Wicks, J. D., Saunders, S., Potier, O., 2014. A protocol for the use of computational fluid dynamics as a supportive tool for wastewater treatment plant modelling. Wat. Sci. Technol. 70 (10), 1575–1584.

Le Dimet, F.-X., Talagrand, O., 1986. Variational algorithms for analysis and assimilation of meteorological observations: theoretical aspects. Tellus A 38 (2), 97–110.

Le Moullec, Y., Gentric, C., Potier, O., Leclerc, J. P., 2010. Comparison of systemic, compartmental and cfd modelling approaches: application to

the simulation of a biological reactor of wastewater treatment. Chem. Eng. Sci. 65 (1), 343–350.

Lesieur, M., 1994. La turbulence. EDP Sciences.

Lesieur, M., Métais, O., 1996. New trends in large-eddy simulations of turbulence. Annu Rev. Fluid Mech. 28, 45–82.

Lions, J.-L., 1971. Optimal Control of Systems Governed by Partial Differential Equations. Springer.

Locatelli, F., 2015. Activated sludge batch settling: from experimental investigation using an ultrasonic transducer to 1 D modelling, sensitivity analysis and parameter identification. Ph.D. thesis, Strasbourg University.

Locatelli, F., Charpentier, I., Fran¸cois, P., Mosé, R., 2015a. Modelling the settling of flocculated suspensions: sensitivity analysis through automatic differentiation. to be submitted in Comput. Chem. Eng.

Locatelli, F., François, P., Laurent, J., Lawniczak, F., Dufresne, M., Vazquez, J., Bekkour, K., 2015b. Detailed velocity and concentration profiles measurement during activated sludge batch settling using an ultrasonic transducer. Separ. Sci. Technol. 50 (7), 1059–1065.

Locatelli, F., Laurent, J., François, P., Dufresne, M., Vazquez, J., Bekkour, K., 2013. Impact de la loi de comportement rhéologique sur la sédimentation en batch de boues activées: approche expérimentale et numérique. Houille Blanche (4), 31–36.

Lotito, V., Spinosa, L., Mininni, G., Antonacci, R., 1997. The rheology of sewage sludge at different steps of treatment. Water Sci. Technol. 36 (11), 79–85.

Manneville, S., Bécu, L., Colin, A., 2004. High-frequency ultrasonic speckle velocimetry in sheared complex fluids. Eur. Phys. J. App. Phys. 28 (03), 361–373.

Morgensten, J., 1985. How to compute fast a function and all its derivatives, a variation on the theorem of baur-strassen. SIGACT News 16, 60–62.

Mori, M., Isaac, J., Seyssiecq, I., Roche, N., 2008. Effect of measuring geometries and exocellular polymeric substances on the rheological behaviour of sewage sludge. Chem. Eng. Res. Des. 86, 554–559.

Mori, M., Seyssiecq, I., Roche, N., 2006. Rheological measurements of sewage sludge for various solids concentrations and geometry. Process Biochem. 41, 1656–1662.

Pollert, J., Pavlíčková, D., Vladimír, T., 2012. Secondary clarifiers optimisation in prague's wastewater treatment plant using a mathematical model. Water Practice and Technology 7 (1).

Ratkovich, N., Horn, W., Helmus, F. P., Rosenberger, S., Naessens, W., Nopens, I., Bentzen, T. R., 2013. Activated sludge rheology: A critical review on data collection and modelling. Water Res. 47, 463–482.

Roche, N., Vaxelaire, J., Prost, C., 1995. A simple empirical model for hindered settling in activated sludge clarifier. Water Environ. Res. 67 (5), 775–780.

Rodi, W., 1993. Turbulence models and their application in hydraulics, 3rd Edition. Balkema, Rotterdam, The Netherlands.

Rushton, A., Ward, A., Holdich, R., 2000. Solid-Liquid Filtration and Separation Technology, Second, Completely Revised Edition. Wiley-Vch Verlag GmbH, Weinheim.

Sanin, F. D., 2002. Effect of solution physical chemistry on the rheological properties of activated sludge. Water SA 28 (2), 207–212.

Seyssiecq, I., Ferrasse, J.-H., Roche, N., 2003. State-of-the-art: rheological characterisation of wastewater treatment sludge. Biochem. Eng. J. 16 (1), 41–56.

Slatter, P., 1997. The rheological characterisation of sludges. Water Sci. Technol. 36 (11), 9–18.

Smagorinsky, J., 1963. General circulation experiments with the primitive equations. Mon. Weather Rev. 91 (3), 99–164.

Sozanski, M., Kempa, E., Grocholski, K., Bien, J., 1997. The rheological experiment in sludge properties research. Water Sci. Technol. 36 (11), 69–78.

Spérandio, M., Heran, M., Gillot, S., 2007. Modélisation dynamique des procédés biologiques de traitement des eaux. Techniques de l'ingénieur W 6 500, 1–18.

Stamou, A. I., Latsa, M., Assimacopoulos, D., 2000. Design of two-storey final settling tanks using mathematical models. J. Hydroinform. 2 (4), 235–245.

Stricker, A.-E., Takacs, I., Marquot, A., 2007. Hindered and compression settling: parameter measurement and modelling. Water Sci. Technol. 56 (12), 101–110.

Takács, I., Patry, G. G., Nolasco, D., 1991. A dynamic model of the clarification-thickening process. Water Res. 25 (10), 1263–1271.

Takeda, Y., 1986. Velocity Profile Measurement by Ultrasound Doppler Shift Method. Int. J. Heat Fluid Fl. 7 (4), 313–318.

Takeda, Y., 1995. Velocity profile measurement by ultrasonic Doppler method. Exp. Therm. Fluid Sci. 10, 444–453.

Takeda, Y., 1999. Ultrasonic doppler method for velocity profile measurement in fluid dynamics and fluid engineering. Exp. Fluids 26 (3), 177–178.

Taylor, G. I., 1923. Stability of a viscous liquid contained between two rotating cylinders. Philos. T. R. Soc. Lond., 289–343.

Tixier, N., 2003. Approche des propriétés rhéologiques de suspensions biologiques floculées. Thèse de doctorat, Université de Limoges.

Tixier, N., Guibaud, G., Baudu, M., 2003a. Towards a rheological parameter for activated sludge bulking characterisation. Enzyme Microb. Tech. 33(2–3), 292–298.

Tixier, N., Guibaud, G., Baudu M., 2003b. Determination of some rheological parameters for the characterization of activated sludge. Bioresource Technol. 90 (2), 215–220.

Torfs, E., Balemans, S., Locatelli, F., Bürger, R., Laurent, J., François, P., Diehl, S., Nopens, I., 2015. Critical analysis of constitutive functions for hindered settling velocity in 1–D settler models. In: Proceedings of the 9th IWA Symposium on Systems Analysis and Integrated Assessment (Watermatex).

Tropea, C., Yarin, A. L., Foss, J. F., 2007. Springer handbook of experimental fluid mechanics. Vol. 1. Springer Science & Business Media.

Van Dyke, M., 1982. An Album of Fluid Motion. Parabolic Press.

Van Wazer, J., Lyons, J., Kim, K., Colwell, R., 1963. Viscosity and flow measurement. New York: Interscience.

Vanhooren, H., Meirlaen, J., Amerlinck, Y., Claeys, F., Vangheluwe, H., Vanrolleghem, P., 2003. West: modelling biological wastewater treatment. J. Hydroinform. 5, 27–50.

Vanrolleghem, P. A., Lee, D. S., 2003. On-line monitoring equipment for wastewater treatment processes: state of the art. Water Sci. Technol. 47 (2), 1–34.

Versteeg, H. K., Malalasekera, W., 1995. An introduction to computational fluid dynamics: the finite volume method. Prentice Hall.

Vesilind, P. A., 1968. Discussion of 'Evaluation of activated sludge thickening theories' by Dick R. I. and Ewing B. B. J. San. Eng. Div. ASCE 94 (SA1), 185–191.

Wang, T., Wang, J., Ren, F., Jin, Y., 2003a. Application of doppler ultrasound velocimetry in multiphase flow. Chem. Eng. J. 92 (1), 111–122.

Wang, T., Wang, J., Ren, F., Jin, Y., 2003b. Application of doppler ultrasound velocimetry in multiphase flow. Chem. Eng. J. 92 (1), 111–122.

White, J., 1990. Principles of Polymer Engineering Rheology. John Wiley & Sons, Inc.

Wicklein, E. A., Samstag, R. W., 2009. Comparing commercial and transport cfd models for secondary sedimentation. Proceedings of the Water Environment Federation 2009 (10), 6066–6081.

Wiklund, J., Shahram, I., Stading, M., 2007. Methodology for in-line rheology by ultrasound doppler velocity profiling and pressure difference techniques. Chem. Eng. Sci. 62 (16), 4277–4293.

Willuweit, L., O'Sullivan, J. J., 2013. A decision support tool for sustainable planning of urban water systems: Presenting the dynamic urban water simulation model. Water Res. 47 (20), 7206–7220.

Wren, D. G., Barkdoll, B. D., Kuhnle, R. A., Derrow, R. W., 2000. Field techniques for suspended-sediment measurement. J. Hydraul. Eng.-ASCE 126 (2), 97–104.

Xanthos, S., Gong, M., Ramalingam, K., Fillos, J., Deur, A., Beckmann, K., McCorquodale, J. A., 2011. Performance Assessment of Secondary Settling Tanks Using CFD Modeling. Water Resour. Manag. 25 (4), 1169–1182.

Xia, M., Wang, Z., Wu, Z., Wang, X., Zhou, Z., Lu, J., 2009. Simulation and assessment of sludge concentration and rheology in the process of waste activated sludge treatment. J. Environ. Sci. 21 (12), 1639–1645.

Yang, F., Bick, A., Shandalov, S., Brenner, A., Oron, G., 2009. Yield stress and rheological characteristics of activated sludge in an airlift membrane bioreactor. J. Membrane Sci. 334 (1–2), 83–90.

Yoshida, T., Mori, M., Nimura, Y., Hikita, G.-I., Takagishi, S., Nakanishi, K., Satomura, S., 1961. Analysis of heart motion with ultrasonic Doppler method and its clinical application. Am. Heart J. 61 (1), 61–75.

Florent LOCATELLI

Activated sludge batch settling: from experimental investigation using an ultrasonic transducer to 1D modelling, sensitivity analysis and parameter identification

Résumé

Ce travail porte sur l'étude expérimentale et la modélisation de la sédimentation des boues activées. Un pilote expérimental associant une colonne de sédimentation et un transducteur ultrasonore est proposé. Des profils de vitesse de sédimentation et de concentration en particules sont obtenus grâce à ce dispositif, ce qui permet de mieux comprendre les mécanismes de décantation des boues. Ces résultats sont utilisés afin de développer une approche numérique. Un modèle de sédimentation est construit en intégrant des fonctions expérimentales. Une méthodologie mettant en œuvre la différentiation automatique du modèle est ensuite élaborée et appliquée, d'une part, à l'analyse de sensibilité du modèle aux paramètres des fonctions utilisées et, d'autre part, à l'identification des valeurs de ces paramètres à l'aide des résultats expérimentaux. La conjonction des approches expérimentale et numérique proposées constitue un processus efficace pour le développement des modèles de sédimentation.

Mots-clés : clarification secondaire, sédimentation de zone, compression, expérimentation en laboratoire, rhéologie, méthode ultrasonore non invasive, modélisation, approche mécaniste, simulation numérique, différentiation automatique

Abstract

This work deals with the experimental investigation and modelling of activated sludge settling. An experimental setup combining a settling column and an ultrasonic transducer is proposed. Settling velocity and concentration profiles are obtained using this setup, allowing for a better understanding of the mechanisms of activated sludge settling. These results are applied to the development of a numerical approach. A settling model using experimental functions is built. A methodology based on the automatic differentiation of the model is developed. This methodology is used, on the one hand, to analyse the sensitivity of the results to the model parameters and, on the other hand, to identify the parameter values on the basis of experimental data. The combination of the proposed experimental and numerical methods yields an efficient process for the development of sedimentation models.

Key-words: secondary clarification, zone settling, compression, laboratory experimentation, rheology, non-invasive ultrasonic method, modelling, mechanistic approach, numerical simulation, automatic differentiation